



中山大学深圳校区

电子与通信工程学院

川渝论坛 2023-09-22



Visible Light Communication-Based Localization: Robust Algorithm, Performance Limits & Resource Deployment Optimization

Bingpeng Zhou

zhoubp3@mail.sysu.edu.cn

School of ECE, Sun Yat-sen University, Shenzhen, 518000

Chongqing, 2023

Outline



- Background
- System Model
- Robust Algorithm
- Performance Limits
- Resource Allocation
- Conclusions

Background

6G-driven Location-Aware intelligent applications:

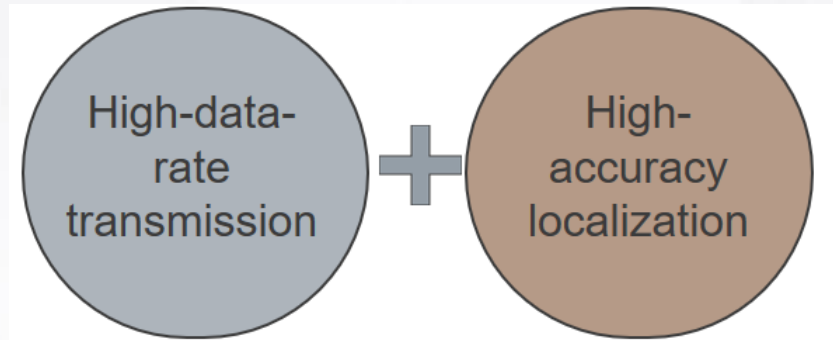
- Robotic navigation; Autonomous parcel sorting;
- UAV-based delivery;
- UE location and orientation are critical parameters.



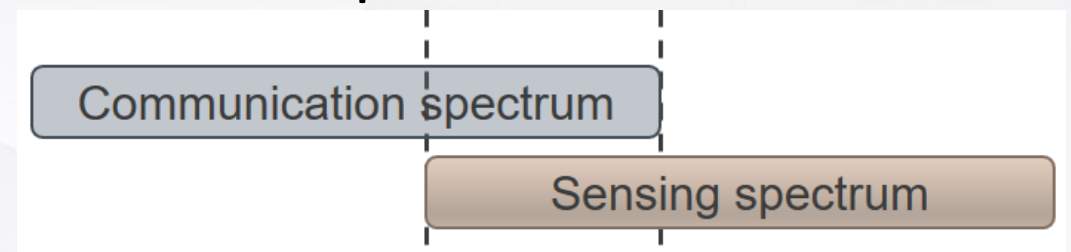
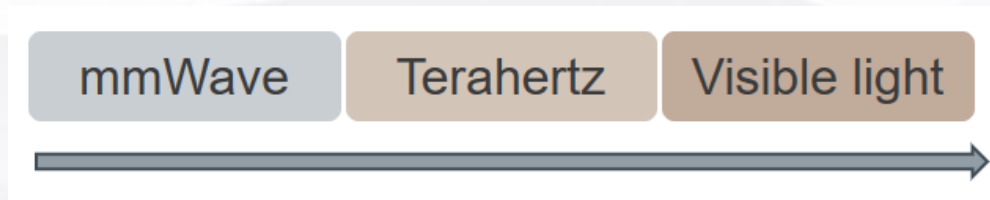


Background

- **Integrated Communication and Sensing, ICAS -> promising solutions**
- Demand: 6G-driven apps requires comm + sensing.



- Supply: software and hardware of C&S are compatible.





Background

Conventional UE localization solutions:

- WiFi-based localization solution: no angular resolution.
- GPS: not accessible for indoor applications.
- Radar: subject to environment.



Background

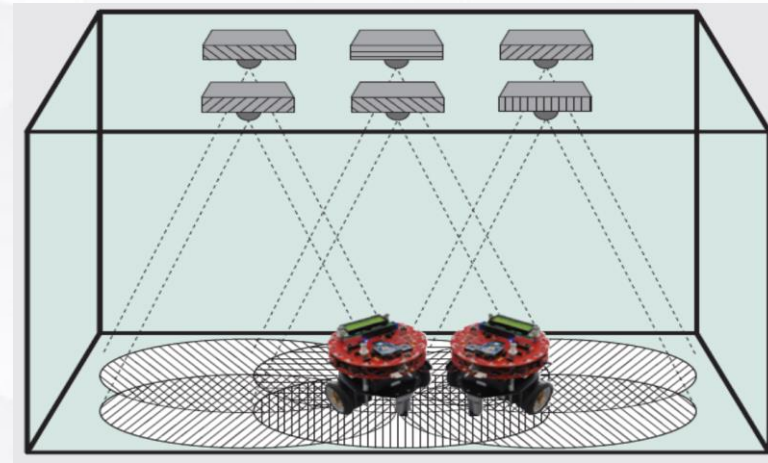
- Matrix view of conventional localization solutions

| 定位技术 | 室内/室外场景 | 定位精度 | 角度分辨率 | 适用范围 | 稳定性 |
|--------|---|--|-------|---------|-------|
| GPS/北斗 |  |  5-20米 | 较低 | 全球 | ★ ☆ ☆ |
| WiFi定位 |   |  5-15米 | 较低 | < 150米 | ☆ ☆ ☆ |
| 激光雷达 |   |  5-10厘米 | 较高 | < 80米 | ★ ★ ☆ |
| 超宽带定位 |   |  10-50厘米 | 较低 | < 250米 | ★ ★ ☆ |
| 蜂窝定位 |  |  15-50米 | 较低 | < 1000米 | ☆ ☆ ☆ |
| 无线传感定位 |   |  5-15米 | 较低 | < 200米 | ★ ☆ ☆ |

Background

VLC integrated with localization:

- Low-cost: localization during indoor illumination.
- High angular resolution due to large free band.
- Simultaneous Communication and Localization





Background

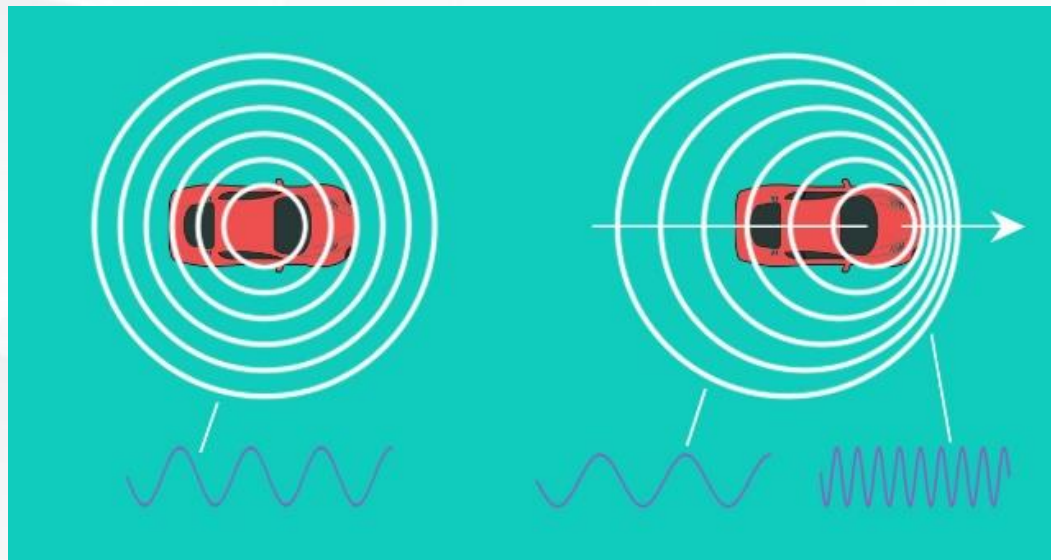
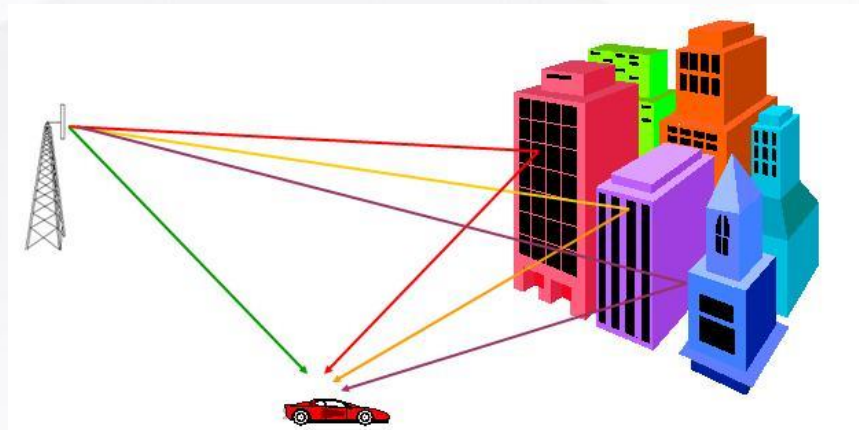
Conventional VLP methods

- Signal propagation model-based VLP
 - Require perfect knowledge of Lambertian model
 - Require perfect alignment of RX and TX orientation angles
 - Prior knowledge of VLP systems, e.g., UE orientation angle, height, ...
 - Channel fading is unresolved
- Fingerprinting-based VLP
- IMU-assisted cooperative VLP
- Deep Learning-based VLP

Background

Great challenge

- Random fading, Multipath interference,
- Lambertian modeling mismatch
- UD mobility -> Time-varying Doppler fading



Outline



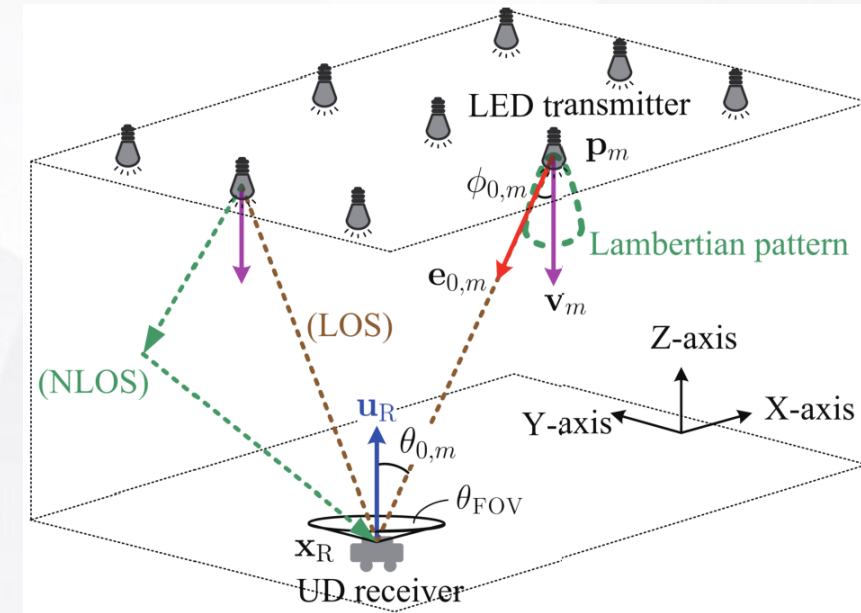
- Background
- **System Model**
- Robust Algorithm
- Performance Limits
- Resource Allocation
- Conclusions



System Model

System setup

- M LEDs with known location $\mathbf{p}_m \in \mathbb{R}^3$ and orientation $\mathbf{v}_m \in \mathbb{R}^3$
- One mobile UD with a PD array
- UD location $\mathbf{x}_R \in \mathbb{R}^3$ and pose angle $\mathbf{u}_R \in \mathbb{R}^3$
- Let $\alpha_R = [\mathbf{x}_R, \mathbf{u}_R] \in \mathbb{R}^6$ be the joint vector.





System Model

Measurement Model

- The received waveform of visible light follows the lambertian model, which is summarized as below (for each tx-rx pair, n-th subcarrier)

$$z_{m,n} = g_{m,n}(\alpha_R; \wp_{m,n}) + \epsilon_{m,n}$$

- where $g_{m,n}(\alpha_R; \wp_{m,n})$ denotes VLC signal propagation function absorbing diffuse scattering and channel fading, depending on UD location
- α_R is UD location parameter
- $\wp_{m,n} = \{\text{fading coefficient, NLOS interference}\}$: system parameters, time varying due to dynamic environment
- $\epsilon_{m,n}$: random measurement noise



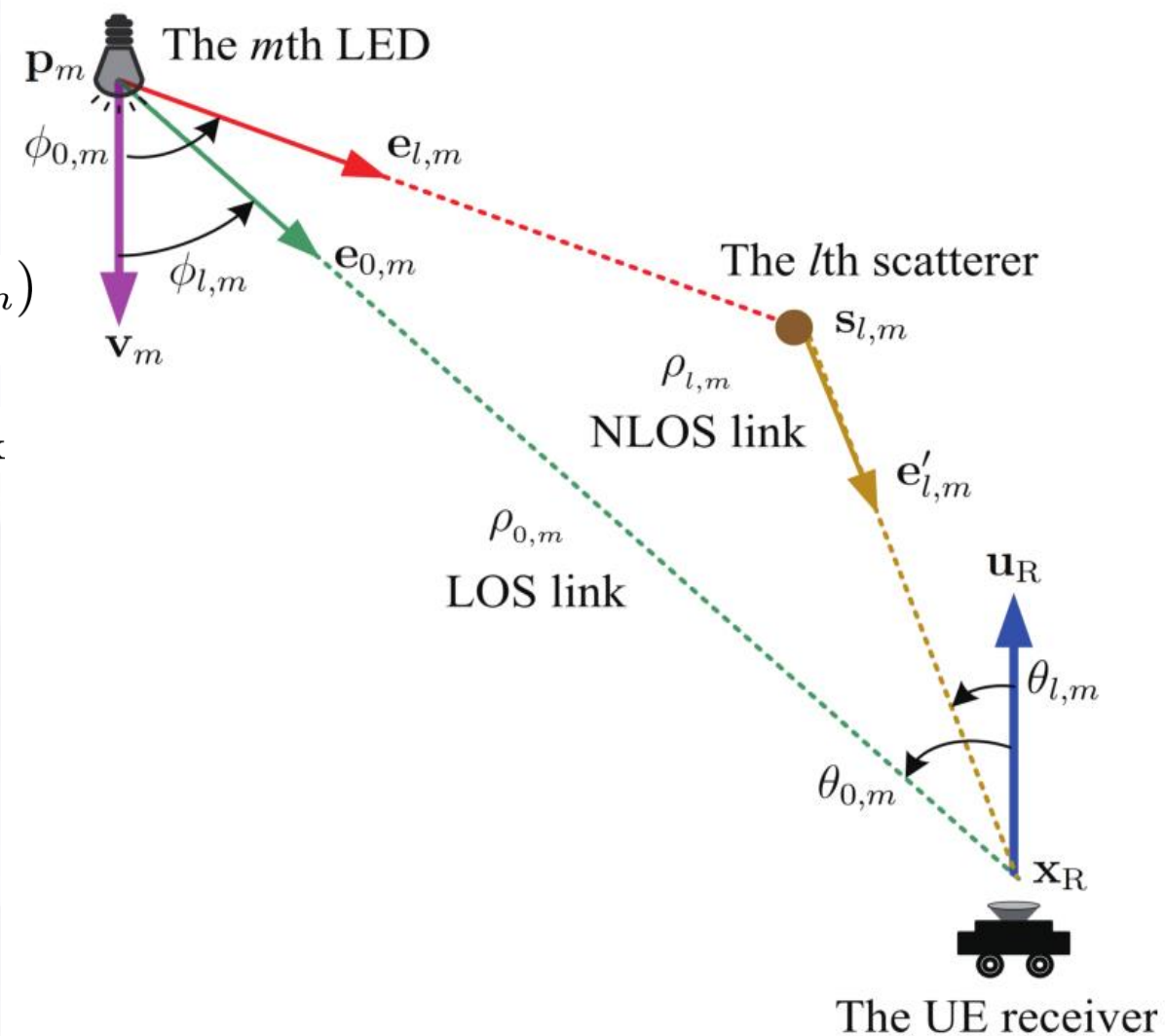
System Model

Lambertian Radiation Model

- Signal propagation model

$$g_{m,n}(\mathbf{a}_R; \mathbf{p}_{m,n}) = \sum_{\ell=0:L-1} a_{m,n} g_{\ell,m,n} \exp(-j2\pi f_{n,m} \tau_{\ell,m})$$

- Gain of each path $g_{\ell,m,n} = G_{\text{rx}} G_{\text{path}} G_{\text{tx}}$
- Known tx OFDM pilot: $a_{m,n}$



System Model

Lambertian Radiation Model

- Gain of LED Transmitters

$$G_{\text{tx}} = \sqrt{W_{\text{tx}}} (r + 1) (\cos(\phi_{l,m}))^r$$

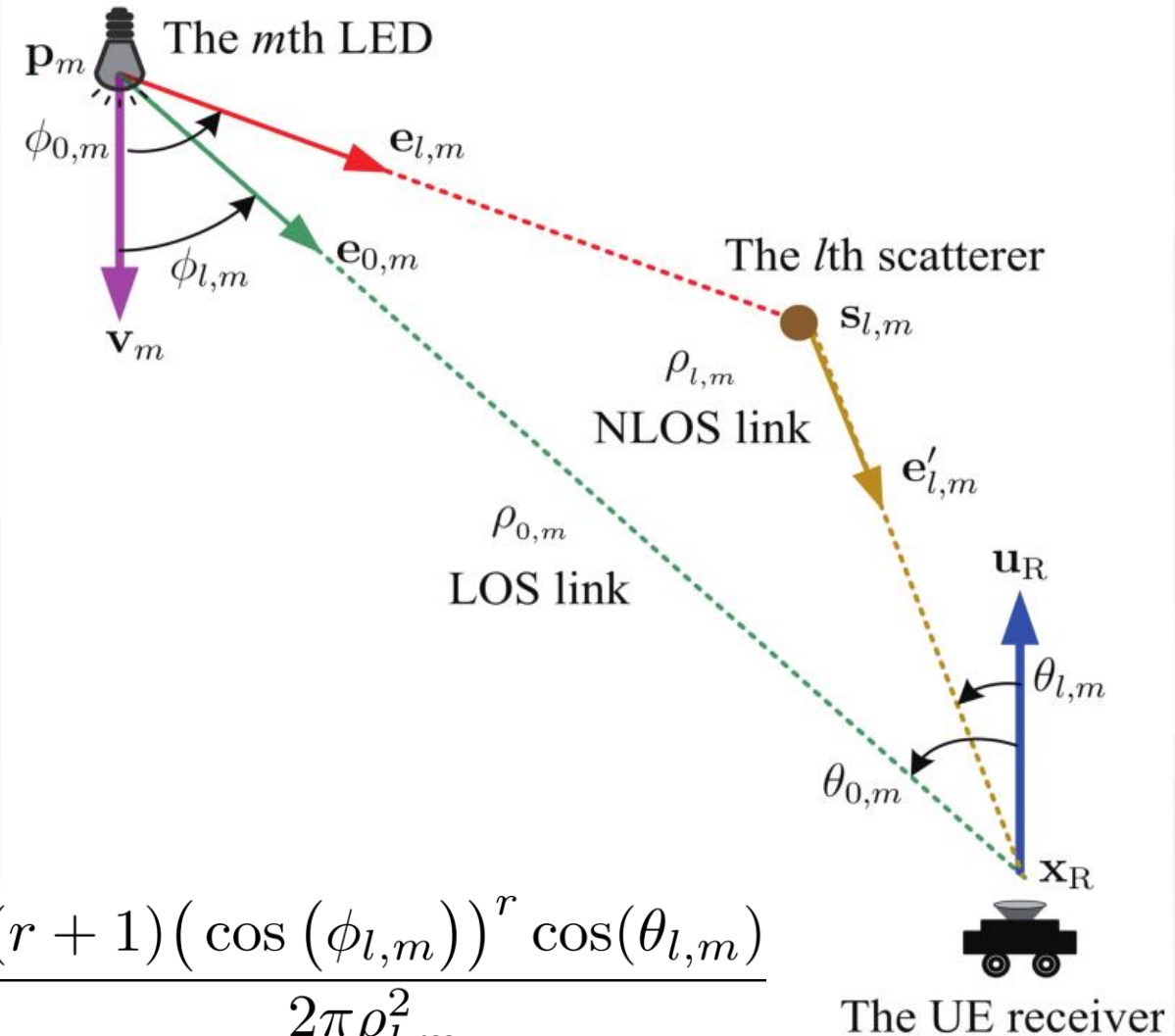
- Lambertian order $r = -\frac{\ln 2}{\ln \cos(A_{\frac{1}{2}})}$

- Response gain of UD's PD

$$G_{\text{rx}} = \Psi_F \Psi_C \Psi_A \cos(\theta_{l,m})$$

- Path loss $G_{\text{path}} = \frac{1}{2\pi \rho_{l,m}^2}$

- Gain of each path $g_{l,m,n} = \sqrt{W_{\text{tx}}} h_{l,m} \frac{(r + 1) (\cos(\phi_{l,m}))^r \cos(\theta_{l,m})}{2\pi \rho_{l,m}^2}$





System Model

Lambertian Radiation Model

- Finally, the received OFDM signal waveform

$$z_{m,n} = \sqrt{W_{tx}} \sum_{\ell=0:L-1} h_{\ell,m} \frac{(r+1)(\cos(\phi_{\ell,m}))^r \cos(\theta_{\ell,m})}{2\pi \rho_{\ell,m}^2} \exp(-j2\pi f_{n,m} \tau_{\ell,m}) + \epsilon_{m,n}$$

- RSS sample $y_m = \sqrt{W_{tx}} \frac{(r+1)(\cos(\phi_{0,m}))^r \cos(\theta_{0,m})}{2\pi \rho_{0,m}^2} + \varsigma_m^{\text{nlos}} + \epsilon_m$
- All propagation parameters depend on UD location and orientation:
Transmission delay (tau), radiation angle (theta), incidence angle (phi),
transmission distance (rho)



Outline

- Background
- System Model
- Robust VLP Algorithm
- Performance Limits
- Resource Allocation
- Conclusions



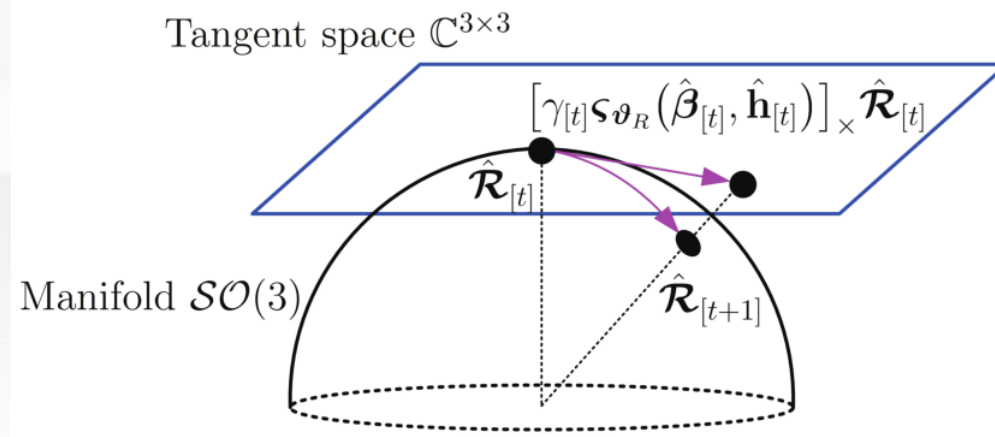
Robust VLP Method

Problem formulation

- UD location and pose tracking based on VLC aims to determine UD location α_R from varying samples $\{z_{m,n} | \forall m, \forall n\}$

$$\mathcal{P}_{\text{VLP}} : (\hat{\alpha}_R, \hat{\mathbf{h}}) = \arg \min_{\alpha_R} \min_{\mathbf{h}} \|\mathbf{z} - \mathbf{G}(\alpha_R) \mathbf{h}\|_2^2, \quad (1)$$

$$\text{s.t. } \mathcal{R}(\mathbf{u}_R) \in \mathcal{SO}(3), \quad (2)$$



Robust VLP Method

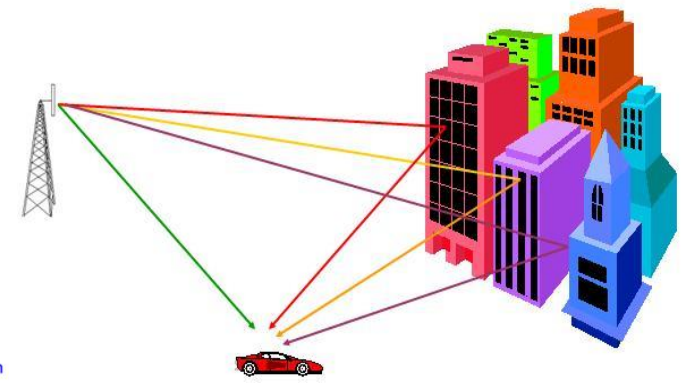
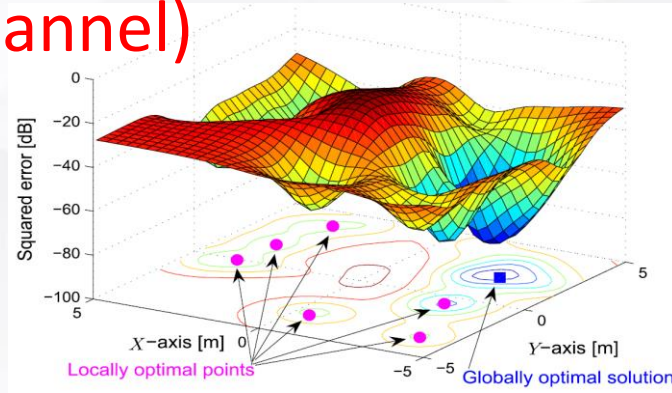
Problem formulation

$$\mathcal{P}_{\text{VLP}} : (\hat{\alpha}_{\text{R}}, \hat{\mathbf{h}}) = \arg \min_{\alpha_{\text{R}}} \min_{\mathbf{h}} \|\mathbf{z} - \mathbf{G}(\alpha_{\text{R}})\mathbf{h}\|_2^2, \quad (1)$$

$$\text{s.t. } \mathcal{R}(\mathbf{u}_{\text{R}}) \in \mathcal{SO}(3), \quad (2)$$

Technical Challenge:

- NLOS interference, random fading (and even UD mobility)
- Non-convex problem nature (cost, constraint)
- Large uncertainty set (pose, channel)





Robust VLP Method

Our Solution:

- Lamberation model-based VLP
 - LRM calibration-enhanced VLP
 - Joint channel estimate with VLP
 - Stochastic sampling
- FG-based VLP:
 - FG interference model optimization-enhanced VLP
- DL-based VLP:
 - Branched ResNet-based VLP;
 - BiRCNN-based VLP



(1) Stochastic Searching



(1) Stochastic Searching

Stochastic searching-based VLP

- Generate a set of random particles (location, orientation)

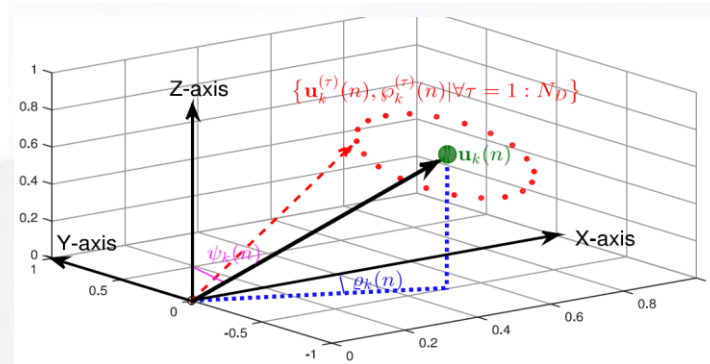
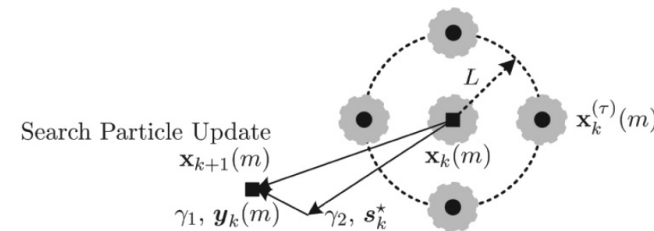
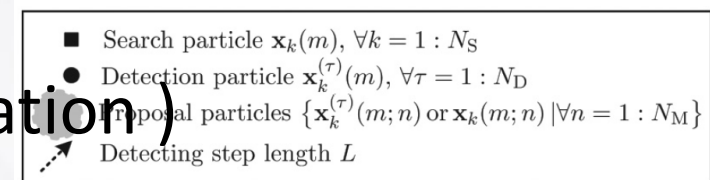
$$\{\alpha_k(n), \varphi_k(n) | \forall n = 1 : N_S\} \sim p(\mathbf{z} | \alpha_R)$$

- Global search $\alpha_k^{GB} = \arg \max_{\alpha_k(n) | \forall n = 1 : N_S} \{\varphi_k(n) | \forall n = 1 : N_S\},$

- Local detection $\alpha_k^{LB}(n) = \arg \max_{\alpha_k^{(\tau)}(n) | \tau = 1 : N_D} \{\varphi_k^{(\tau)}(n) | \forall \tau = 1 : N_D\},$

- Stochastic update $\alpha_{k+1}(n) = \alpha_k^b(n), \text{ if } \varphi_k^b(n) \geq \varphi_k(n),$

$$\alpha_k^b(n) = \text{decison}(\alpha_k^{GB}, \alpha_k^{LB})$$

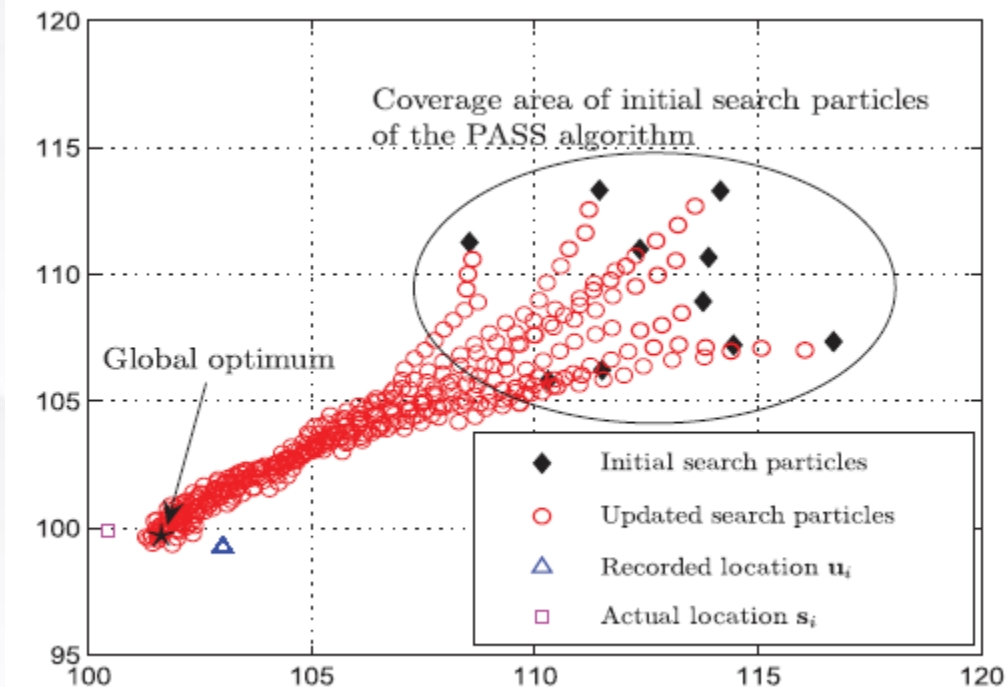
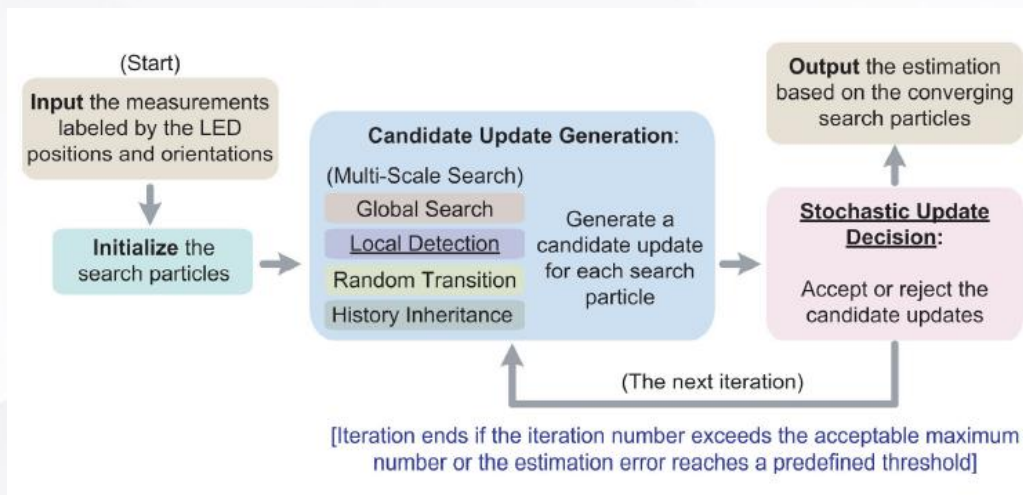


(1) Stochastic Searching

Stochastic searching-based VLP

- Update particle until they converge

- Localization decision $\hat{\alpha}_k = \sum_{n=1:N_S} \varphi_k(n) \alpha_k(n),$





(1) Stochastic Searching

What is different in our solution

- Statistical optimality-guided localization decision
- Robust search (local + global, location + **angle rotation**)
- Guaranteed convergence

$$\hat{\alpha}_k = \sum_{n=1:N_S} \varphi_k(n) \alpha_k(n),$$

Theorem 1 (Convergence of PASS to Global Optimum):

Given the sufficiently large number of iterations, the PASS-based estimate $\hat{\alpha}_k(N_S)$ in Eq. (30) will converge in probability to the globally optimal solution α_R^* , i.e.,

$$\lim_{\substack{N_S \rightarrow \infty, \\ k \rightarrow \infty}} \Pr\{\|\hat{\alpha}_k(N_S) - \alpha_R^*\|_2 \leq \varepsilon\} = 1, \forall \varepsilon > 0, \quad (31)$$

where $\|\cdot\|_2$ denotes the ℓ_2 -norm on a vector.

Theorem 2 (Convergence of PASS to True Value): Given a sufficient number of search particles and iterations for an unbiased SPAO system, the PASS-based estimate $\hat{\alpha}_k(N_S, |\Omega_R|)$ will converge in probability to the true value α_R , asymptotically, with a large measurement sample limit,

$$\lim_{\substack{N_S \rightarrow \infty, \\ k \rightarrow \infty, \\ |\Omega_R| \rightarrow \infty}} \Pr\{\|\hat{\alpha}_k(N_S, |\Omega_R|) - \alpha_R\|_2 \leq \varepsilon\} = 1, \forall \varepsilon > 0.$$



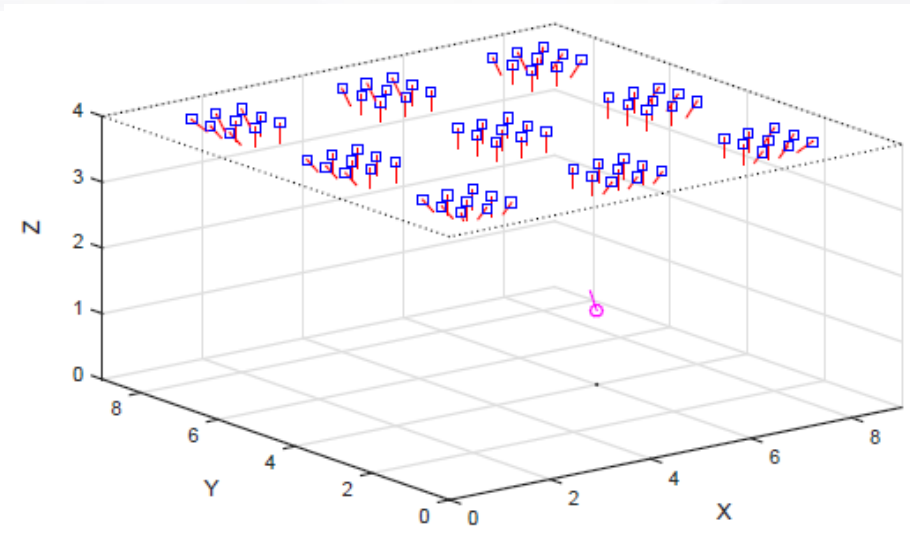
(1) Stochastic Searching

Simulation Settings

- SNR=20 dB, 81 LEDs on the ceiling, 9*9*4 space, RSS samples used

- NLOS propagation scenario: $s_{nlos,m} = \frac{\varphi_{nlos}}{1 - \varphi_{nlos}} h_m(\mathbf{x}_R, \mu_R), \varphi_{nlos} \in [0, 0.5)$

- Baselines
 - (*Baseline 1*): Geometric trilateration algorithm [14] with perfect alignment of LED and UE orientation angles;
 - (*Baseline 2*): Brute force search (BFS)-assisted maximum likelihood estimate (MLE) algorithm;
 - (*Baseline 3*): Newton-Raphson positioning (NRP) method [9] using locally linear approximation for nonlinear system model;
 - (*Baseline 4*): Traditional PSO method [22] dedicated to non-convex optimization;
 - (*Baseline 5*): Traditional SA method [25] dedicated to non-convex optimization.



(1) Stochastic Searching

Simulation results

- Convergence
- RMSE vs SNR

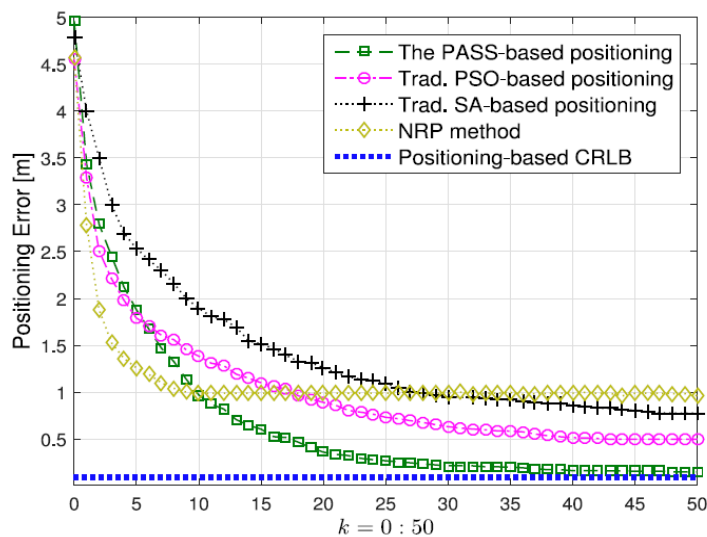
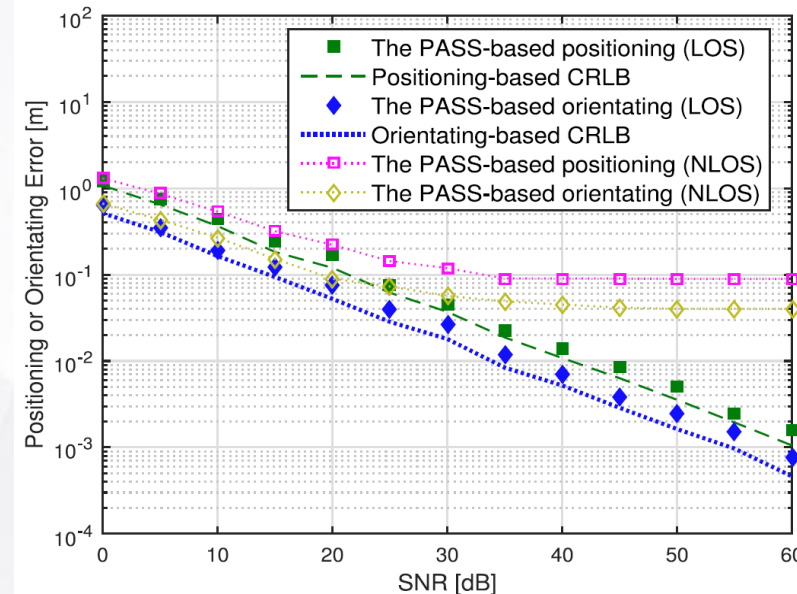
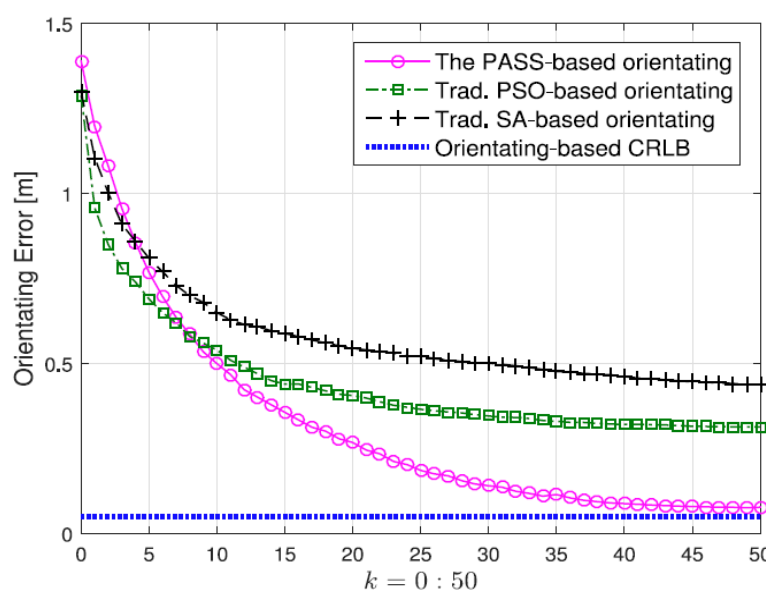


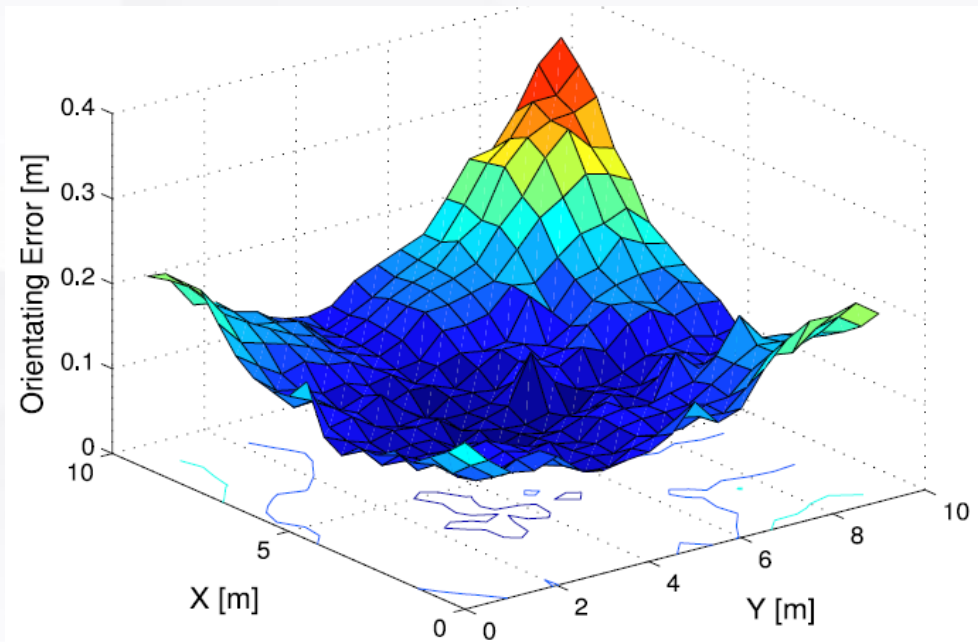
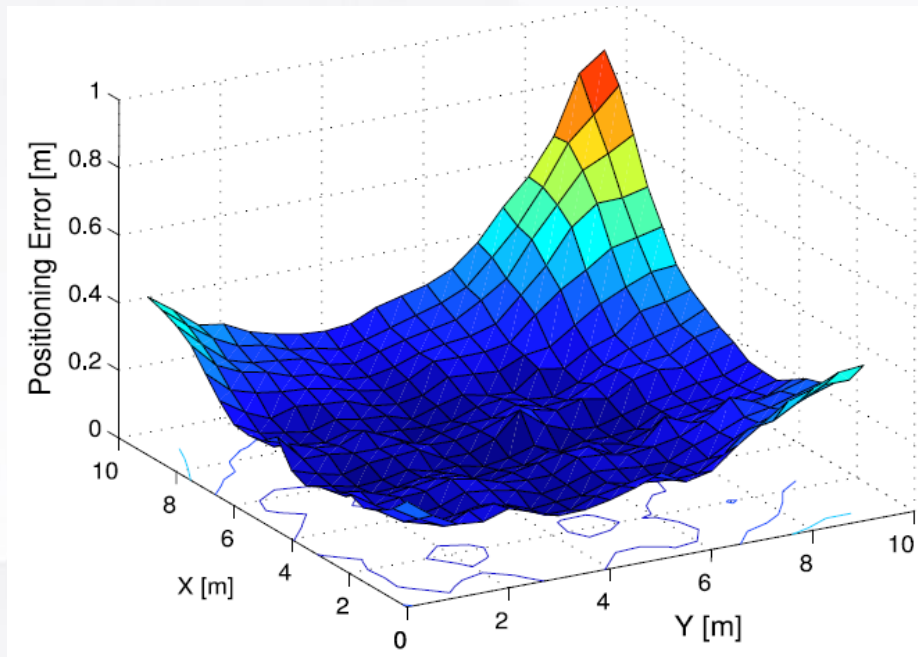
Fig. 4. The convergence of positioning errors $\|\hat{\mathbf{x}}_R - \mathbf{x}_R\|_2$ (SNR = 20 dB).



(1) Stochastic Searching

Simulation results

- RMSE vs UD Location

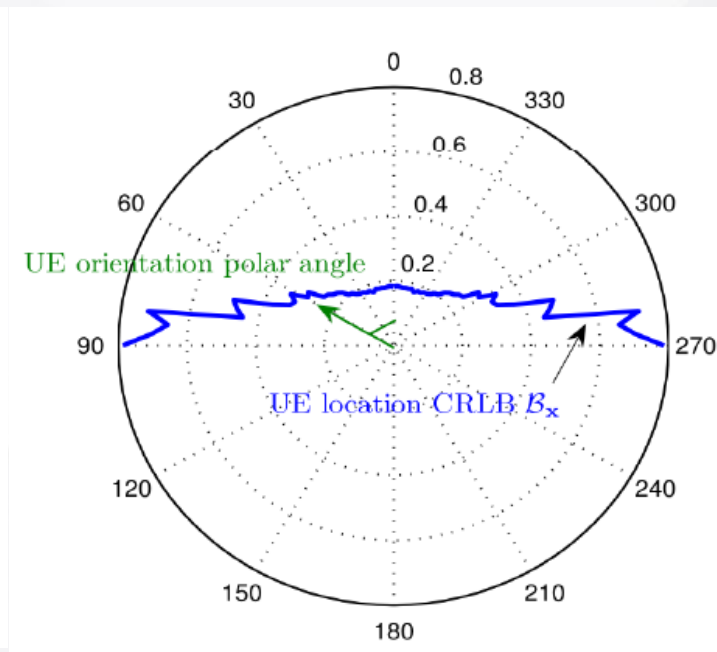
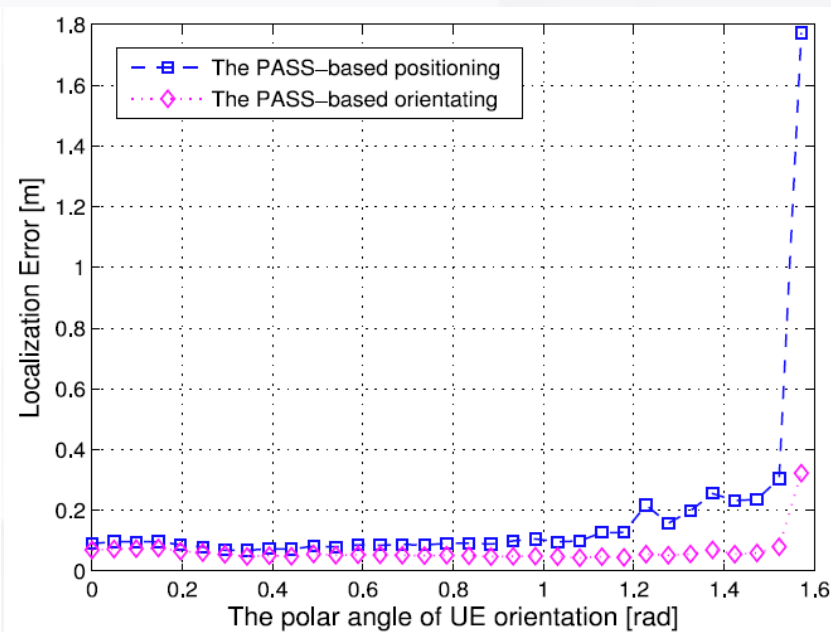
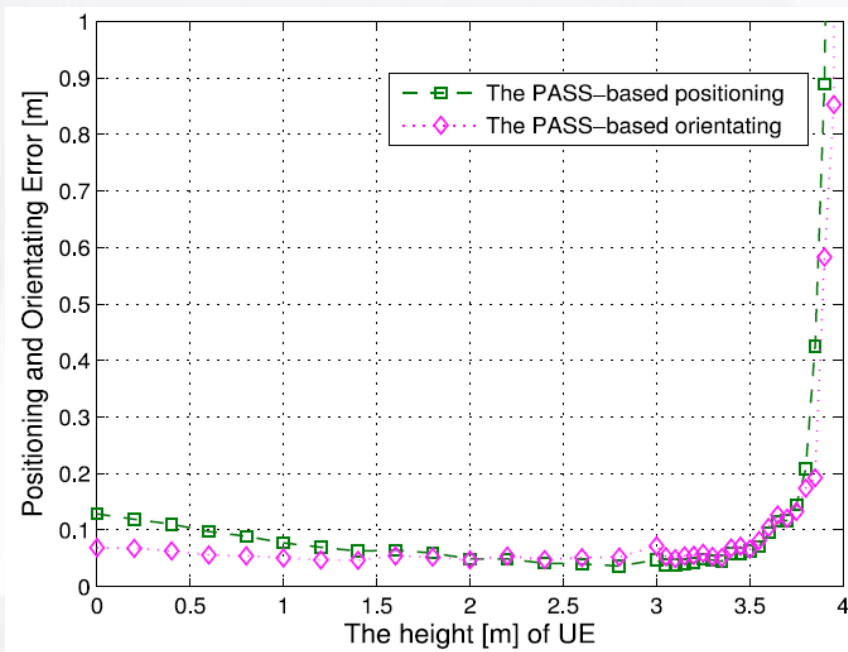




(1) Stochastic Searching

Simulation results

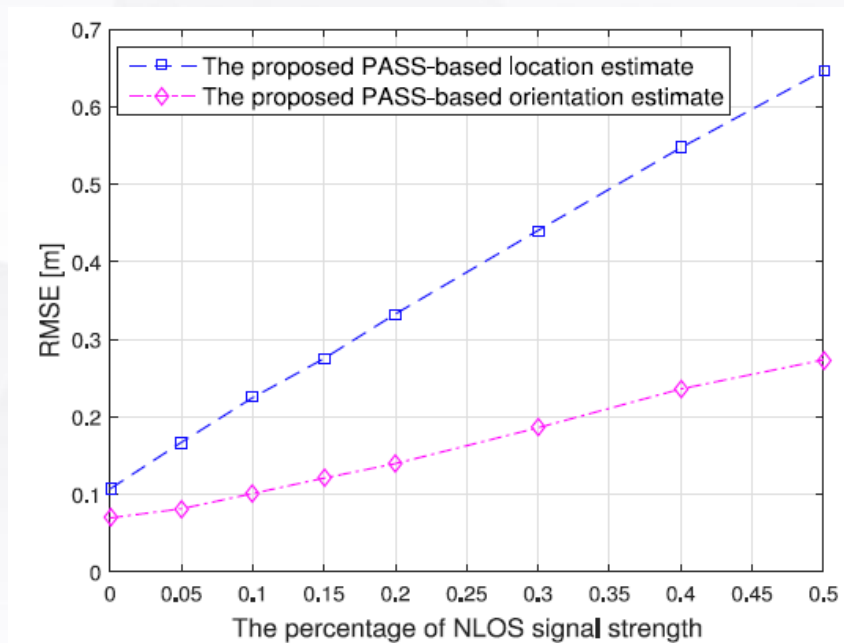
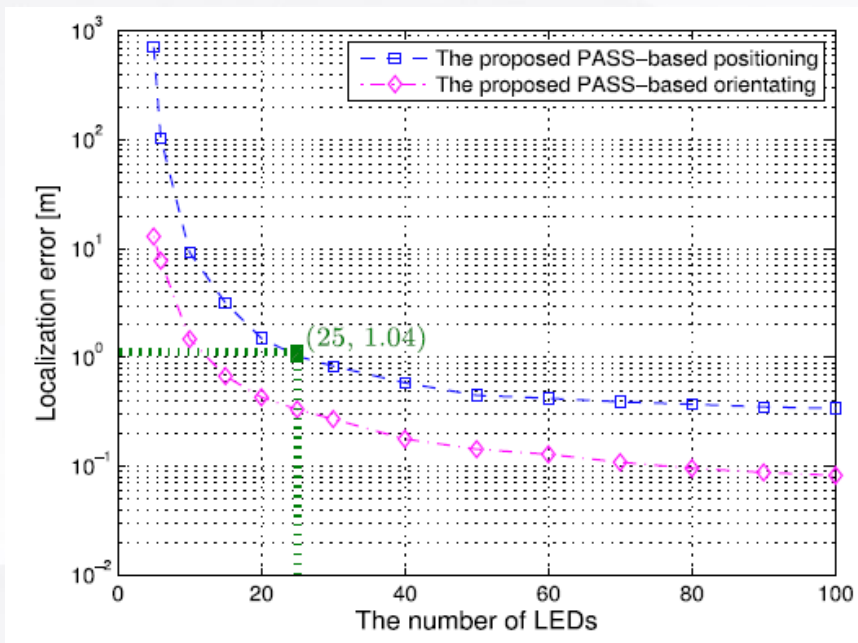
- RMSE vs UD height and polar angle



(1) Stochastic Searching

Simulation results

- RMSE vs the number of LEDs and NLOS interference





(1) Stochastic Searching

Conclusion:

- MMSE-guided stochastic searching is used for addressing non-convexity challenge.
- Convergence of stochastic searching is ensured, which can hit the global optimum **almost surely** as the number of particles tends to be infinity.

Theorem 1 (Convergence of PASS to Global Optimum):

Given the sufficiently large number of iterations, the PASS-based estimate $\hat{\alpha}_k(N_S)$ in Eq. (30) will converge in probability to the globally optimal solution α_R^* , i.e.,

$$\lim_{\substack{N_S \rightarrow \infty, \\ k \rightarrow \infty}} \Pr\{\|\hat{\alpha}_k(N_S) - \alpha_R^*\|_2 \leq \varepsilon\} = 1, \forall \varepsilon > 0, \quad (31)$$

where $\|\cdot\|_2$ denotes the ℓ_2 -norm on a vector.

Theorem 2 (Convergence of PASS to True Value): Given a sufficient number of search particles and iterations for an unbiased SPAO system, the PASS-based estimate $\hat{\alpha}_k(N_S, |\Omega_R|)$ will converge in probability to the true value α_R , asymptotically, with a large measurement sample limit,

$$\lim_{\substack{N_S \rightarrow \infty, \\ k \rightarrow \infty, \\ |\Omega_R| \rightarrow \infty}} \Pr\{\|\hat{\alpha}_k(N_S, |\Omega_R|) - \alpha_R\|_2 \leq \varepsilon\} = 1, \forall \varepsilon > 0.$$



(2) Channel Estimate-Based VLP



(2) Channel Est-Enhanced VLP

Challenge:

- VLP problem is **convex** w.r.t. channel state and emitting power.

$$\mathcal{P}_{\text{SPAO}} : (\hat{\mathbf{x}}_R, \hat{\boldsymbol{\mu}}_R) = \arg \min_{\mathbf{x}_R, \boldsymbol{\mu}_R} \|\mathbf{z} - \mathbf{G}(\mathbf{x}_R)\boldsymbol{\mu}_R\|_2^2, \quad (10)$$

$$\text{s.t. } \|\boldsymbol{\mu}_R\|_2^2 \leq W_{\max}. \quad (11)$$

- SCA-based iteration by exploiting **hidden-convex substructure** is employed for addressing non-convex location estimate.

(2) Channel Est-Enhanced VLP

Solution :

- SCA-guided Iteration between localization and channel estimation

$$\text{The original VLP problem } \mathcal{P}_{\text{VLP}} : (\hat{\mathbf{x}}_R, \hat{\boldsymbol{\mu}}_R) = \arg \min_{\mathbf{x}_R, \boldsymbol{\mu}_R} \|\mathbf{z} - \mathbf{G}(\mathbf{x}_R)\boldsymbol{\mu}_R\|_2^2, \quad (12)$$

$$\text{s.t. } \|\boldsymbol{\mu}_R\|_2^2 = 1. \quad (13)$$

⇓ (be composed into two subproblem)

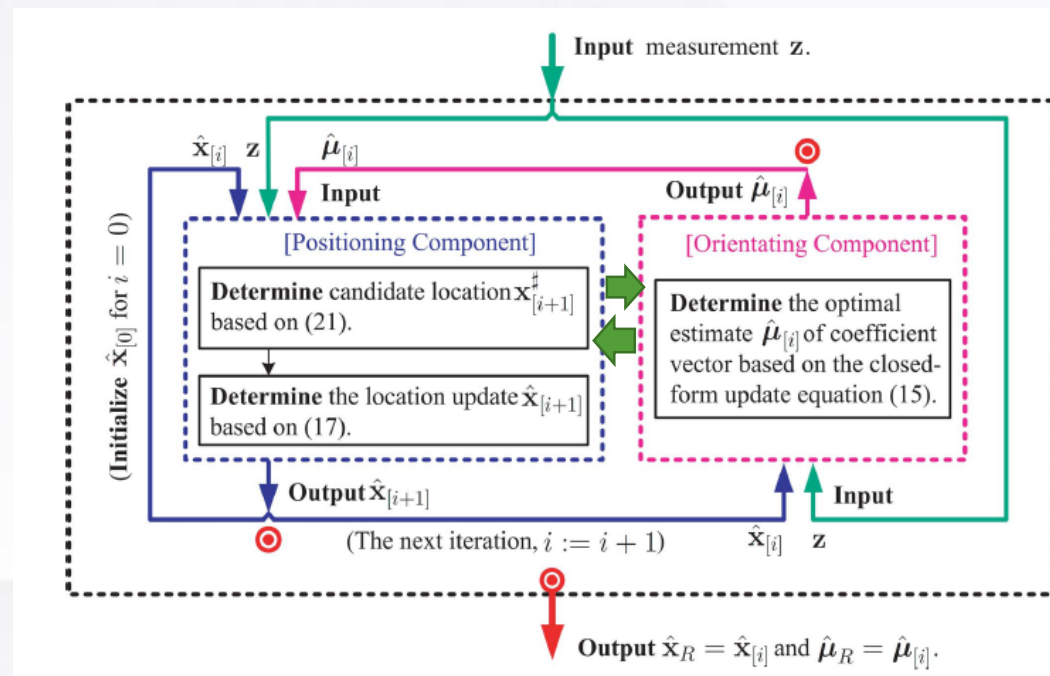
$$\begin{aligned} & \text{UE orientation update subproblem } \mathcal{P}_O : \hat{\boldsymbol{\mu}}_{[i]} = \arg \min_{\boldsymbol{\mu}_R} \|\mathbf{z} - \mathbf{G}(\hat{\mathbf{x}}_{[i]})\boldsymbol{\mu}_R\|_2^2. \\ & \text{(iteration)} \quad \text{s.t. } \|\boldsymbol{\mu}_R\|_2^2 \leq 1. \quad (14) \\ & \text{UE position update subproblem } \mathcal{P}_P : \hat{\mathbf{x}}_{[i+1]} = \arg \min_{\mathbf{x}_R} \|\mathbf{z} - \mathbf{G}(\mathbf{x}_R)\hat{\boldsymbol{\mu}}_{[i]}\|_2^2 \end{aligned}$$



(2) Channel Est-Enhanced VLP

Solution :

- SCA-guided Iteration between localization and channel estimation



Algorithm 1 The SLLS-Based SPAO Algorithm

Input : The measurement vector \mathbf{z} .

1 Initialize $\hat{\mathbf{x}}_{[0]}$.

2 **While** not converge **do** (for $i = 1 : K$)

[Orientation Update: input $\{\hat{\mathbf{x}}_{[i]}, \mathbf{z}\}$ and output $\hat{\boldsymbol{\mu}}_{[i]}$]

3 - Determine $\hat{\boldsymbol{\mu}}_{[i]}$ as per (15).

[Position Update: input $\{\hat{\boldsymbol{\mu}}_{[i]}, \mathbf{z}\}$ and output $\hat{\mathbf{x}}_{[i]}$]

4 - Determine $\mathbf{x}_{[i]}^\#$ as per (21).

5 - Determine $\gamma_{[i]}$ as per (22).

6 - Determine $\hat{\mathbf{x}}_{[i]}$ as per (17).

7 **End**

8 Determine \hat{W}_T and $\hat{\mathbf{u}}_R$ as per (12) and (13), respectively.

Output: $\hat{\mathbf{x}}_R = \hat{\mathbf{x}}_i$, \hat{W}_T and $\hat{\mathbf{u}}_R$.



(2) Channel Est-Enhanced VLP

Simulation results

- Settings: 20 dB, 20 LEDs on the ceiling, 9*9*4 space
- Using RSS measurements

- NLOS propagation scenario: $\zeta_{\text{nlos},m} = \frac{\varphi_{\text{nlos}}}{1 - \varphi_{\text{nlos}}} h_m(\mathbf{x}_R, \mu_R), \varphi_{\text{nlos}} \in [0, 0.5)$

- Baselines

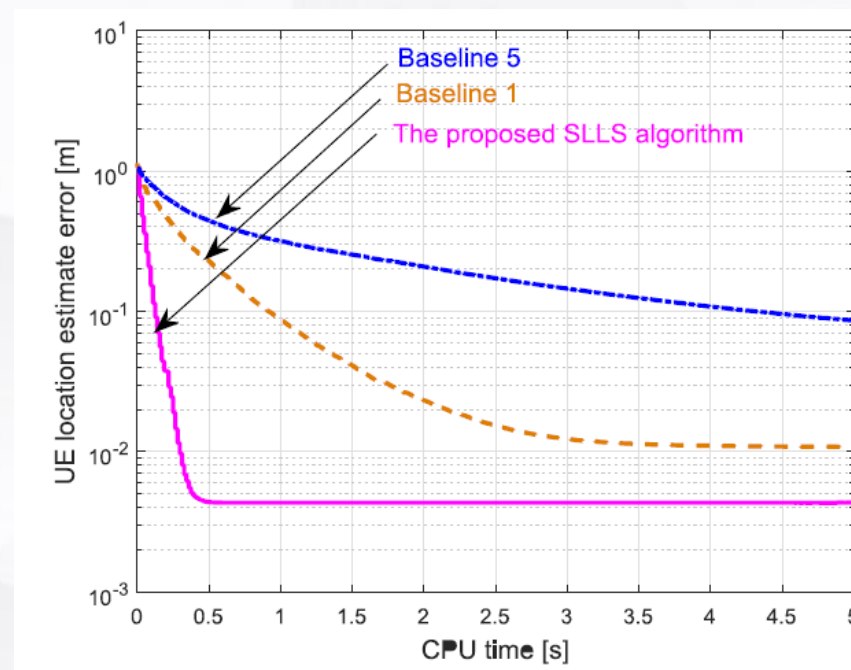
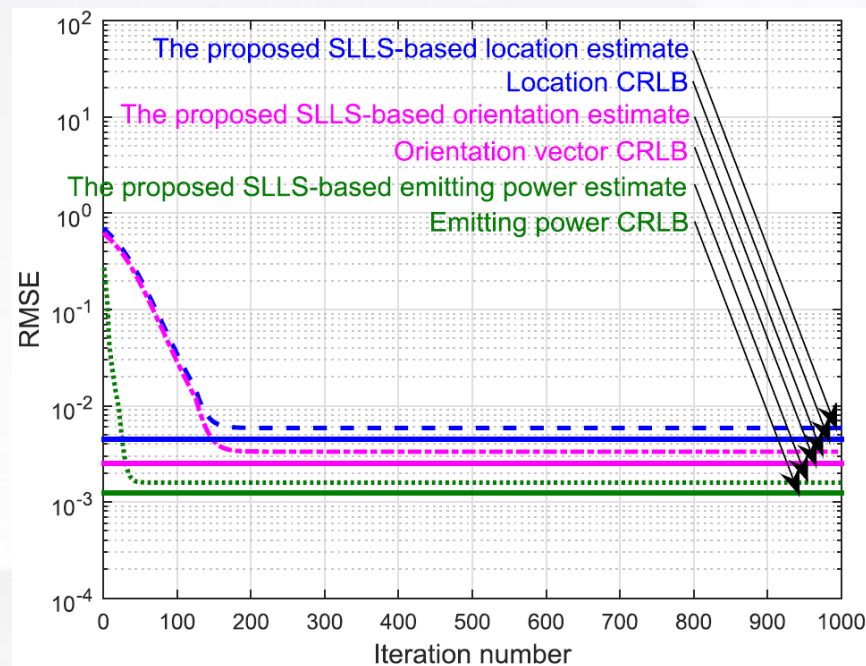
- *Baseline 1*: Gradient descent-based SPAO method [12].
- *Baseline 2*: Line search-based SPAO method [13].



(2) Channel Est-Enhanced VLP

Simulation results:

- Convergence, and CPU time

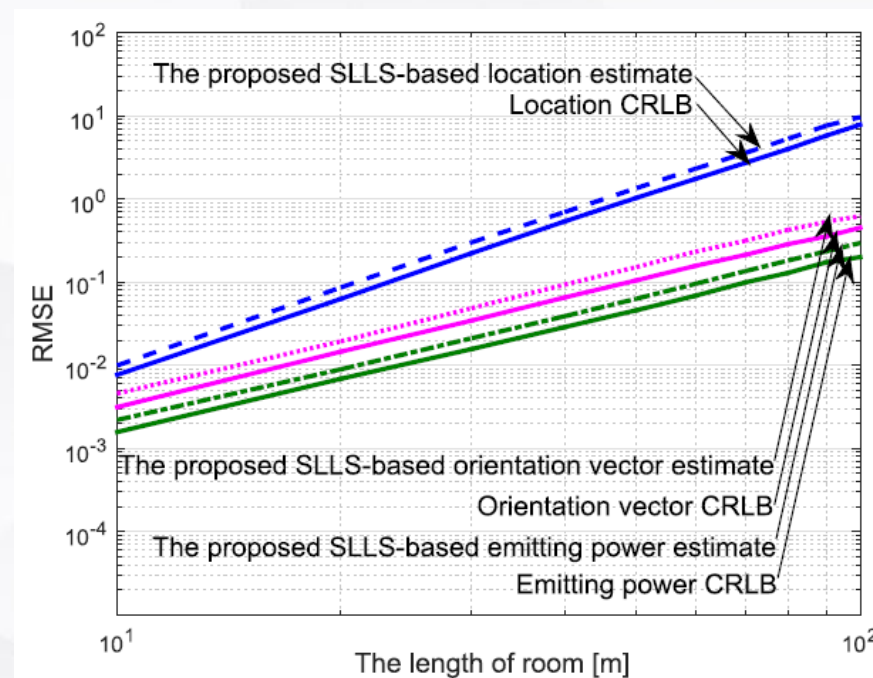
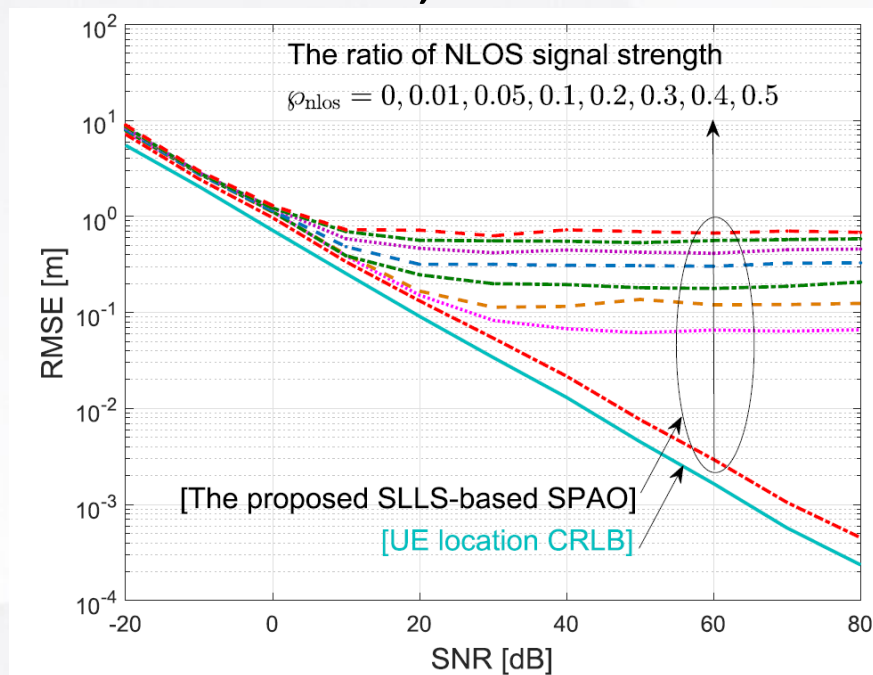




(2) Channel Est-Enhanced VLP

Simulation results:

- RMSE vs SNR, room size



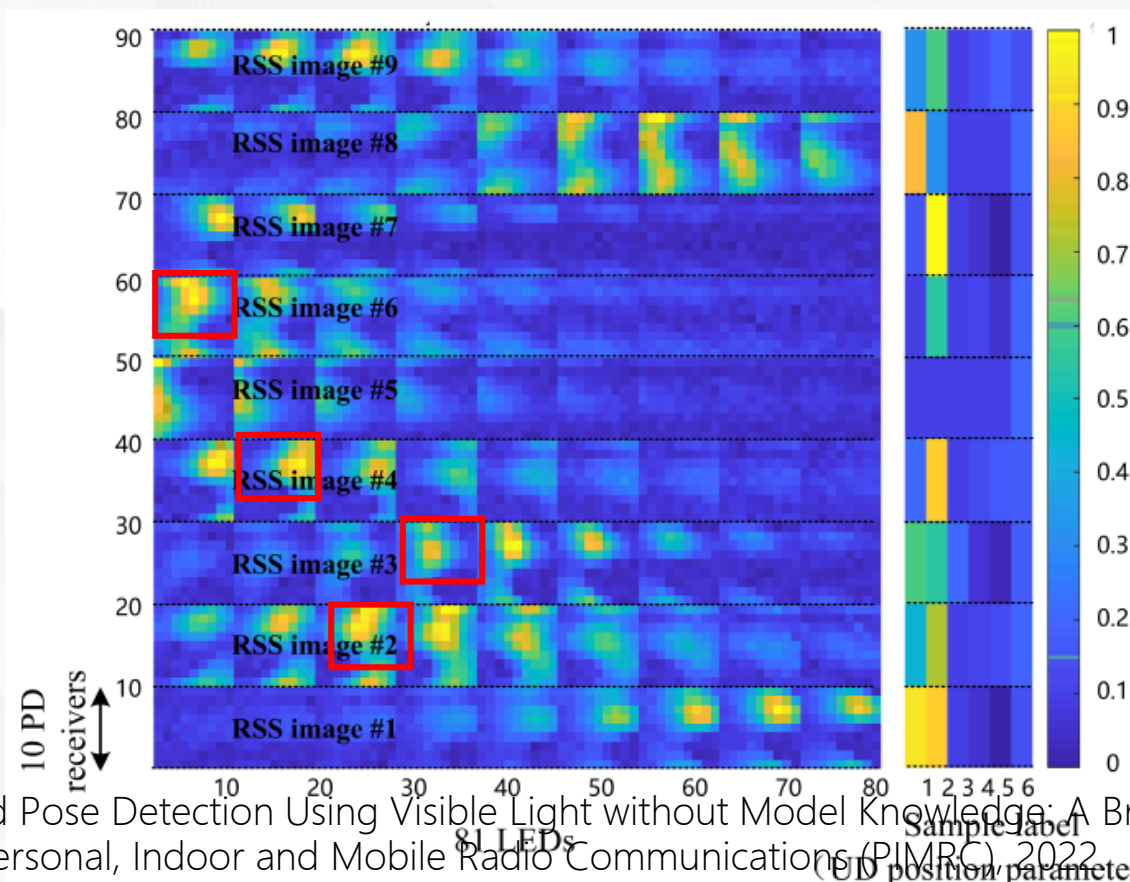


(3) Multi-branched ResNet



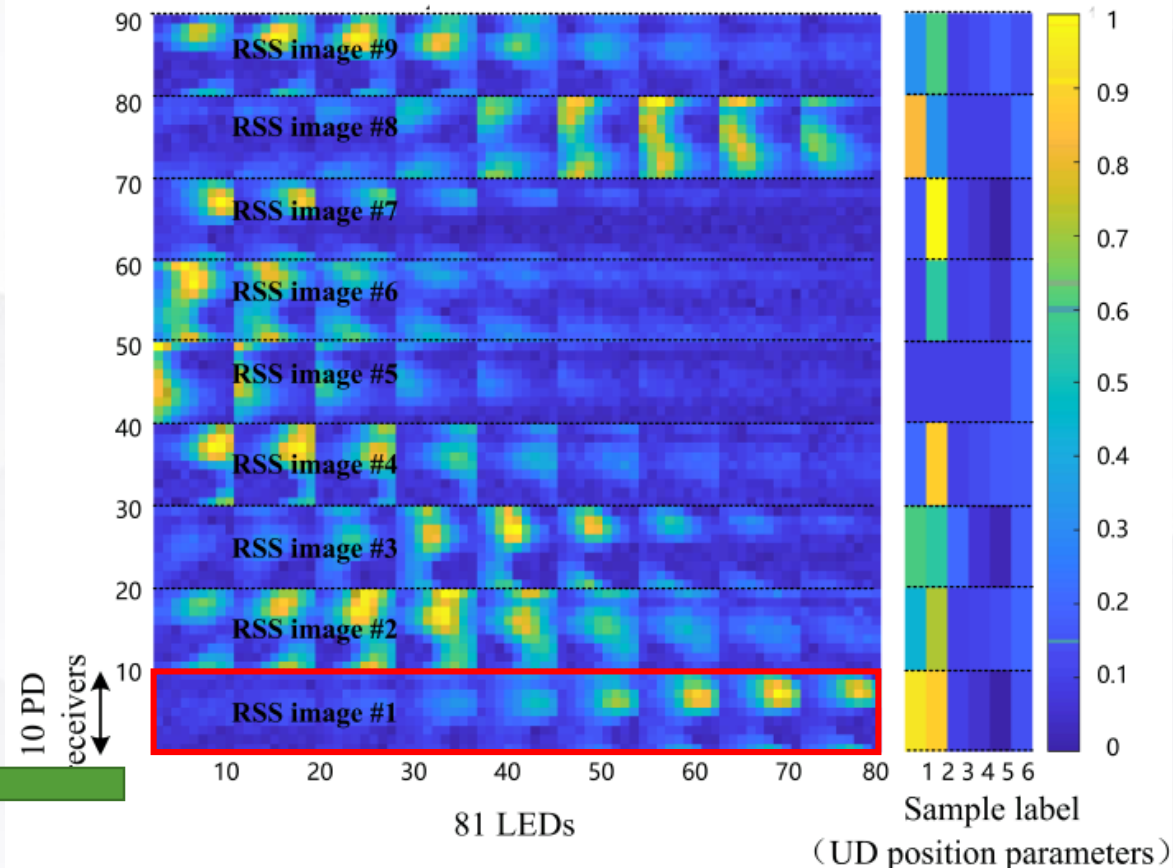
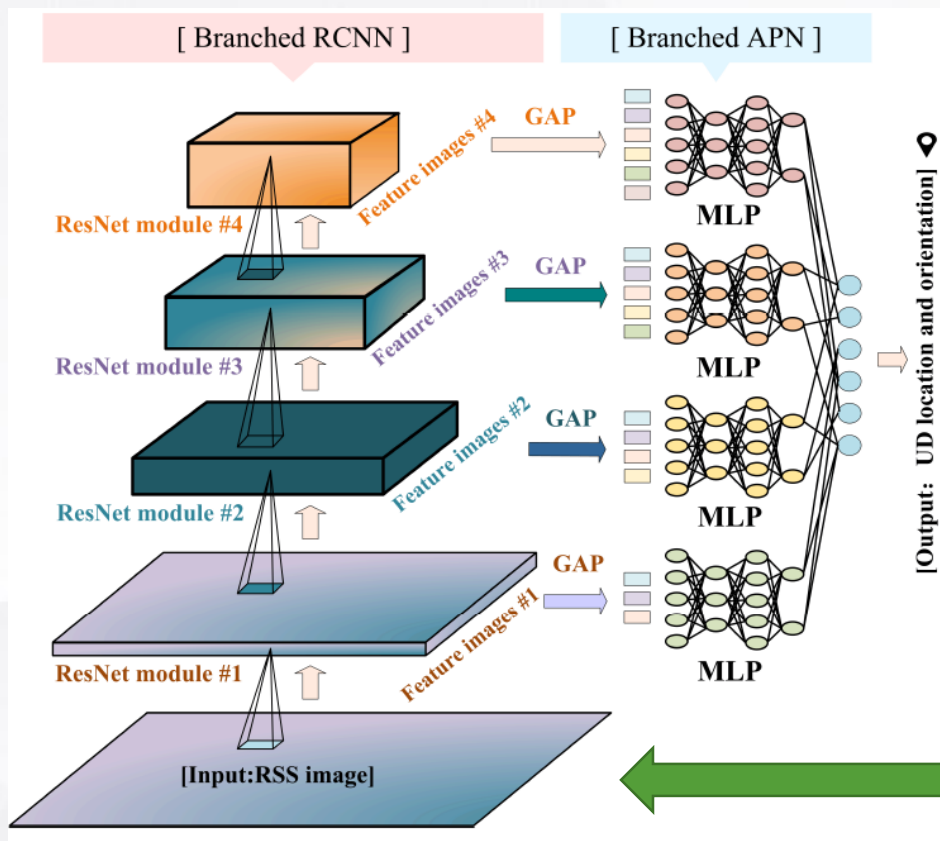
(3) Multi-branched ResNet

- **Intuition** : spatial-time texture/correlation structure in RSS sample image.
- 9 PDs and 81 LEDs
- Sample image
$$\mathbf{A} = \text{mat}[z_{m,n} | m = 1 : M, n = 1 : N]$$
- Texture structure fundamentally stems from the signal propagation and hence depends on UD location
- This texture structure can be used as **feature** to derive UD location



(3) Multi-branched ResNet

- Motivated by this intuition, we develop a **branch-structured RCNN** to extract texture features and learn its mapping to UD location parameters

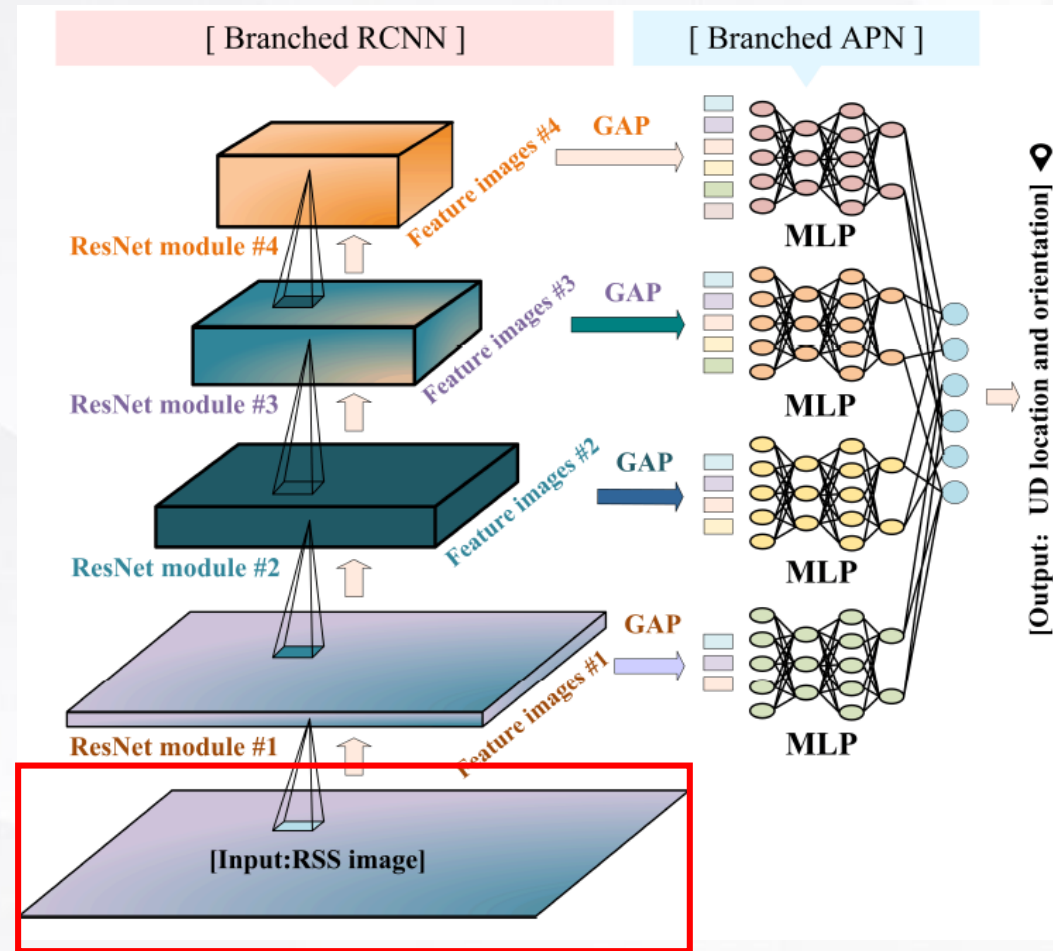




(3) Multi-branched ResNet

Architecture: branch-structured recurrent convolutional neural network, RCNN

- Input: 3D RSS sample images
- Branched residual network, ResNet
- Global average pooling, GAP
- Aggregative perception network, APN
- Output: UD location estimate

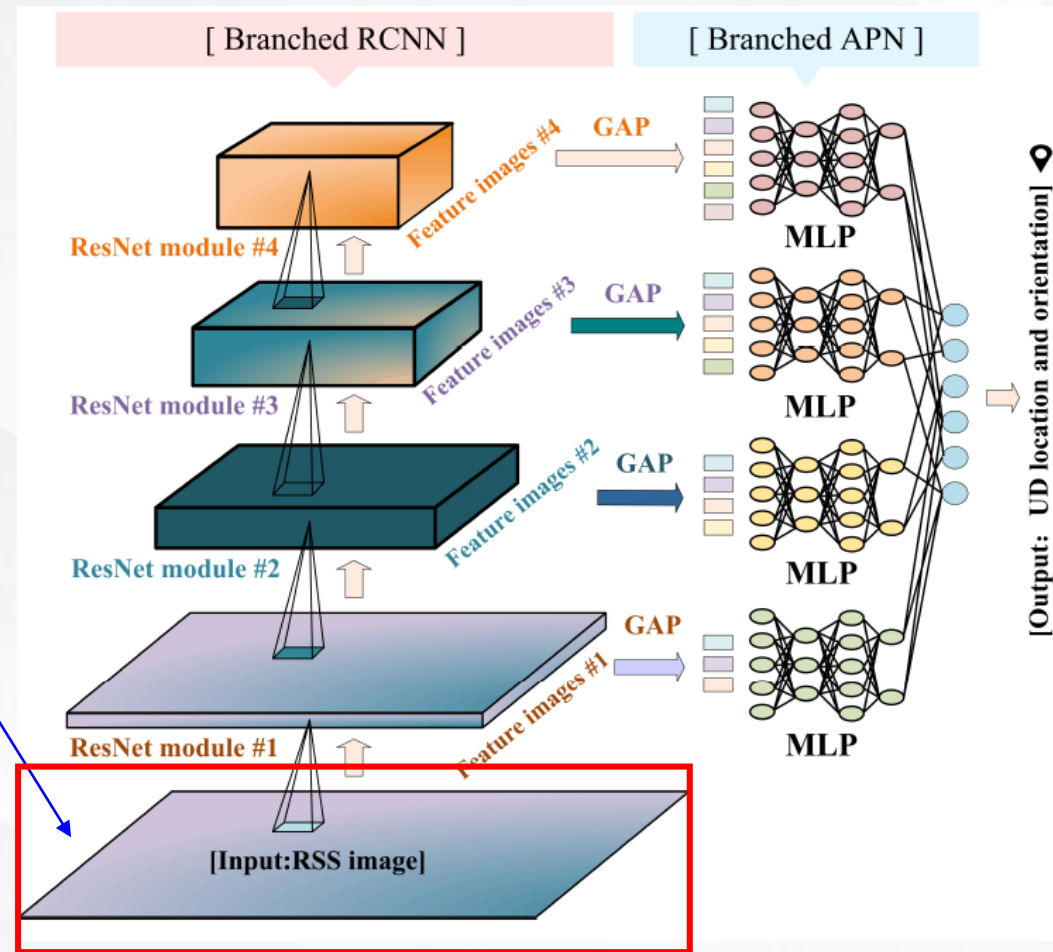
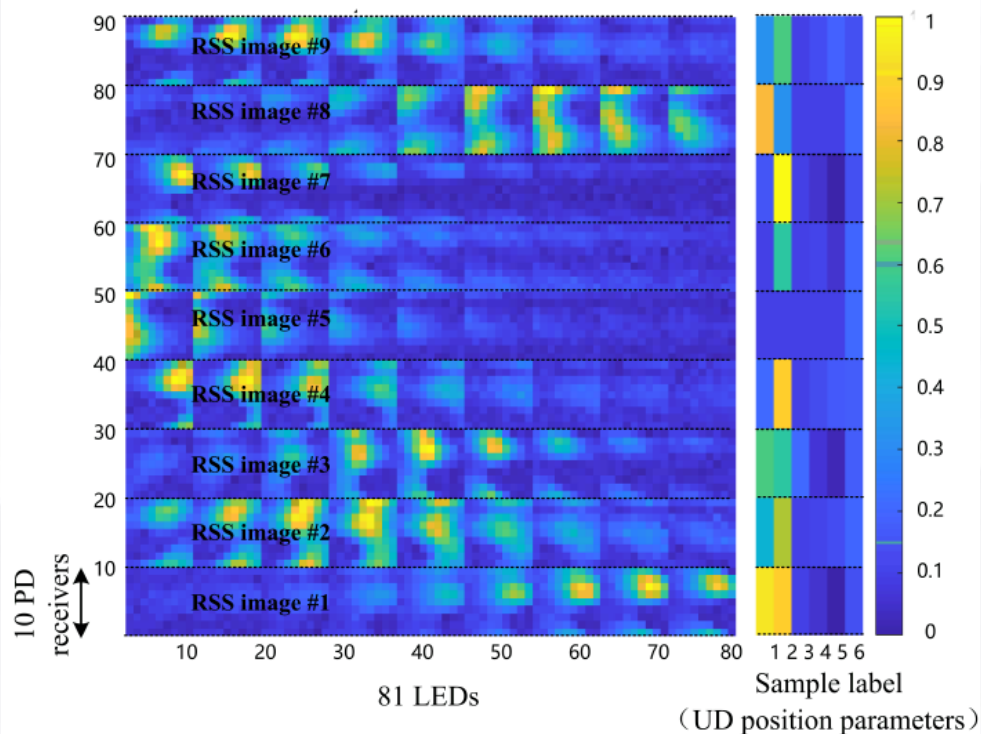


(3) Multi-branched ResNet

Architecture: branch-structured recurrent convolutional neural network, RCNN

- **Input: 3D RSS sample images**

$$\mathbf{A} = \text{mat}[z_{m,n} | m = 1 : M, n = 1 : N]$$





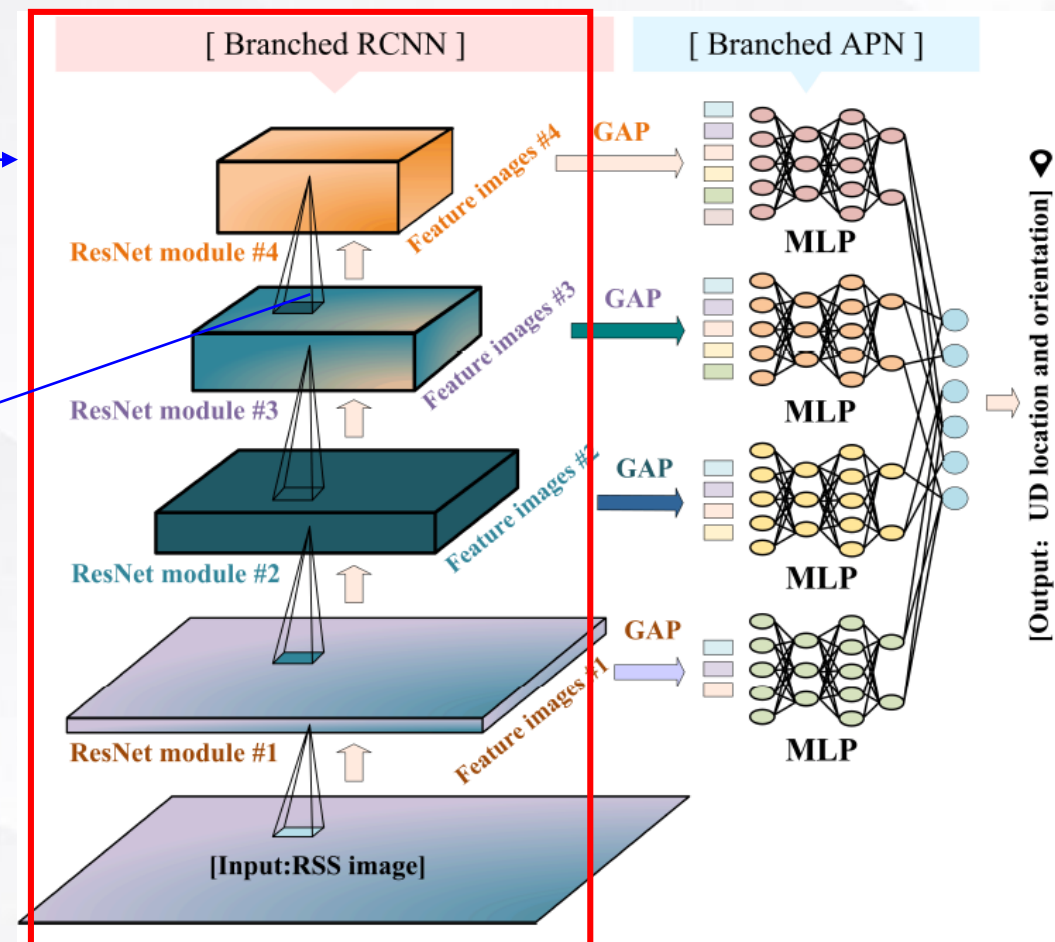
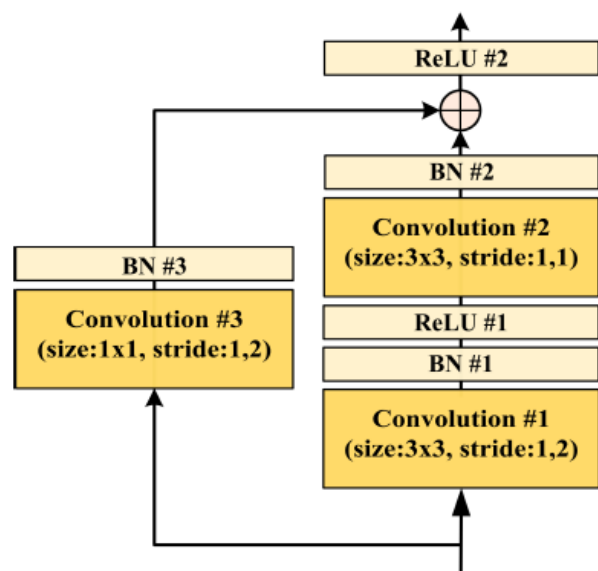
(3) Multi-branched ResNet

Architecture: branch-structured recurrent convolutional neural network, RCNN

- Input: 3D RSS sample images

- **Branched residual network, ResNet**

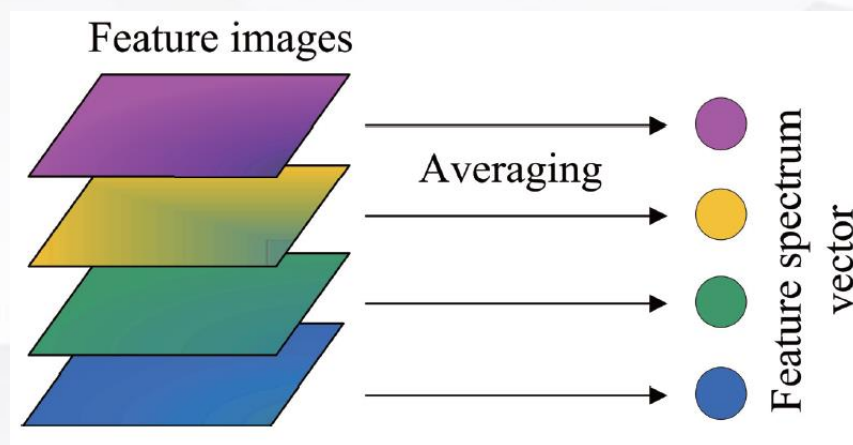
$$C_{\#}^{(\gamma)} = \varphi_{\text{RES}}(C_{\#}^{(\gamma-1)}; \mu^{(\gamma)}, \varsigma^{(\gamma)}, G^{(\gamma)}), \forall \gamma = 1 : \mathcal{J}_G,$$



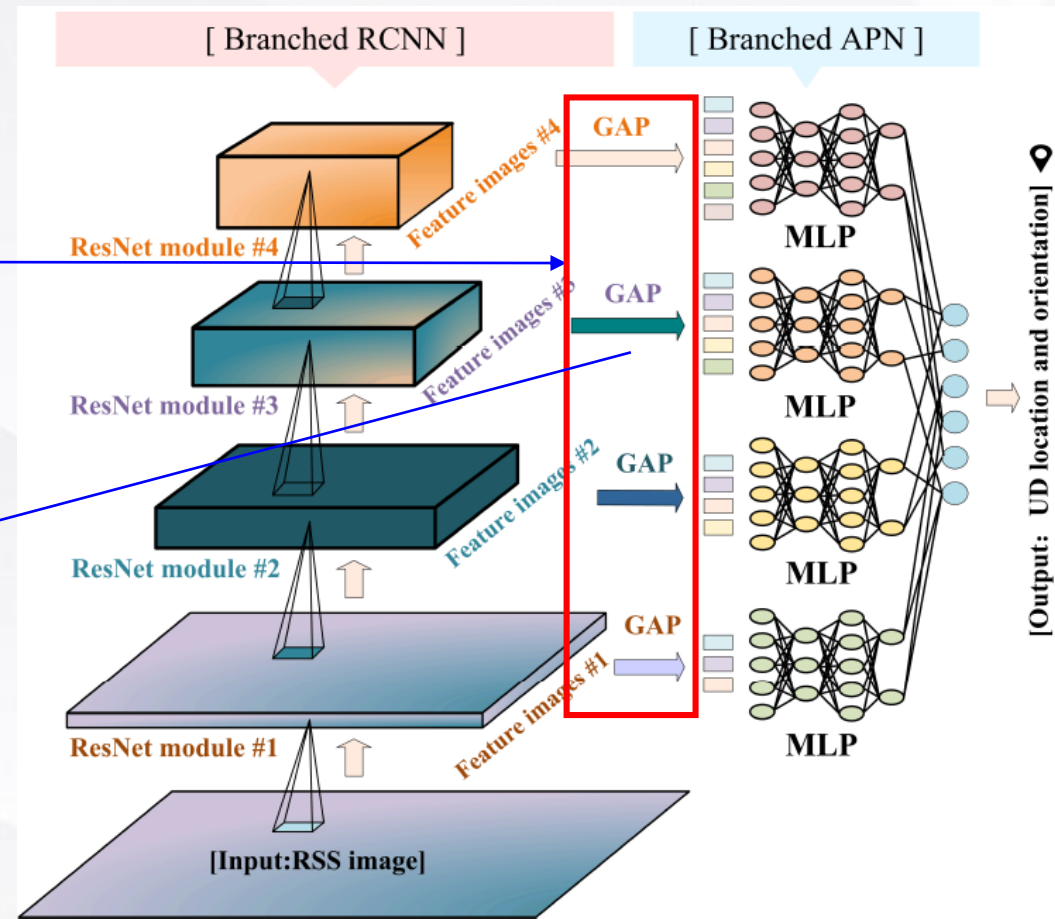
(3) Multi-branched ResNet

Architecture: branch-structured recurrent convolutional neural network, RCNN

- Input: 3D RSS sample images
- Branched residual network, ResNet
- Global average pooling, GAP



$$\chi^{(\gamma)} = \varphi_{\text{GAP}}(\mathbf{C}_{\#}^{(\gamma)}), \forall \gamma = 1 : \mathcal{J}_G$$



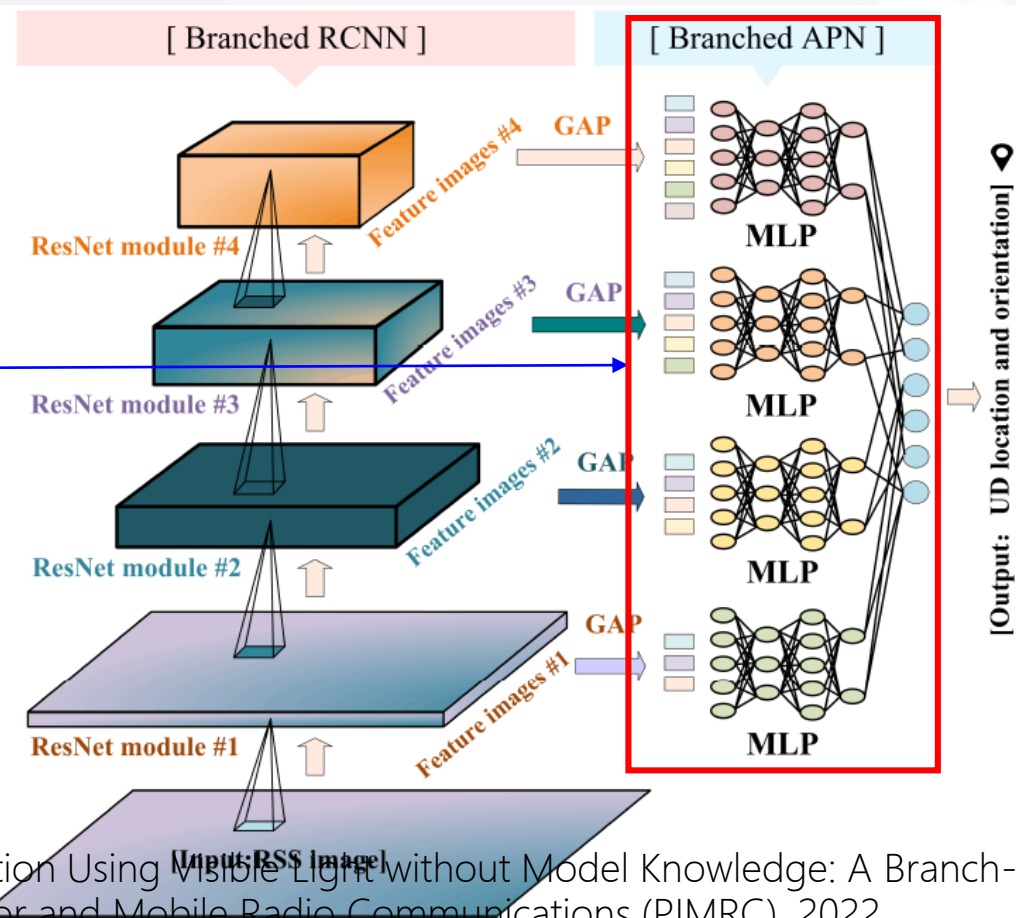


(3) Multi-branched ResNet

Architecture: branch-structured recurrent convolutional neural network, RCNN

- Input: 3D RSS sample images
- Branched residual network, ResNet
- Global average pooling, GAP
- **Aggregative perception network, APN**

$$\hat{\alpha}_R = \varphi_{\text{MLP}}(\chi; \mathbf{w})$$

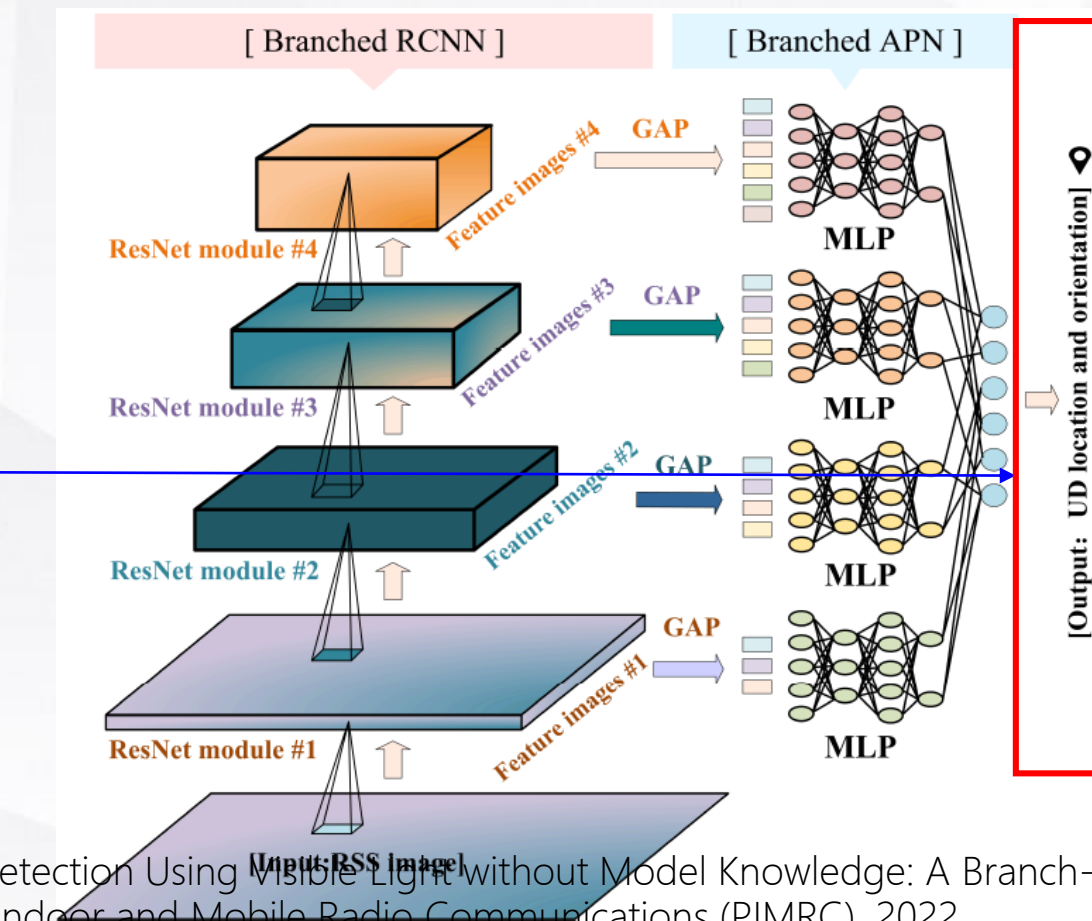




(3) Multi-branched ResNet

Architecture: branch-structured recurrent convolutional neural network, RCNN

- Input: 3D RSS sample images
- Branched residual network, ResNet
- Global average pooling, GAP
- Aggregative perception network, APN
- **Output: UD location estimation**





(3) Multi-branched ResNet

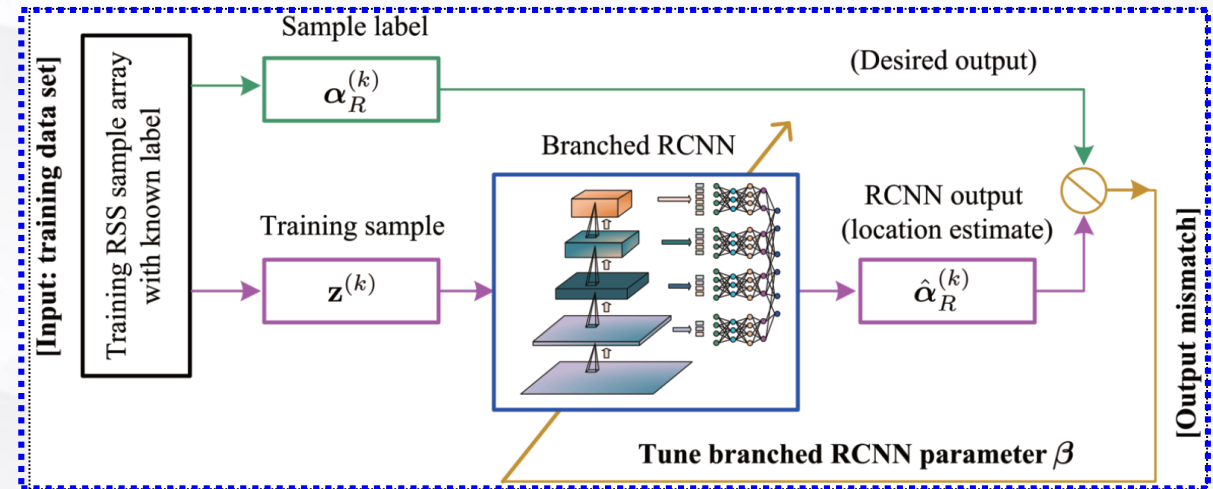
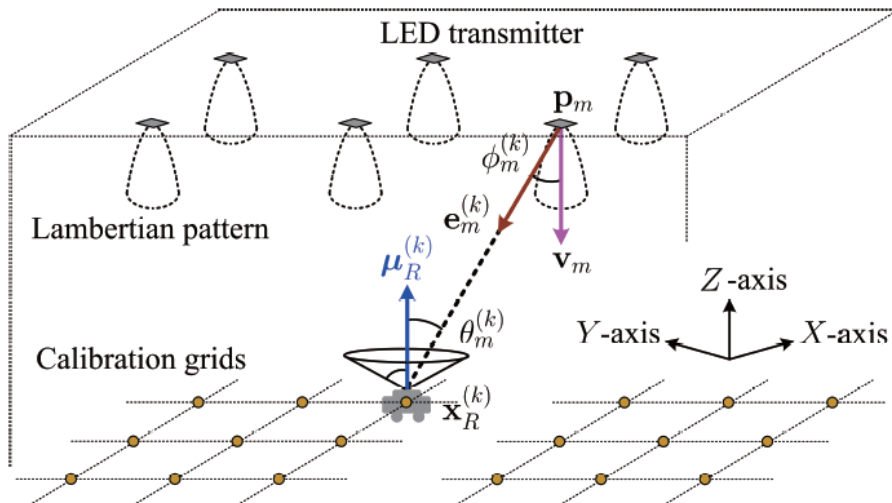
Architecture: branch-structured recurrent convolutional neural network, RCNN

- The proposed multi-branch RCNN will behave as parallel pipelines to capture environmental-invariant clustering structures from diverse-level sample texture features,
- thus rendering a reliable VLP solution over dynamic environments.

(3) Multi-branched ResNet

Procedures: First train and then test

- Training: derive the optimal network parameter with lowest mismatch
- Testing: determine UD location and pose for a given sample, using the well-trained branched RCNN.

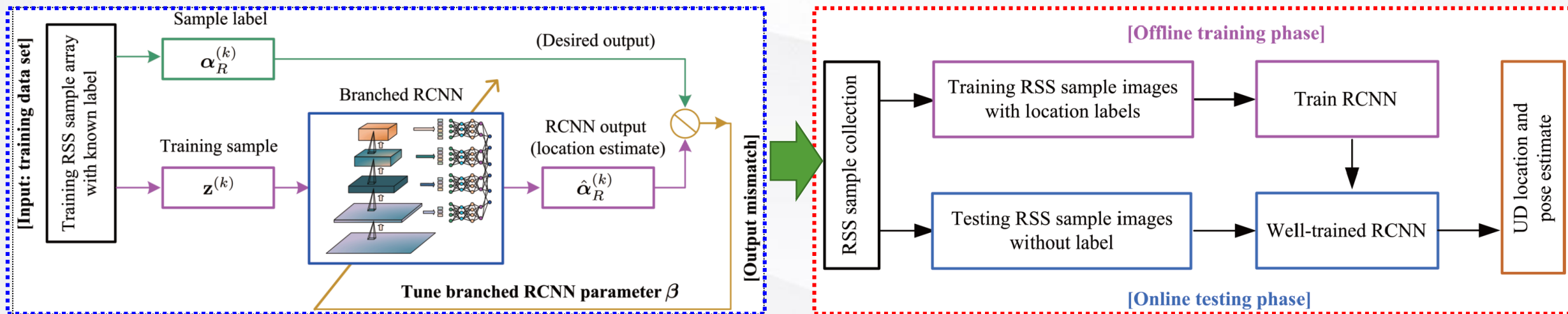




(3) Multi-branched ResNet

Procedures: First train and then test

- Training: derive the optimal network parameter with lowest mismatch
- Testing: determine UD location and pose for a given sample, using the well-trained branched RCNN.





(3) Multi-branched ResNet

Pseudo codes

Algorithm 1: Branched RCNN-based VLP method

Input : \mathbf{z} , $\{\mathbf{G}^{(\gamma)}, \boldsymbol{\mu}^{(\gamma)}, \boldsymbol{\varsigma}^{(\gamma)} | \forall \gamma = 1 : \mathcal{J}_G\}$ and \mathbf{w} .

- 1 Determine \mathbf{A} based on \mathbf{z} as per (5).
- 2 Set the input of the first ResNet to be $\mathbf{C}_{\#}^{(0)} = \mathbf{A}$.
- 3 **For** $\gamma = 1 : \mathcal{J}_G$
- 4 [ResNet]: $\mathbf{C}_{\#}^{(\gamma)} = \varphi_{\text{RES}}(\mathbf{C}_{\#}^{(\gamma-1)}; \boldsymbol{\mu}^{(\gamma)}, \boldsymbol{\varsigma}^{(\gamma)}, \mathbf{G}^{(\gamma)})$;
- 5 [GAP]: determine $\boldsymbol{\chi}^{(\gamma)} = \varphi_{\text{GAP}}(\mathbf{C}_{\#}^{(\gamma)})$, as per (19);
- 6 **End**
- 7 [Branched MLP]: $\hat{\alpha}_R = \varphi_{\text{MLP}}(\boldsymbol{\chi}; \mathbf{w})$, as per (20).

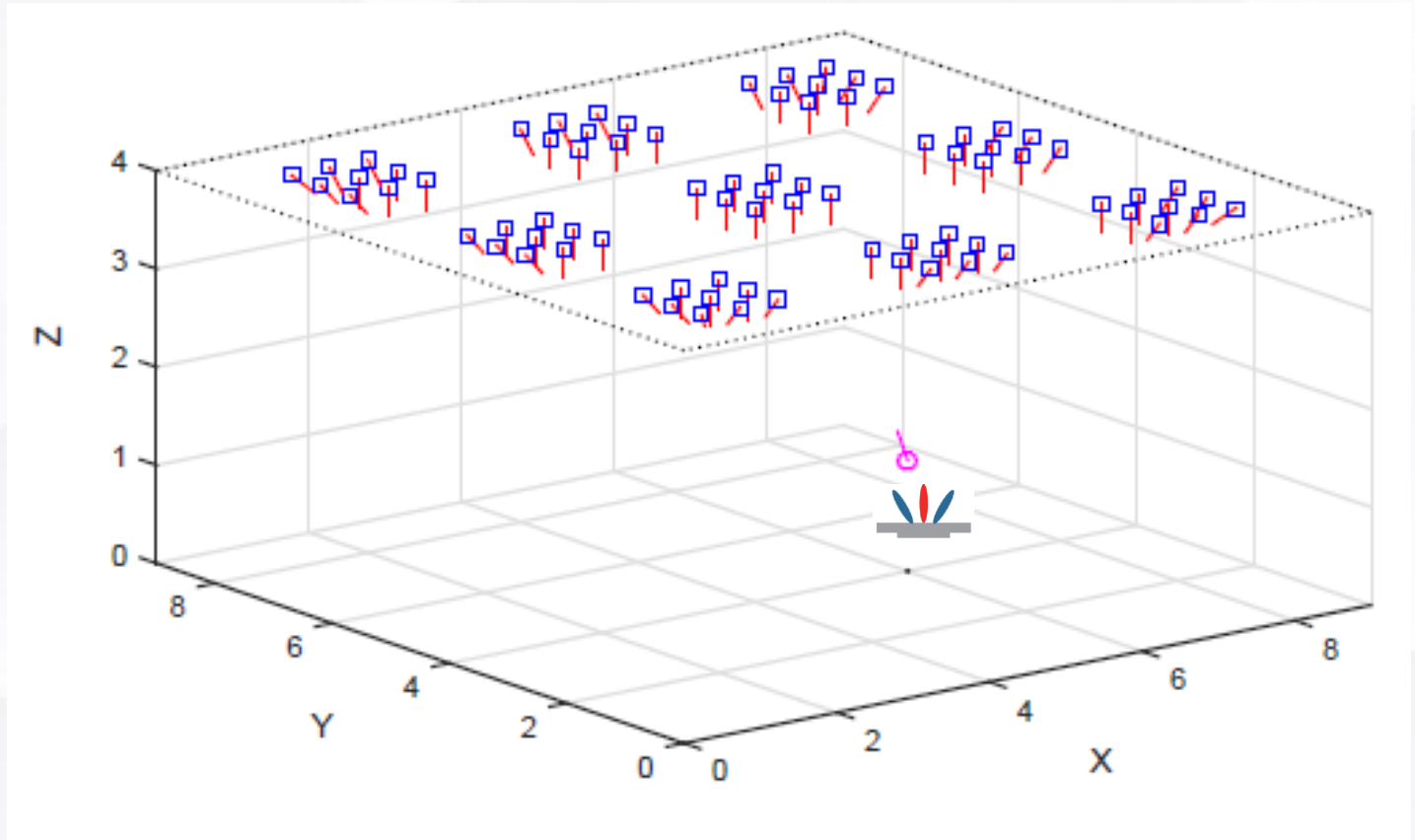
Output: UD location parameter estimate $\hat{\alpha}_R$.



(3) Multi-branched ResNet

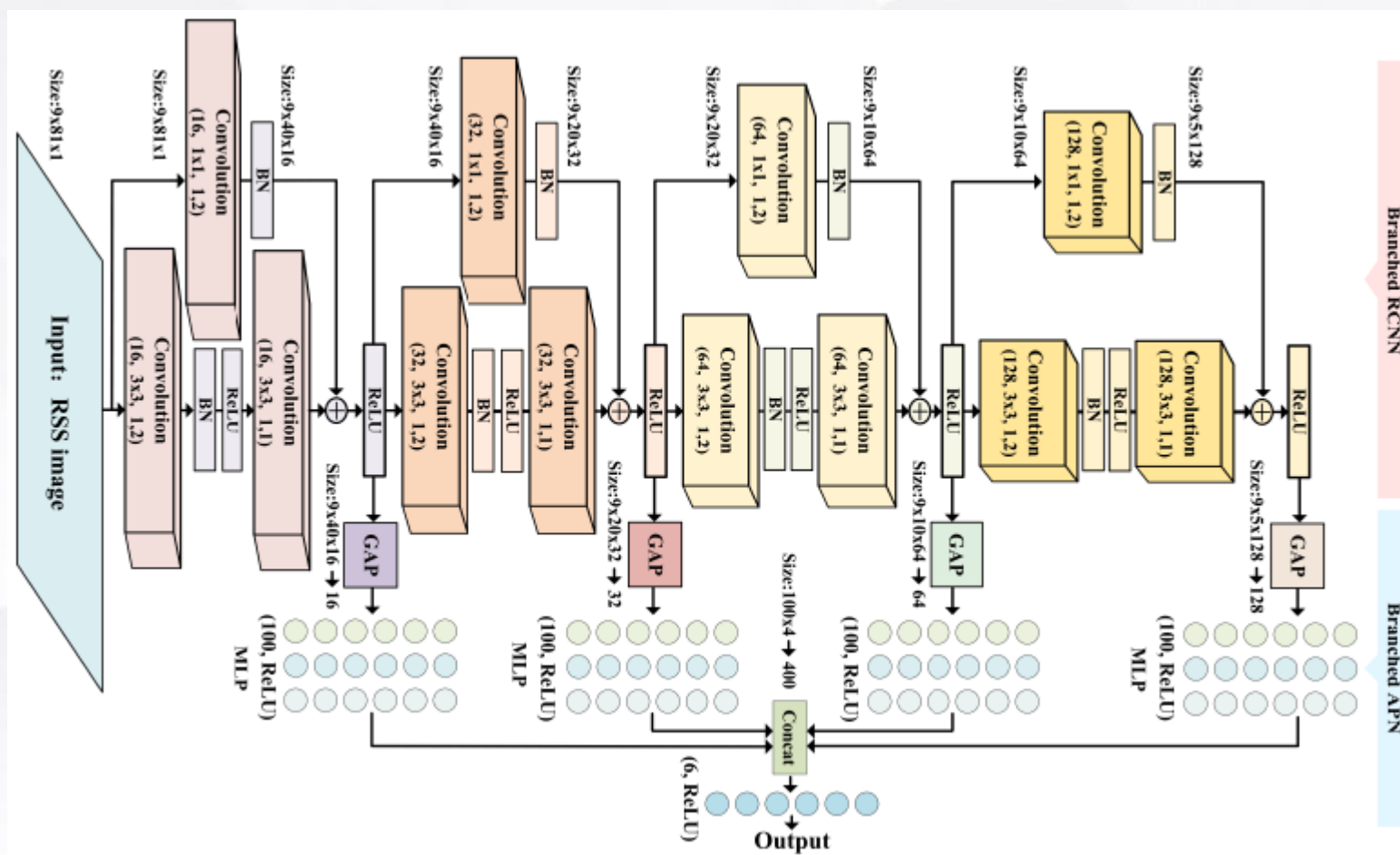
Setup:

- A room: $9\text{m} \times 9\text{m} \times 4\text{m}$
- SNR = 20 dB
- 81 LEDs
- 9 PDs
- RSS samples image



(3) Multi-branched ResNet

Branched RCNN configuration





(3) Multi-branched ResNet

Baselines:

- **Baseline 1:** GCNN-based VLP, which uses Gabor filters for feature extraction.
- **Baseline 2:** MLP-based VLP, adopting a five-layer fully-connected network.
- **Baseline 3:** CNN-based VLP, which models the UD localization as a classification problem.
- **Baseline 4:** Straightforward ResNet-based VLP, which has four residual convolution modules and five-layer fully connected network. Each convolution module has 10 kernels of dimension 3×3 , and the width of fully connected layers is 100.

(3) Multi-branched ResNet

Results: UD 6D localization performance versus SNR

- Our RCNN outperforms baselines due to our multi-branch RCNN design

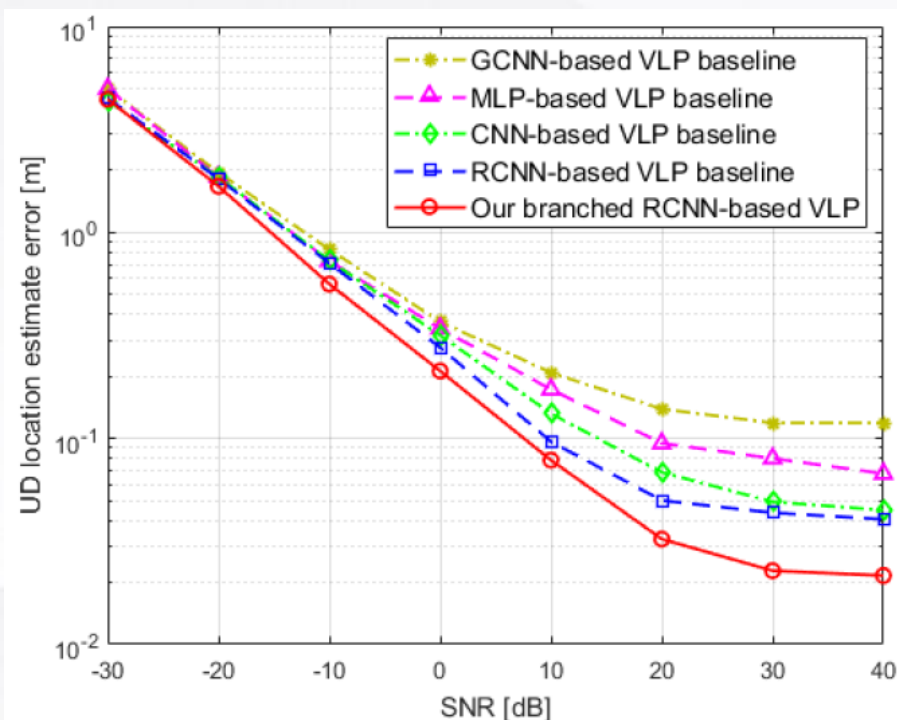


Fig. 6. UD location estimate error versus SNR.

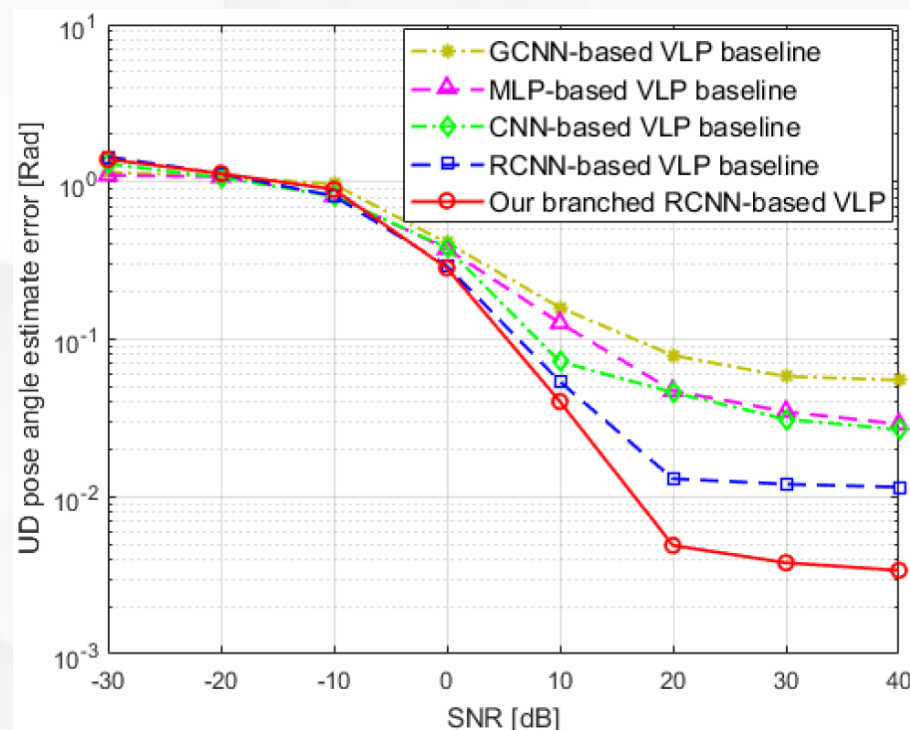


Fig. 7. UD pose angles estimate error versus SNR.

(3) Multi-branched ResNet

Results: VLP error over deployment range and RCNN size

- It is sensitive to deployment range: larger distance, larger VLP error
- Benefit from enlarged RCNN: larger RCNN size, lower VLP error

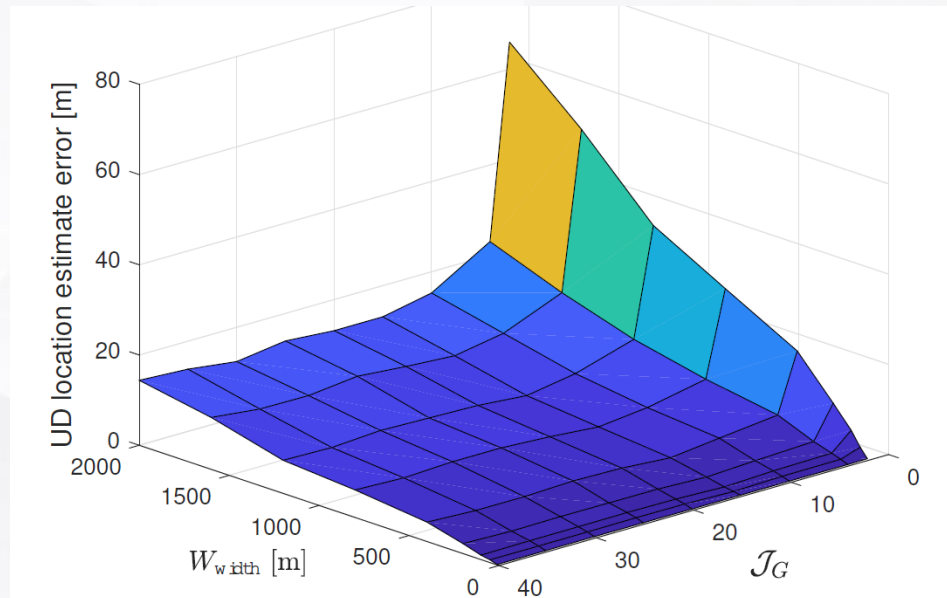


Figure 14. UD location estimate error versus localization area width W_{width} and RCNN size J_G .

(3) Multi-branched ResNet

Results: VLP error versus different degree of dynamics (system, environment)

- Serious dynamics, less discriminative feature, and hence large VLP error

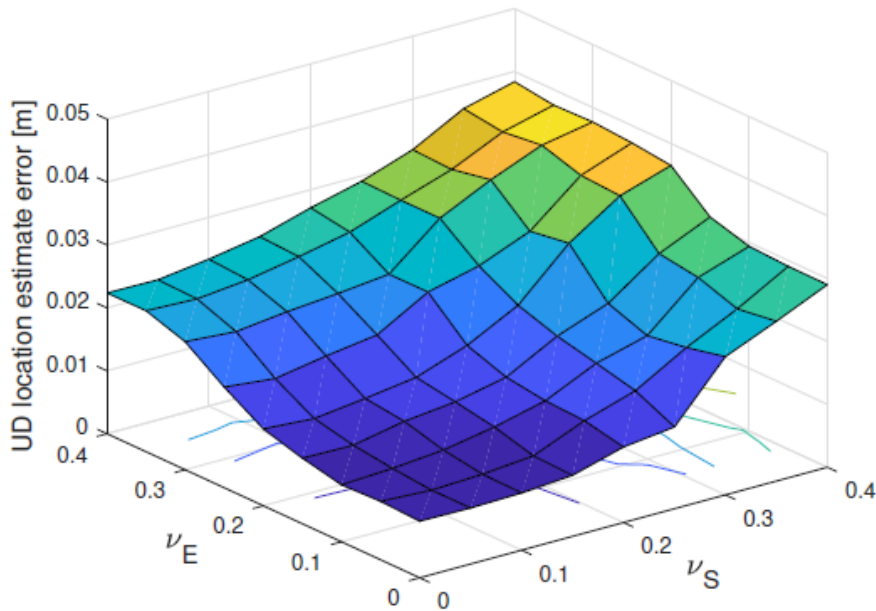


Figure 12. UD location estimation error under various variation degrees of system and environment.

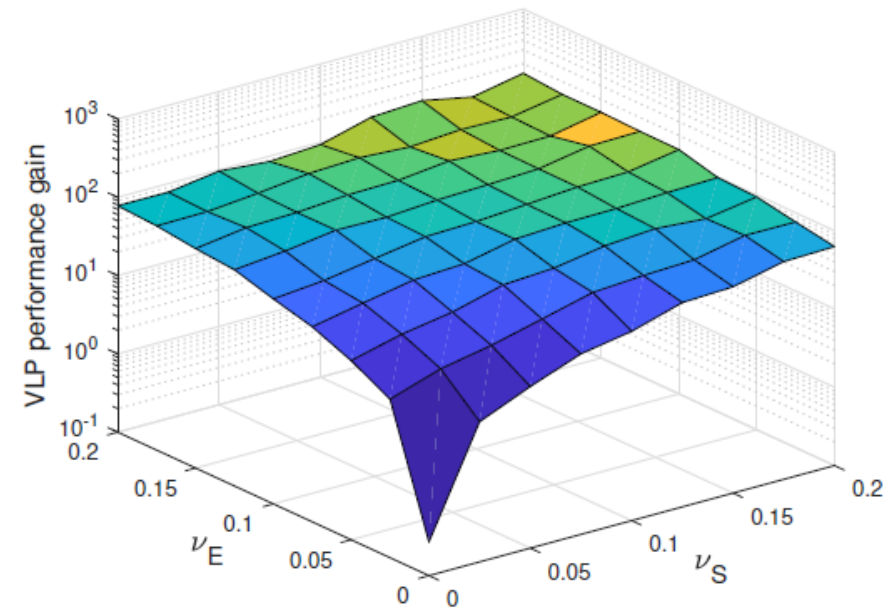


Figure 13. Performance gain of our VLP method over SPM-based VLP under different choices of ν_S and ν_E .

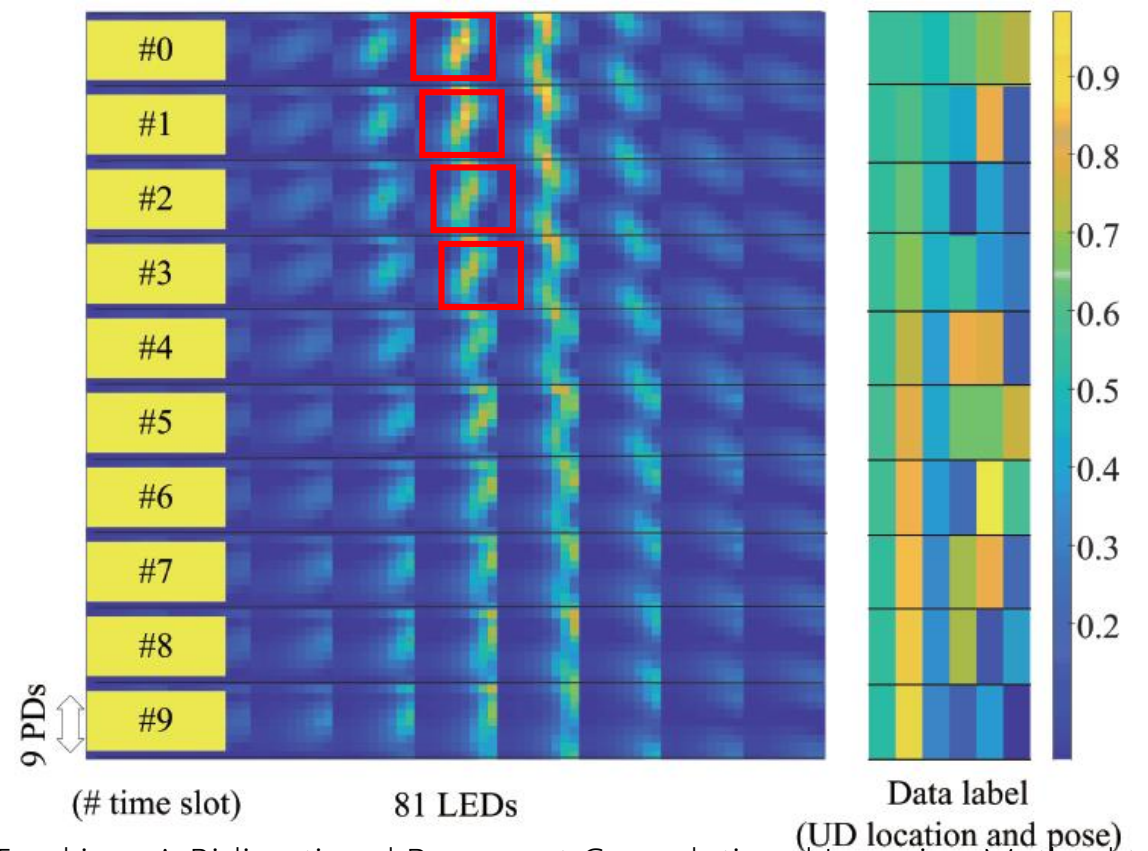


(4) Bidirectional RCNN

(4) Bidirectional RCNN

- Intuition : RSS sample image with spatial-time texture/correlation structure.
- 9 PDs and 81 LEDs
- Sample image

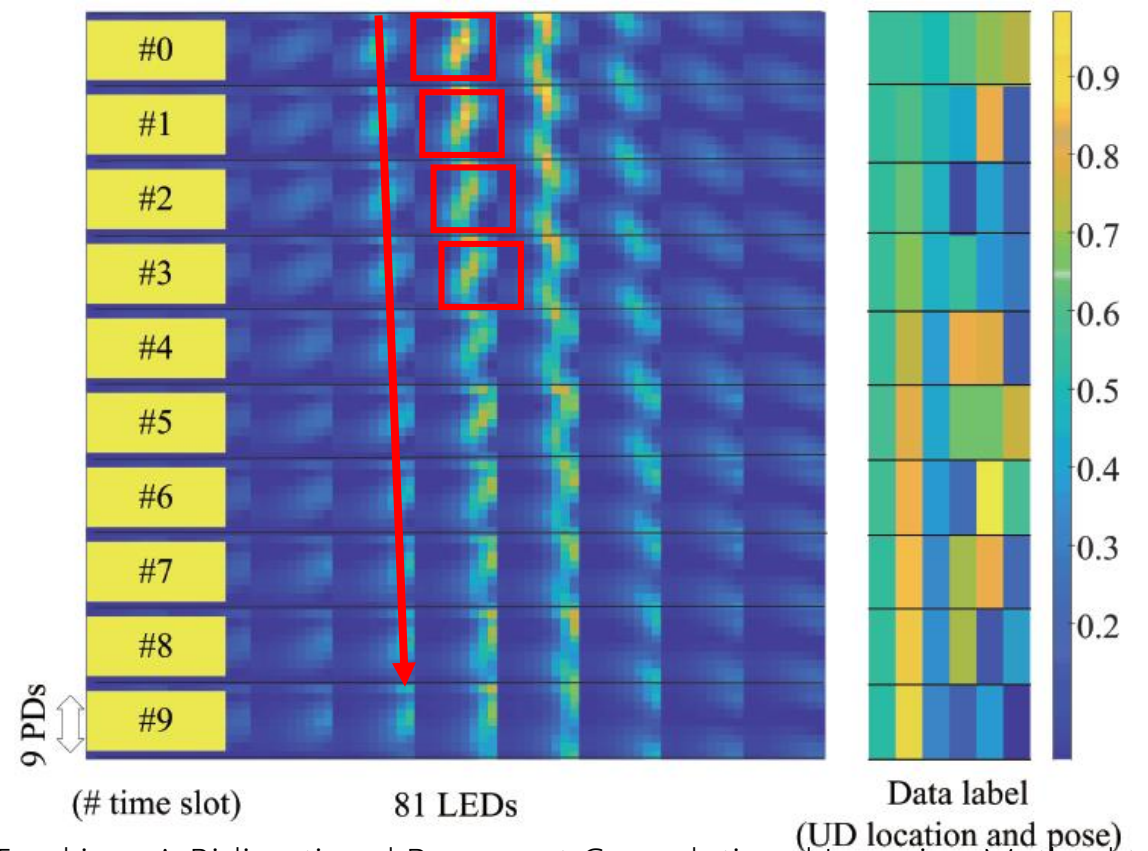
$$\mathbf{A} = \text{mat}[z_{m,n}^{(t)} | m = 1 : M, n = 1 : N]$$





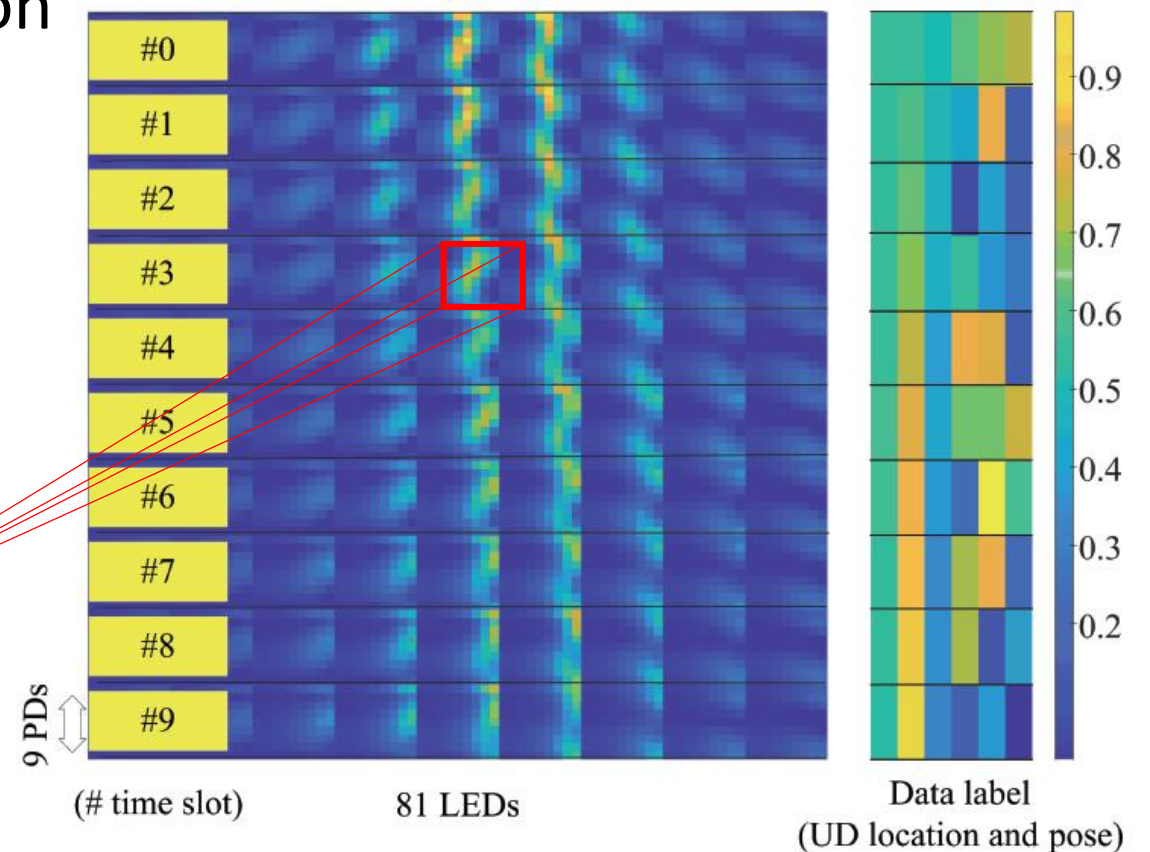
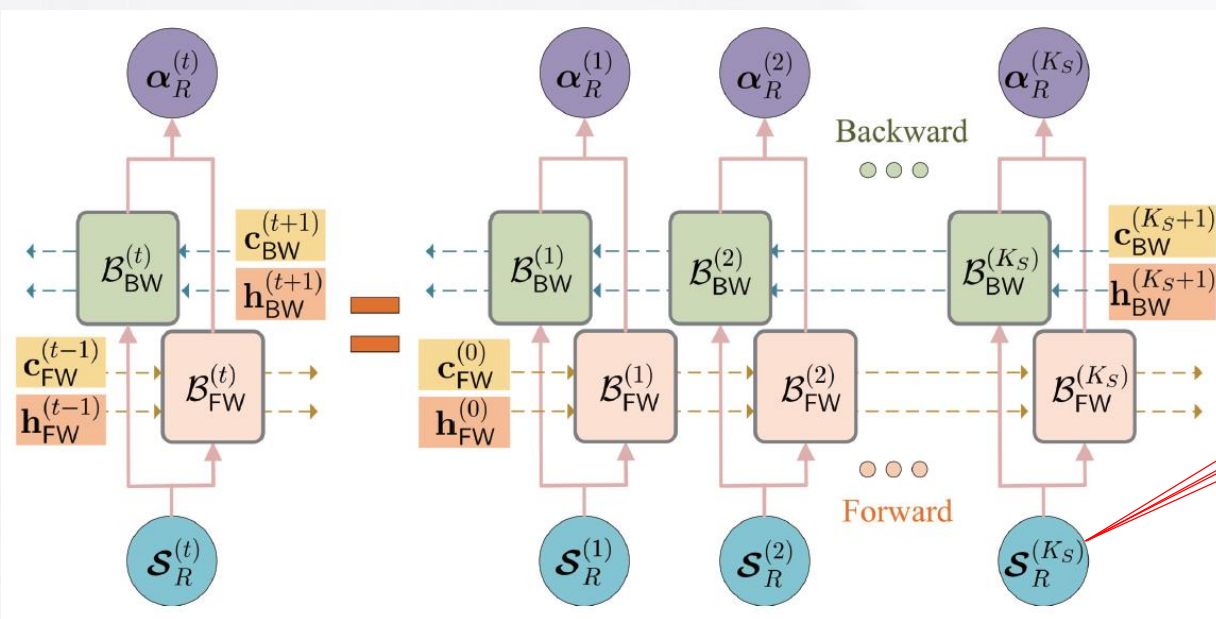
(4) Bidirectional RCNN

- Intuition : RSS sample image with **spatial-time texture/correlation structure**.
- 9 PDs and 81 LEDs
- Sample image
$$\mathbf{A} = \text{mat}[z_{m,n}^{(t)} | m = 1 : M, n = 1 : N]$$
- Texture structure fundamentally stems from the signal propagation and hence **depends on UD location**
- This texture structure can be used as **feature** to derive UD location



(4) Bidirectional RCNN

- Motivated by this intuition, we develop a BiRCNN to extract texture features and learn its mapping to UD location

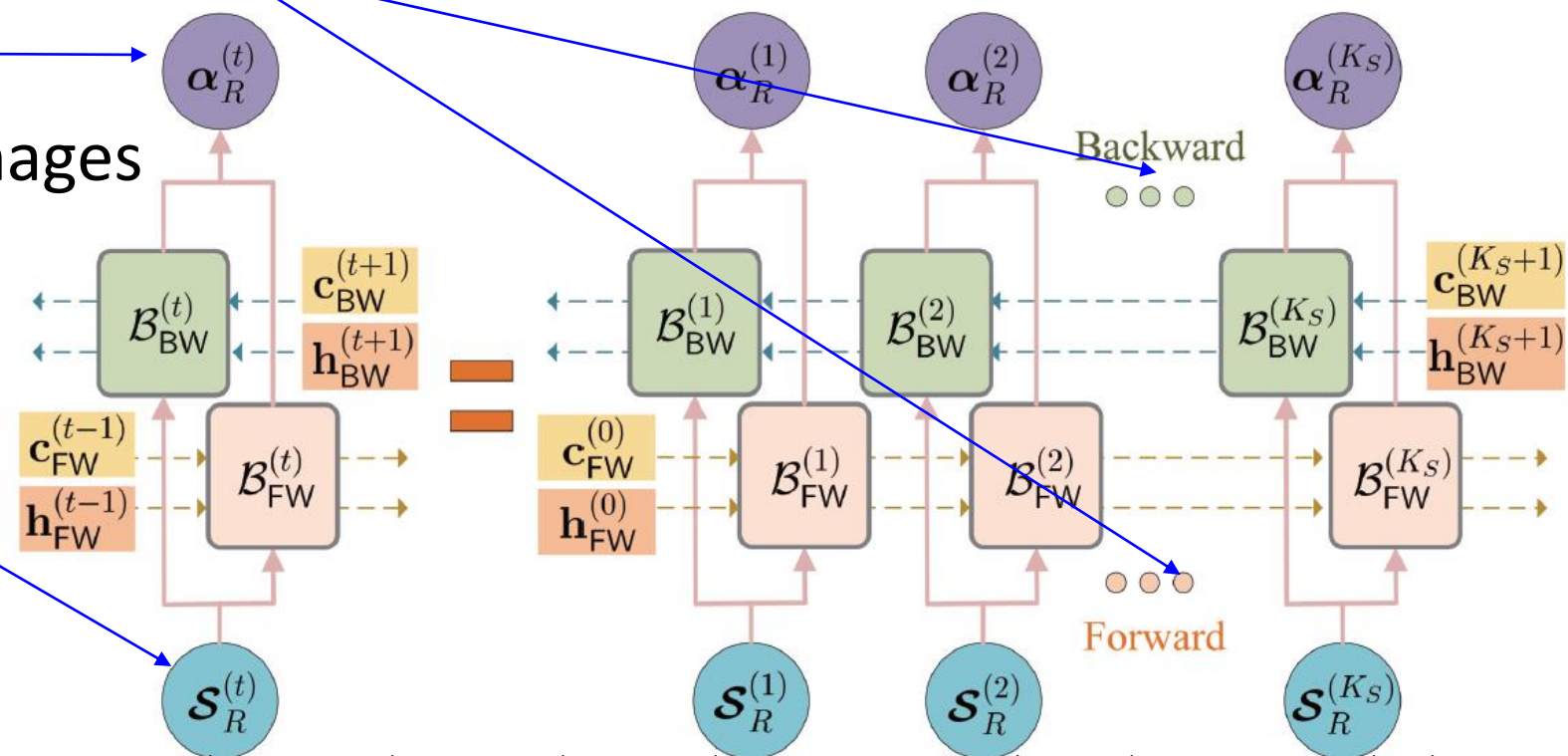




(4) Bidirectional RCNN

Architecture: Bi-directional recurrent convolutional neural network, BiRCNN

- Bi-directional recurrent flows
- Output: UD location
- Input: 3D RSS sample images

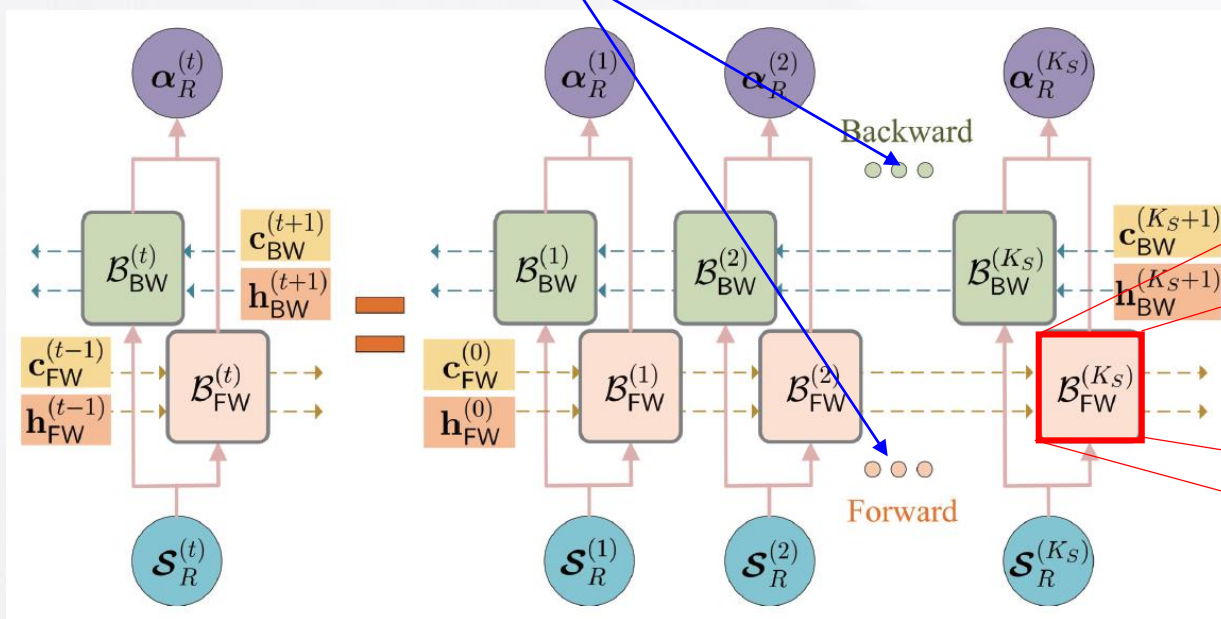




(4) Bidirectional RCNN

Architecture: Bi-directional recurrent convolutional neural network, BiRCNN

- Bi-directional recurrent information flow

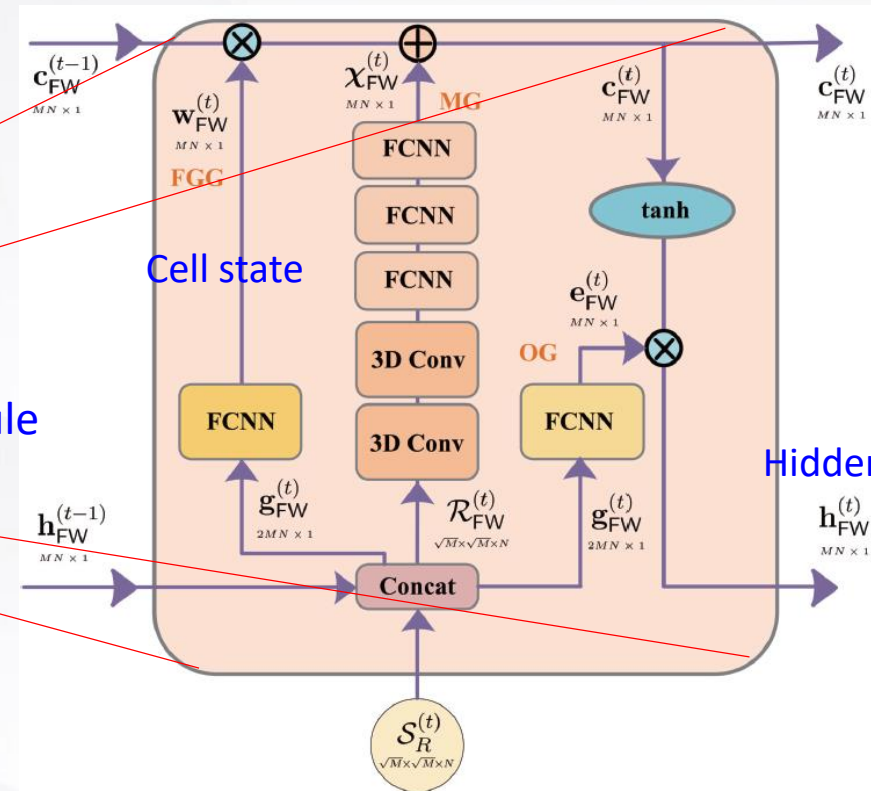


Cell state

Cell state

Forward module

Hidden state

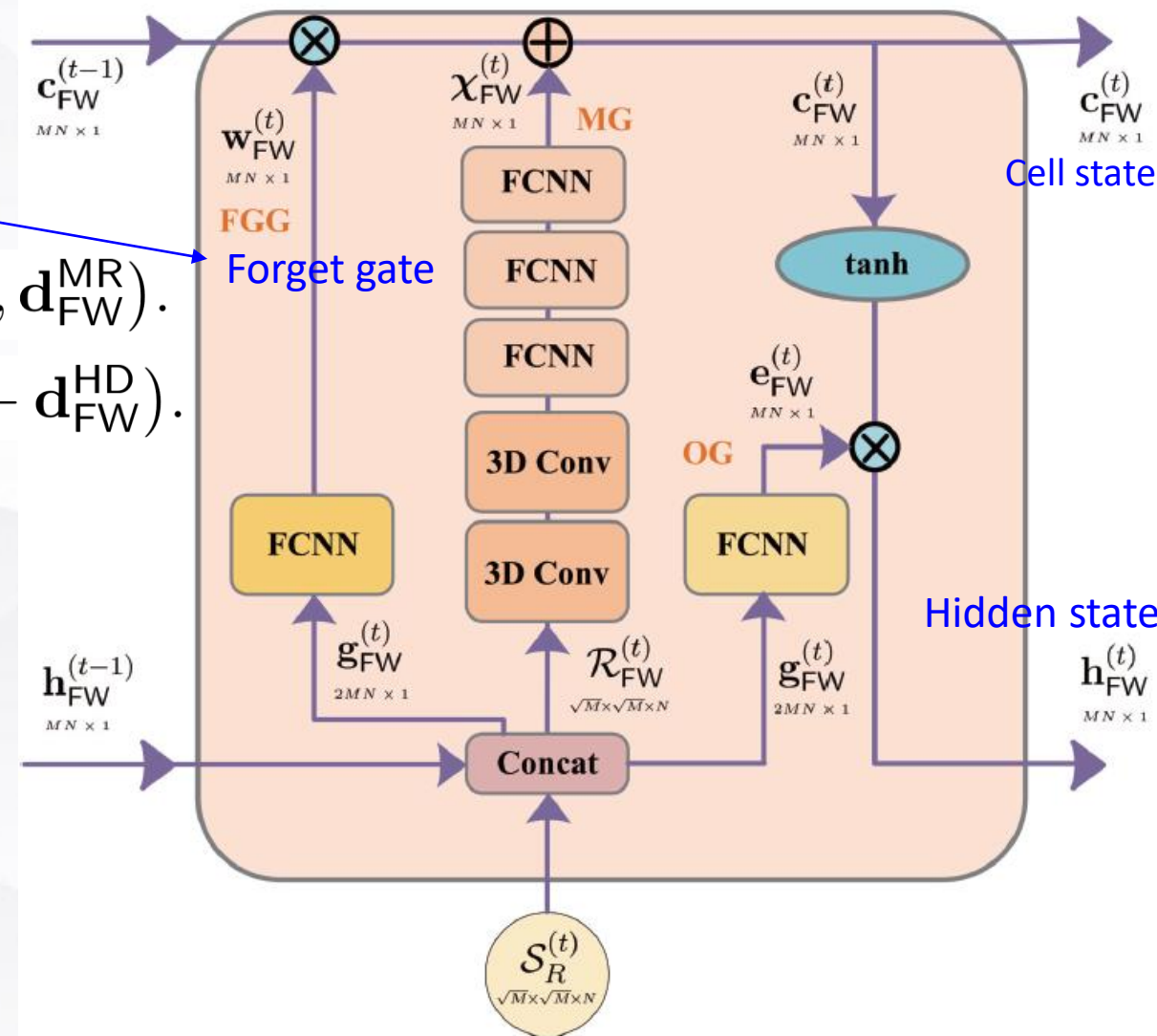




(4) Bidirectional RCNN

Forward module:

- Forget gate $g_{FW}^{(t)} = \text{vec}[\mathbf{h}_{FW}^{(t-1)}, \bar{\mathbf{z}}_R^{(t)}]$.
- Memory gate $\chi_{FW}^{(t)} = \kappa_{FW,FC}^{MR}(\mathbf{a}_{FW}^{(t)}; \omega_{FW}^{MR}, \mathbf{d}_{FW}^{MR})$.
- Output gate $e_{FW}^{(t)} = \text{sigmoid}(\mathcal{W}_{FW}^{HD} g_{FW}^{(t)} + \mathbf{d}_{FW}^{HD})$.
- Hidden state $\mathbf{h}_{FW}^{(t)} = \tanh(\mathbf{c}_{FW}^{(t)}) \odot \mathbf{e}_{FW}^{(t)}$
- Cell state $\mathbf{c}_{FW}^{(t)} = \mathbf{w}_{FW}^{(t)} \odot \mathbf{c}_{FW}^{(t-1)} + \chi_{FW}^{(t)}$,

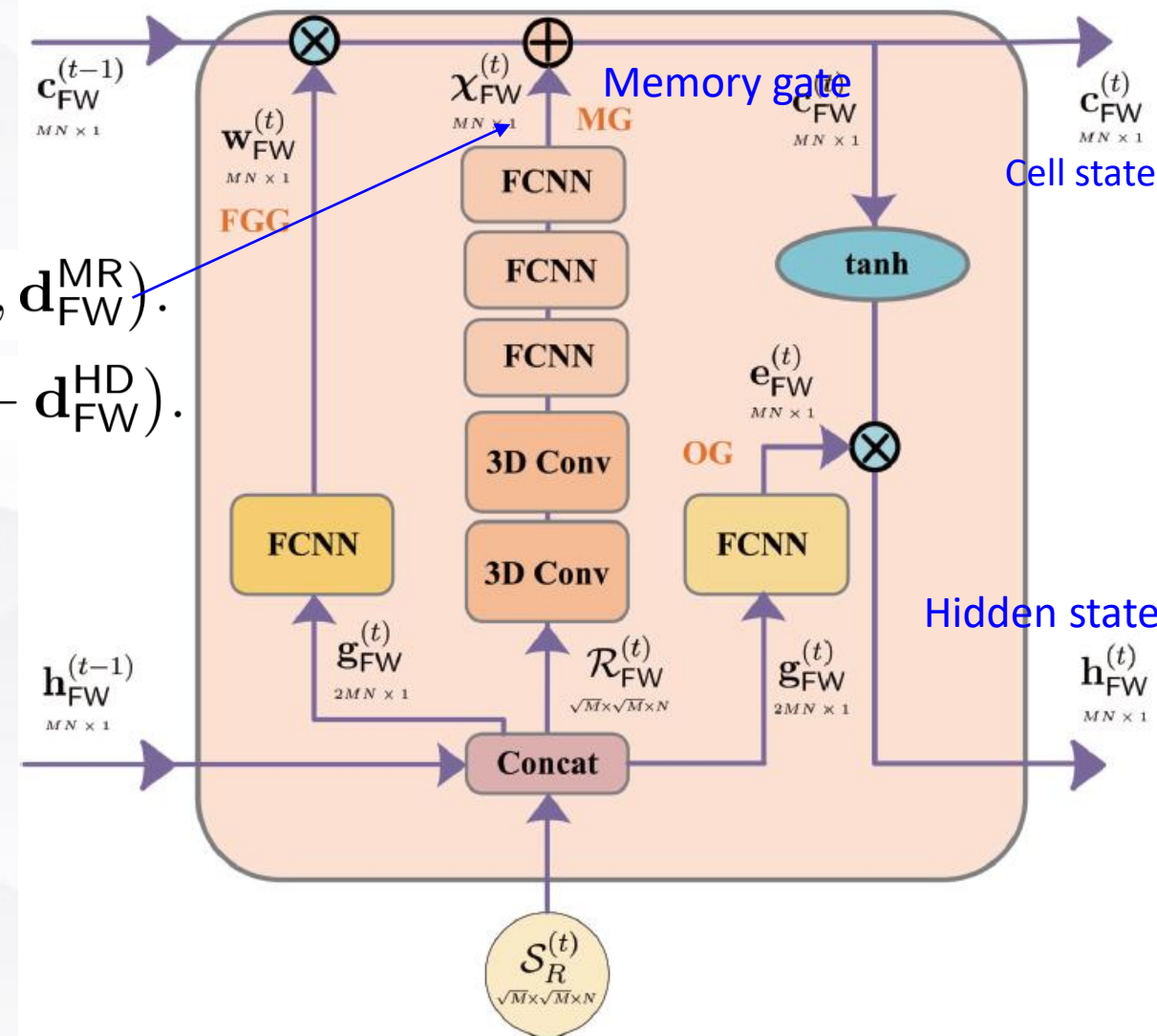




(4) Bidirectional RCNN

Forward module:

- Forget gate $g_{FW}^{(t)} = \text{vec}[\mathbf{h}_{FW}^{(t-1)}, \bar{\mathbf{z}}_R^{(t)}]$.
- Memory gate $\chi_{FW}^{(t)} = \kappa_{FW,FC}^{MR}(\mathbf{a}_{FW}^{(t)}; \omega_{FW}^{MR}, \mathbf{d}_{FW}^{MR})$.
- Output gate $e_{FW}^{(t)} = \text{sigmoid}(\mathcal{W}_{FW}^{HD} g_{FW}^{(t)} + \mathbf{d}_{FW}^{HD})$.
- Hidden state $\mathbf{h}_{FW}^{(t)} = \tanh(\mathbf{c}_{FW}^{(t)}) \odot \mathbf{e}_{FW}^{(t)}$
- Cell state $\mathbf{c}_{FW}^{(t)} = \mathbf{w}_{FW}^{(t)} \odot \mathbf{c}_{FW}^{(t-1)} + \chi_{FW}^{(t)}$,

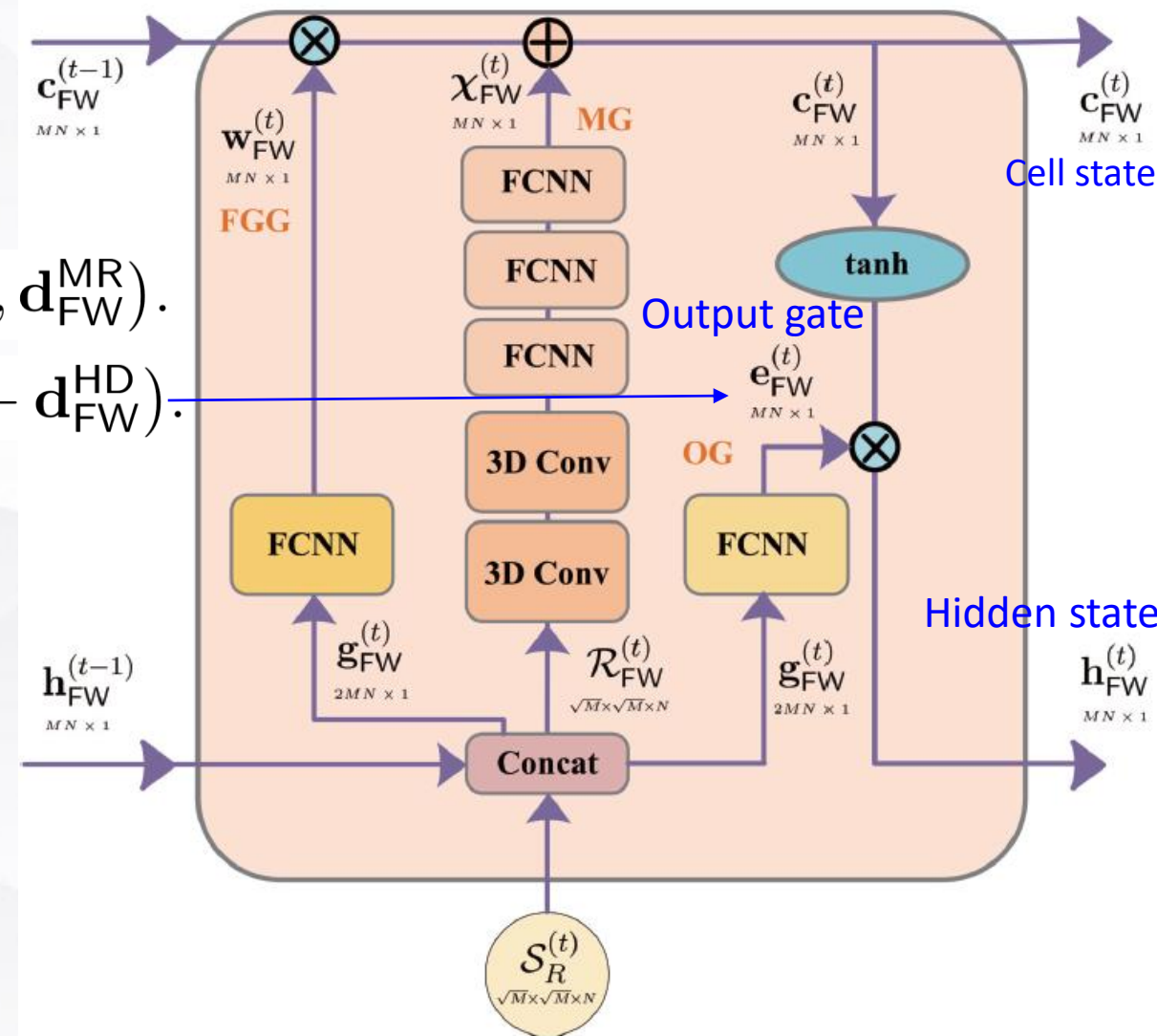




(4) Bidirectional RCNN

Forward module:

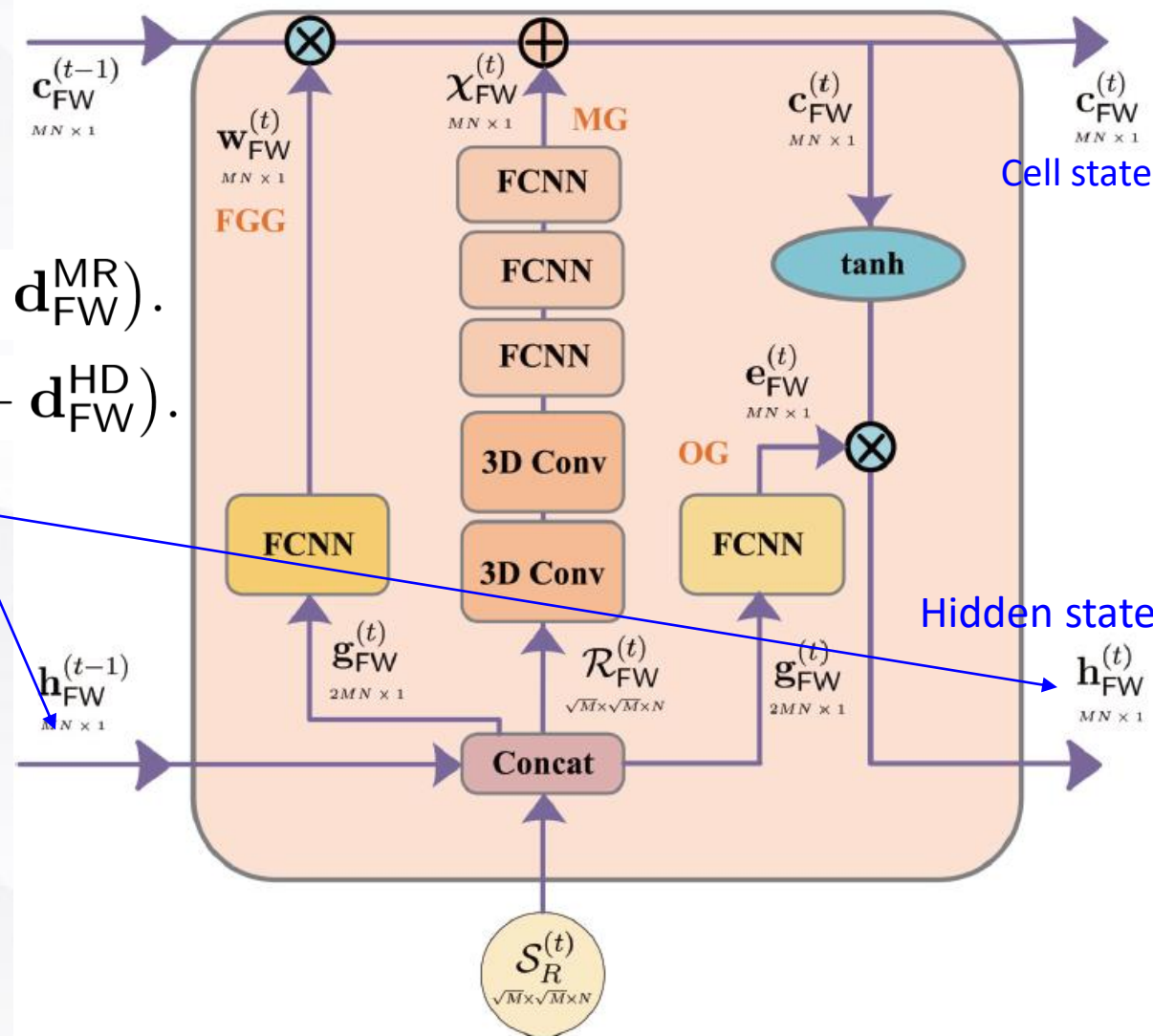
- Forget gate $g_{FW}^{(t)} = \text{vec}[\mathbf{h}_{FW}^{(t-1)}, \bar{\mathbf{z}}_R^{(t)}]$.
- Memory gate $\chi_{FW}^{(t)} = \kappa_{FW,FC}^{MR}(\mathbf{a}_{FW}^{(t)}; \omega_{FW}^{MR}, \mathbf{d}_{FW}^{MR})$.
- Output gate $e_{FW}^{(t)} = \text{sigmoid}(\mathcal{W}_{FW}^{HD} g_{FW}^{(t)} + \mathbf{d}_{FW}^{HD})$.
- Hidden state $\mathbf{h}_{FW}^{(t)} = \tanh(\mathbf{c}_{FW}^{(t)}) \odot \mathbf{e}_{FW}^{(t)}$
- Cell state $\mathbf{c}_{FW}^{(t)} = \mathbf{w}_{FW}^{(t)} \odot \mathbf{c}_{FW}^{(t-1)} + \chi_{FW}^{(t)}$,



(4) Bidirectional RCNN

Forward module:

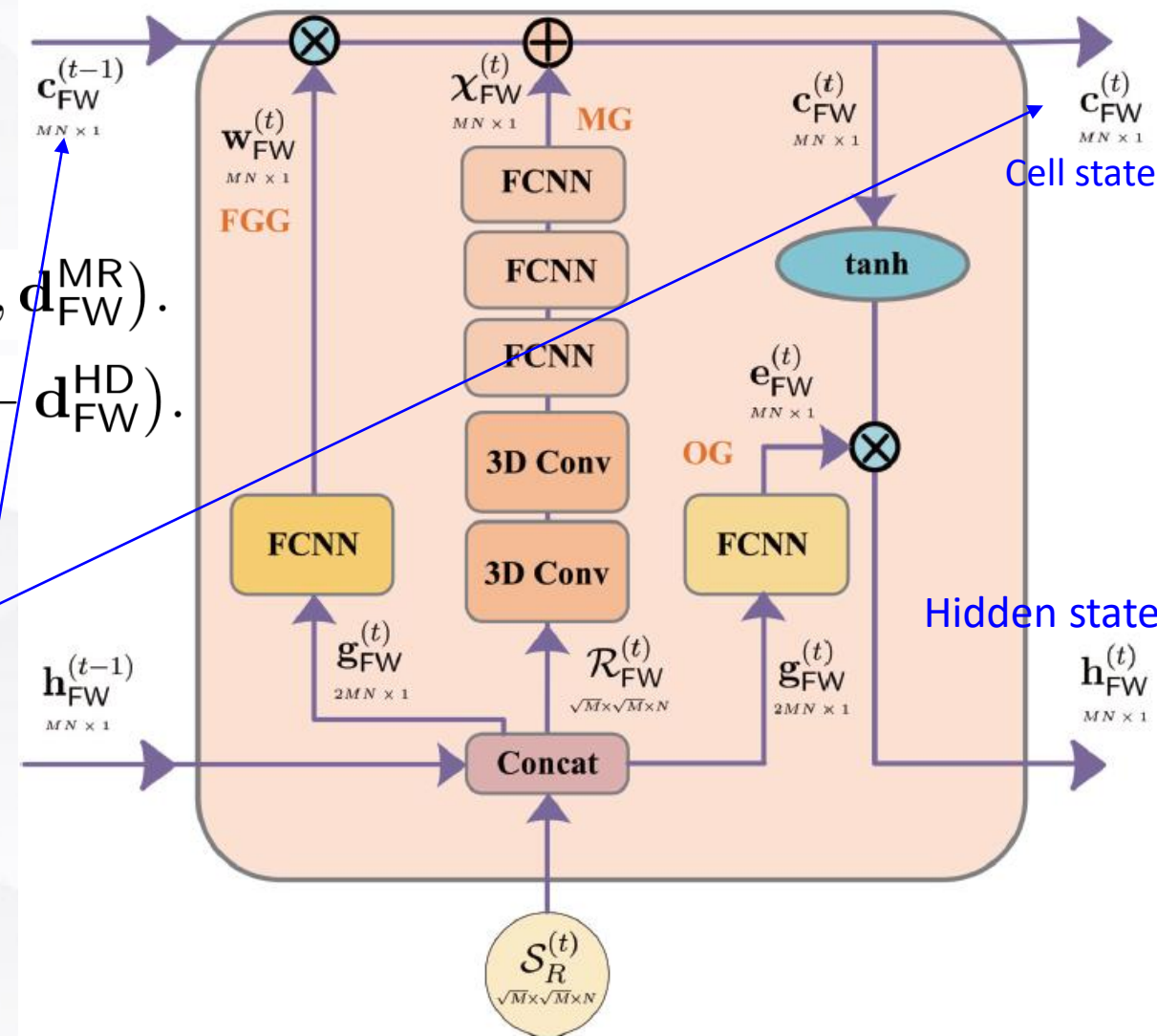
- Forget gate $g_{FW}^{(t)} = \text{vec}[\mathbf{h}_{FW}^{(t-1)}, \bar{\mathbf{z}}_R^{(t)}]$.
- Memory gate $\chi_{FW}^{(t)} = \kappa_{FW,FC}^{MR}(\mathbf{a}_{FW}^{(t)}; \omega_{FW}^{MR}, \mathbf{d}_{FW}^{MR})$.
- Output gate $e_{FW}^{(t)} = \text{sigmoid}(\mathcal{W}_{FW}^{HD} g_{FW}^{(t)} + \mathbf{d}_{FW}^{HD})$.
- Hidden state $\mathbf{h}_{FW}^{(t)} = \tanh(\mathbf{c}_{FW}^{(t)}) \odot \mathbf{e}_{FW}^{(t)}$
- Cell state $\mathbf{c}_{FW}^{(t)} = \mathbf{w}_{FW}^{(t)} \odot \mathbf{c}_{FW}^{(t-1)} + \chi_{FW}^{(t)}$,



(4) Bidirectional RCNN


Forward module:

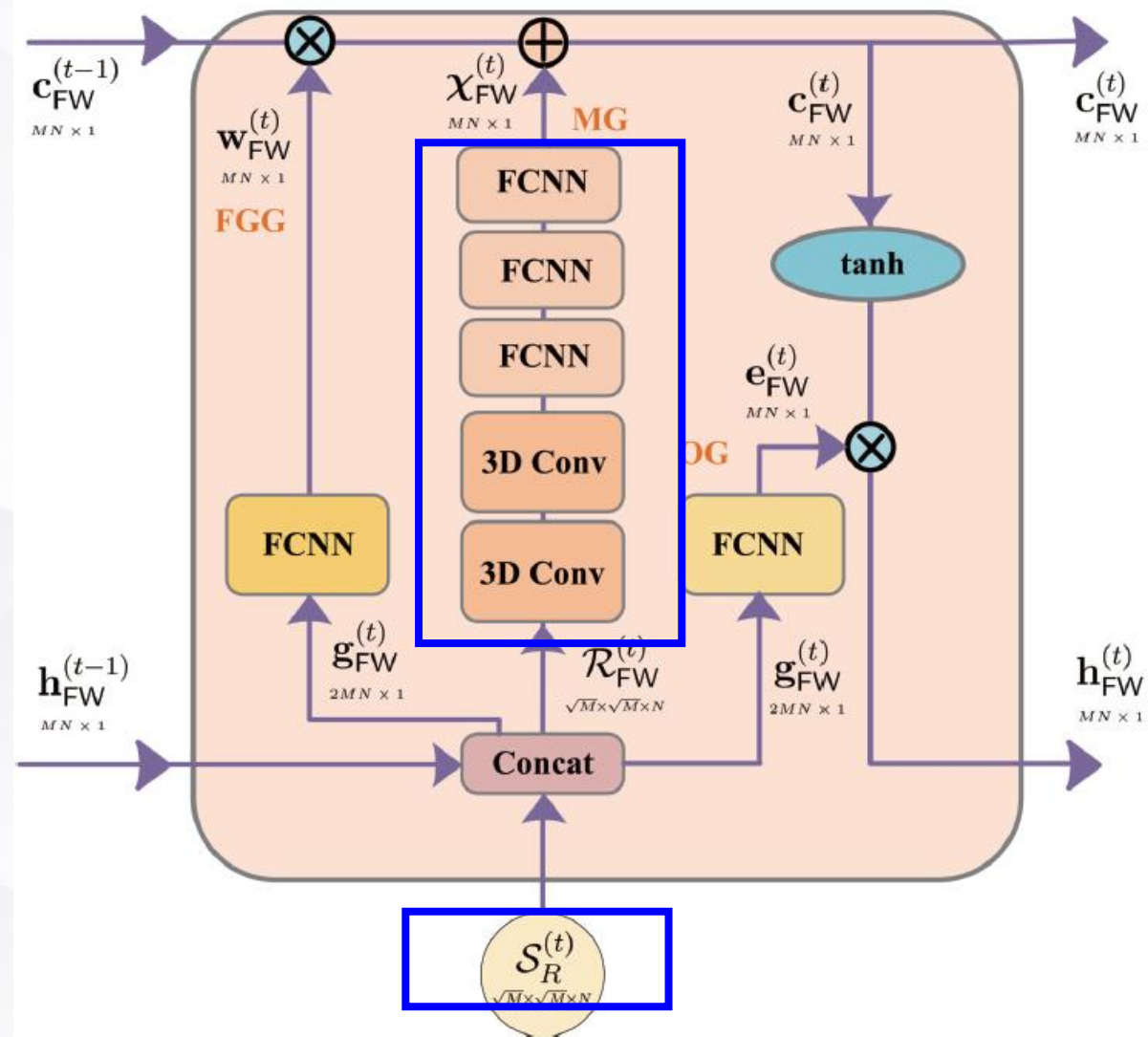
- Forget gate $g_{FW}^{(t)} = \text{vec}[\mathbf{h}_{FW}^{(t-1)}, \bar{\mathbf{z}}_R^{(t)}]$.
- Memory gate $\chi_{FW}^{(t)} = \kappa_{FW,FC}^{MR}(\mathbf{a}_{FW}^{(t)}; \omega_{FW}^{MR}, \mathbf{d}_{FW}^{MR})$.
- Output gate $e_{FW}^{(t)} = \text{sigmoid}(\mathcal{W}_{FW}^{HD} g_{FW}^{(t)} + \mathbf{d}_{FW}^{HD})$.
- Hidden state $\mathbf{h}_{FW}^{(t)} = \tanh(\mathbf{c}_{FW}^{(t)}) \odot \mathbf{e}_{FW}^{(t)}$
- Cell state $\mathbf{c}_{FW}^{(t)} = \mathbf{w}_{FW}^{(t)} \odot \mathbf{c}_{FW}^{(t-1)} + \chi_{FW}^{(t)}$,



(4) Bidirectional RCNN

Something different:

- Texture feature in 3D sample image
 - 3D CNN-based memory gate for enhancing texture extraction
 - Bidirectional time-recursive model to extend time-correlation features
- 
- Boosting UD tracking performance in terms of feature and its extraction



(4) Bidirectional RCNN

Procedures: First train and then test

- Train: derive the optimal network parameter with lowest mismatch
- Test: determine UD location and pose for a given sample, using the well-trained Bi-RCNN.

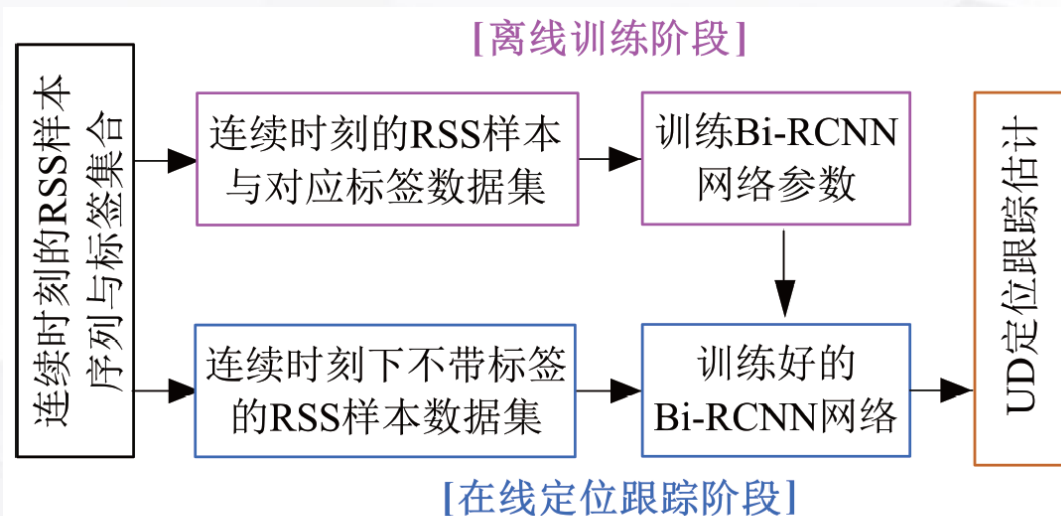


图 5 基于 Bi-RCNN 的 VLP 方法

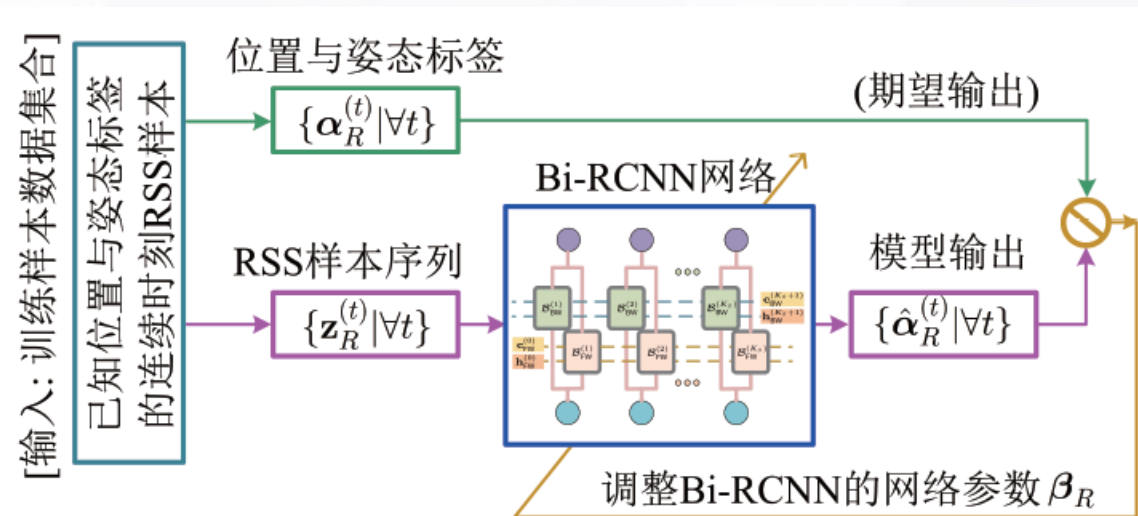


图 14 网络模型训练过程



(4) Bidirectional RCNN

Pseudo codes

Algorithm 1: Our Bi-RCNN-based VLP method

Input : RSS sample sequence $\{z_R^{(\tau)} | \forall \tau = 1 : K\}$.

- 1 **For** $\tau = 1 : K$
- 2 Abstract a subsequence $\{z_R^{(t+\tau-1)} | \forall t = 1 : K_S\}$.
- 3 Initialize $\{h_{FW}^{(t)}, h_{BW}^{(t)}, c_{FW}^{(t)}, c_{BW}^{(t)} | \forall t = 1 : K_S\}$.
- 4 **For** $t = 1 : K_S$
- 5 Determine $\mathcal{S}_R^{(t)}$ by (4),
- 6 Get $\bar{\mathcal{S}}_R^{(t)}$ via normalizing $\mathcal{S}_R^{(t)}$ as per (5).
- 7 Get $\bar{z}_R^{(t)}$ via normalizing $z_R^{(t)}$ as per (6).
- 8 Determine FGG input $g_{FW}^{(t)}$ by (7).
- 9 Determine FGG output $w_{FW}^{(t)}$ by (9).
- 10 Determine OG input $\mathcal{R}_{FW}^{(t)}$ as per (10).
- 11 Determine $A_{FW}^{(t)}$ as per (11).
- 12 Determine MG output $\chi_{FW}^{(t)}$ as per (12),
- 13 Update memory cells $c_{FW}^{(t)}$ as per (14).
- 14 Update the OG state $e_{FW}^{(t)}$ as per (13).
- 15 Update the hidden state $h_{FW}^{(t)}$ as per (16).
- 16 Update backward modules $\{c_{BW}^{(t)}, h_{BW}^{(t)}\}$.
- 17 Update $\hat{\alpha}_R^{(t)}$ as per (17).
- 18 **End**
- 19 **End**

Output: UD location trace $\{\hat{\alpha}_R^{(\tau)} | \forall \tau = 1 : K\}$.



(4) Bidirectional RCNN

Setup:

- A room: $9\text{m} \times 9\text{m} \times 4\text{m}$
- 20 dB SNR
- 81 LEDs
- 9 PDs

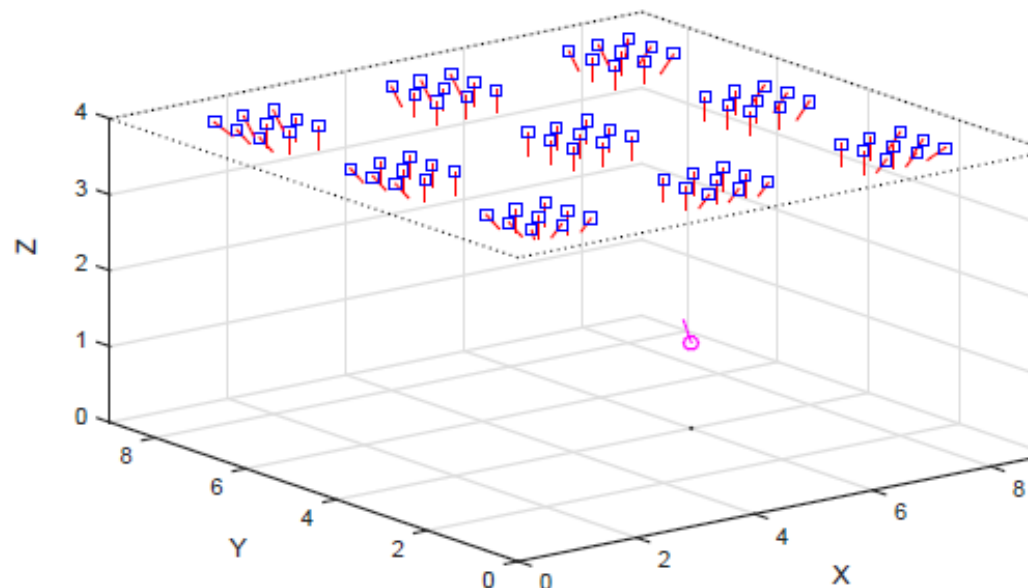
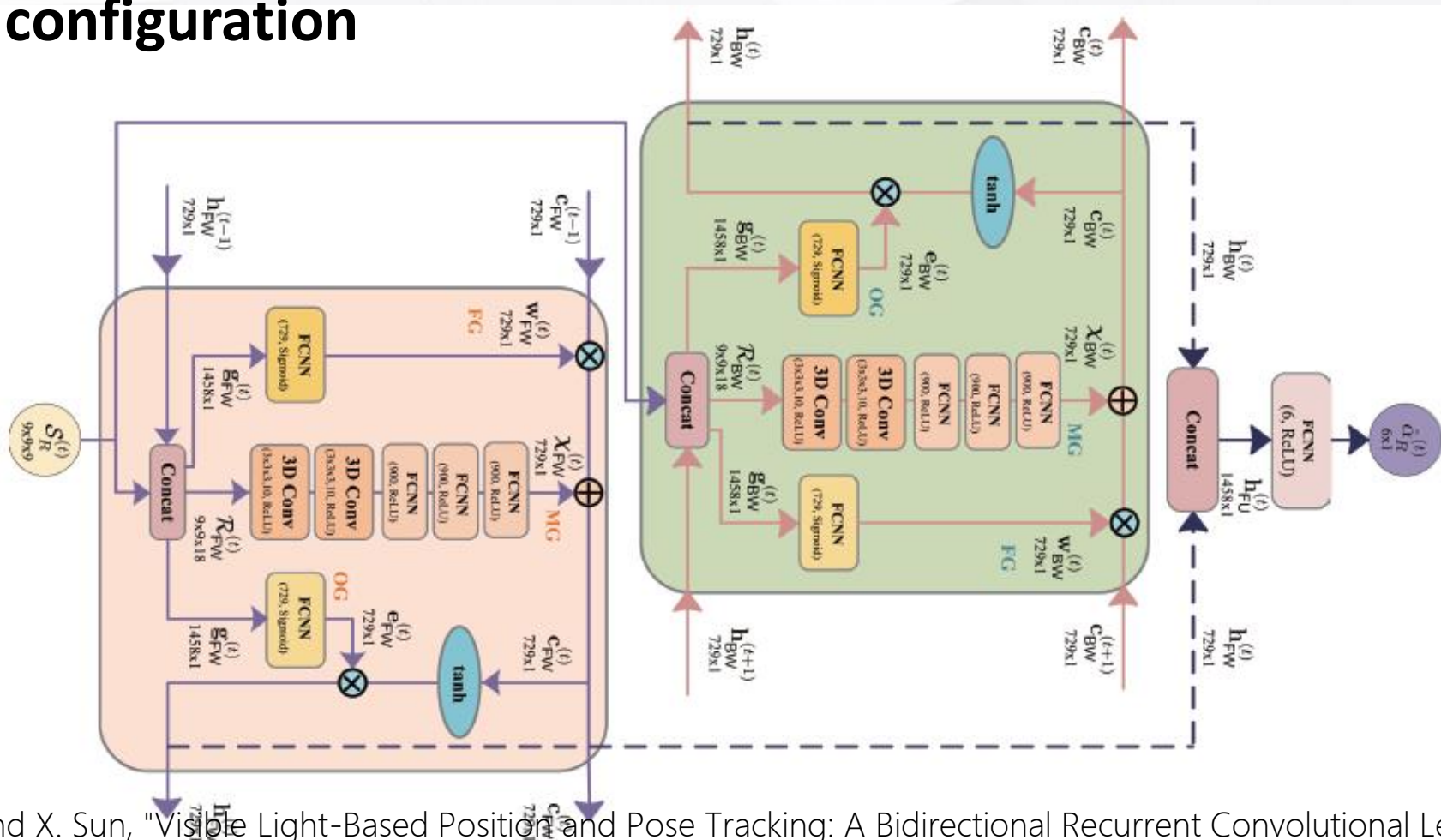


表 3 可见光定位系统参数设定

| 参数名称 | 参数设定 |
|------------------------------|--|
| LED 数量 M | 81 |
| PD 数量 N | 9 |
| LED 发射功率 $W_m^{(t)}$ | [10, 11] Watt |
| PD 视场角 θ_{FOV} | 90 度 |
| 光学聚光器增益 $G_n^{(t)}$ | [2, 2.2] |
| 朗伯辐射阶数 r | 1 |
| 小反射系数 $h_{m,n,\ell}^{(t)}$ | [0.7, 0.77] |
| 机动目标运动速度 v_u | 0.5 m/s |
| 随机运动参数 $\mathbf{v}_R^{(t)}$ | $\mathcal{N}(\mathbf{0}, 0.5\mathbf{I}_3)$ |
| 信噪比 SNR | 20dB |

(4) Bidirectional RCNN

Bi-RCNN configuration





(4) Bidirectional RCNN

Baselines:

- **Baseline 1:** GCNN-based VLP, which uses Gabor filters for feature extraction.
- **Baseline 2:** MLP-based VLP, adopting a five-layer fully-connected network.
- **Baseline 3:** CNN-based VLP, which models the UD localization as a classification problem.
- **Baseline 4:** ResNet-based VLP, which has four residual convolution modules and five-layer fully connected network. Each convolution module has 10 kernels of dimension 3×3 , and the width of fully connected layers is 100.
- **Baseline 5:** Long short-term memory (LSTM)-based VLP.



(4) Bidirectional RCNN

Results: UD 6D tracking performance versus SNR

- Our BiRCNN outperforms baselines due to problem-specific design

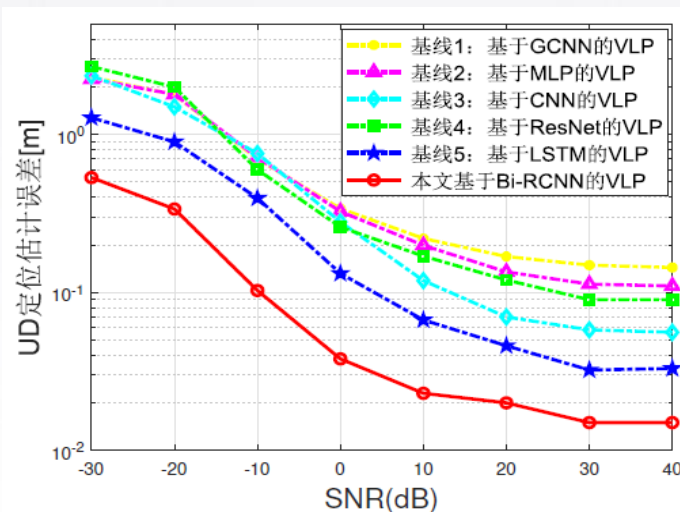


图 17 不同信噪比下的定位误差

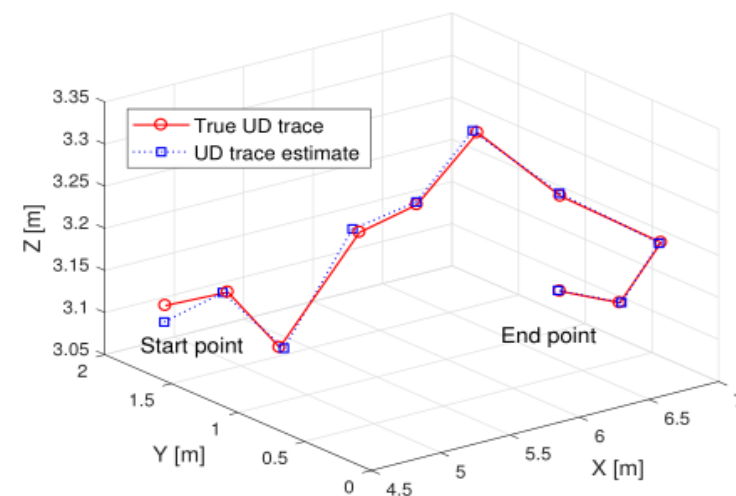
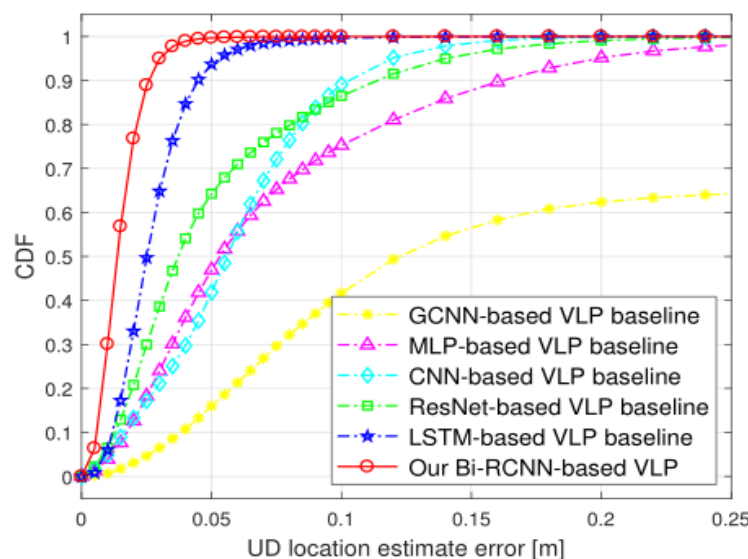


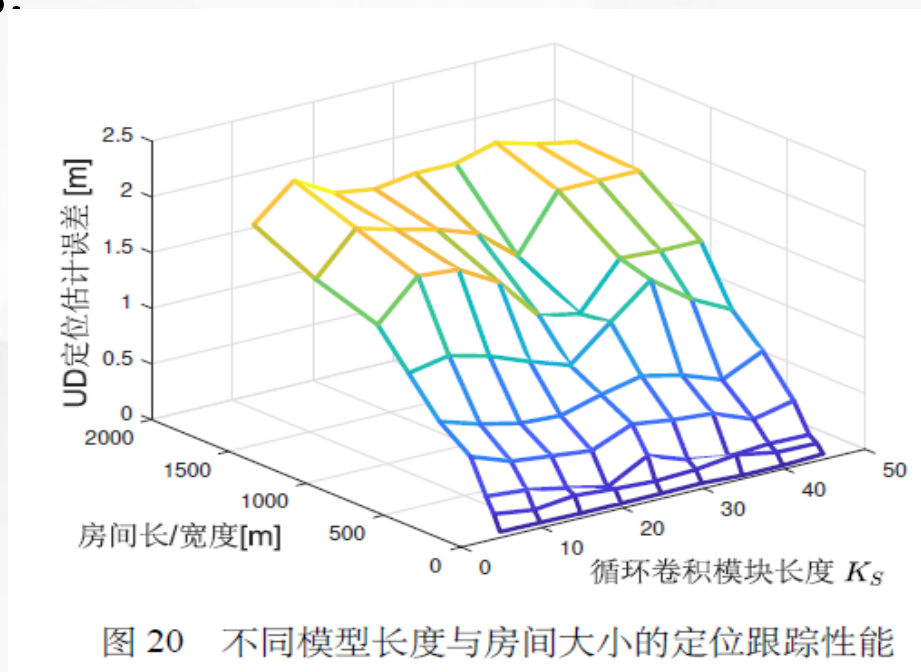
Fig. 7. UD trace and its estimate.



(4) Bidirectional RCNN

Results: VLP error over deployment range and recursive depth

- It is sensitive to deployment range: larger distance, larger error
- but not sensitive to recursive depth since first-order structure is dominant in RSS sample series.





(4) Bidirectional RCNN

Results: VLP error versus different degree of UD mobility

- Large degree of mobility, less time correlation, and hence large VLP error

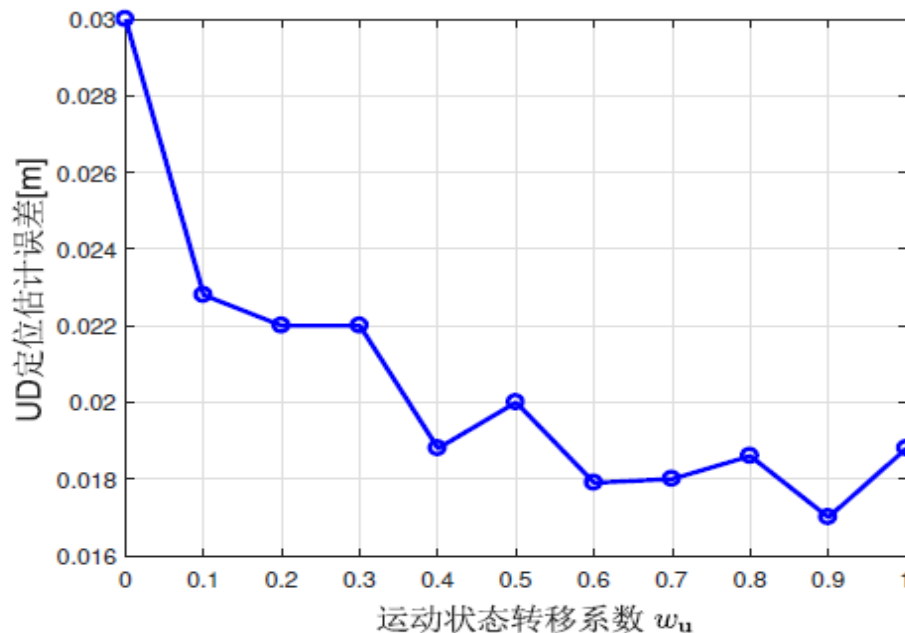


图 21 不同运动系数下的定位跟踪性能



(4) Bidirectional RCNN

- UD location and pose tracking using VLC is challenging due to RSS model mismatch caused by random channel fading and multipath interference.
- In this paper, we develop a novel BiRCNN-based VLP method to offer a robust UD tracking solution via learning reliable structures of dynamic propagation environment.
- We propose to extract spatial-time texture feature of RSS sample series for enhancing VLP performance.
- Simulation results verified the performance gain of our solution over state-of-the-art VLP baselines.
- DL-based VLP vs SPM-based VLP



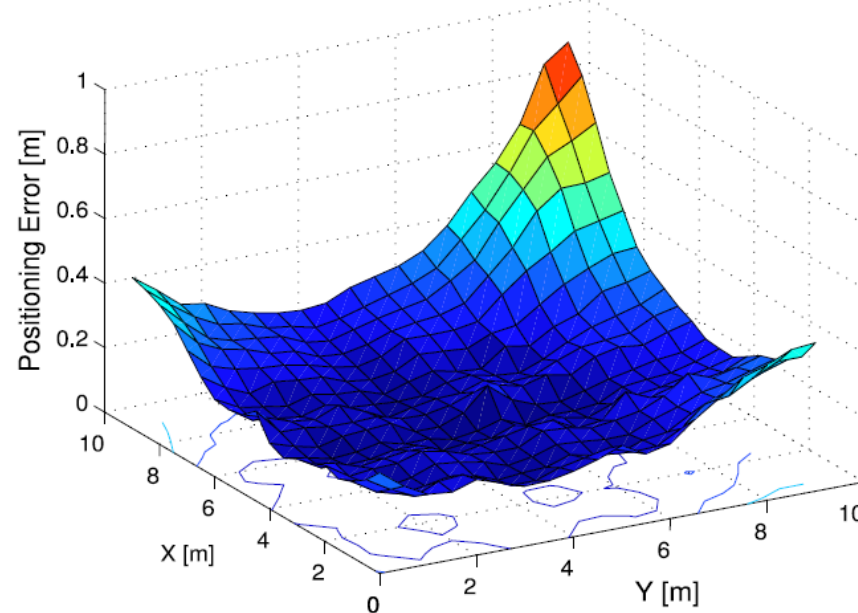
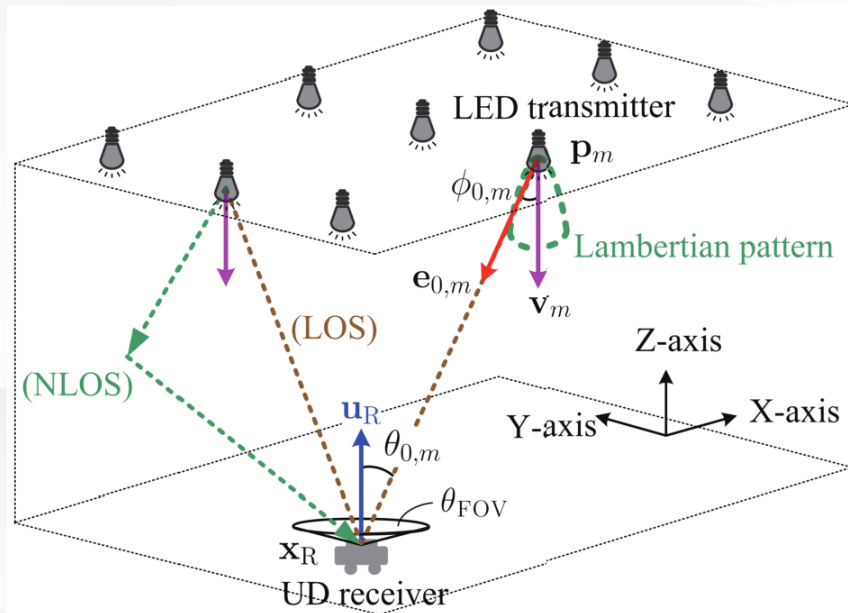
Outline

- Background
- System Model
- Robust VLP Algorithm
- Performance Limits
- Resource Allocation
- Conclusions

VLP Performance Limits

Intuition: **resource** and **environment** are two dominant factors affecting VLP performance

- System resource (bandwidth, SNR, the number of tx, deployment)
- Environments (NLOS interference, fading)

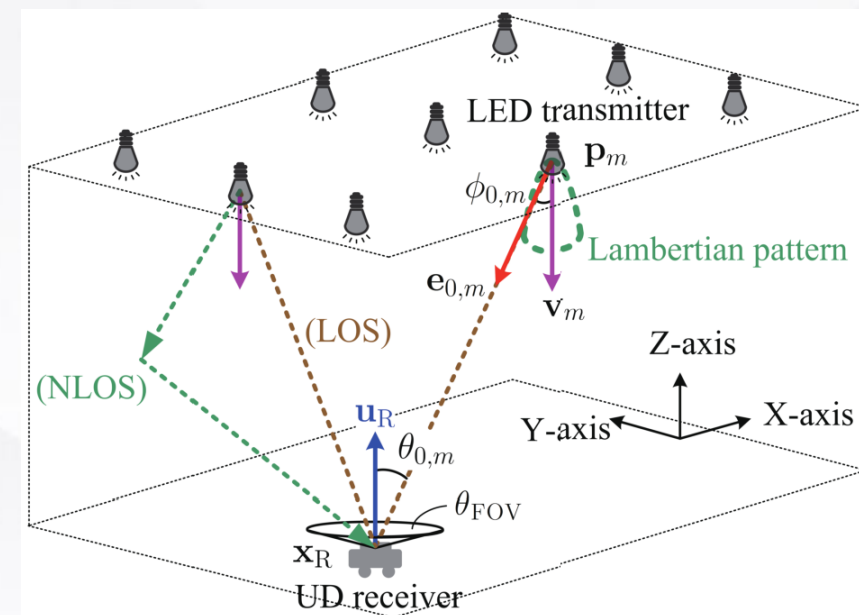




VLP Performance Limits

System Setup

- M LEDs with known location $\mathbf{p}_m \in \mathbb{R}^3$ and orientation $\mathbf{v}_m \in \mathbb{R}^3$
- One mobile UD with a PD array
- UD location $\mathbf{x}_R \in \mathbb{R}^3$ and pose angle $\mathbf{u}_R \in \mathbb{R}^3$
- Let $\alpha_R = [\mathbf{x}_R, \mathbf{u}_R] \in \mathbb{R}^6$ be the joint vector.



- [1] B. Zhou, A. Liu, and V. Lau, "Performance Limits of Visible Light-Based Positioning Using Received Signal Strength Under NLOS Propagation", IEEE Transactions on Wireless Communications, Vol. 18, No.11, 2019, pp. 5227-5241
- [2] B. Zhou, Y. Cao, and Y. Zhuang, "On the Performance Gain of Harnessing Non-Line-Of-Sight Propagation for Visible Light-Based Positioning," IEEE Transactions on Wireless Communications, Vol. 19, No.7, 2020, pp. 4863-4878
- [3] B. Zhou, A. Liu, V. Lau, J. Wen, S. Mumtaz, A. K. Bashir, and S. H. Ahmed, "Performance Limits of Visible Light-Based Positioning for Internet-of-Vehicles: Time-Domain Localization Cooperation Gain," IEEE Transactions on Intelligent Transportation Systems, vol. 22, no. 8, 2021, pp. 5374-5388.

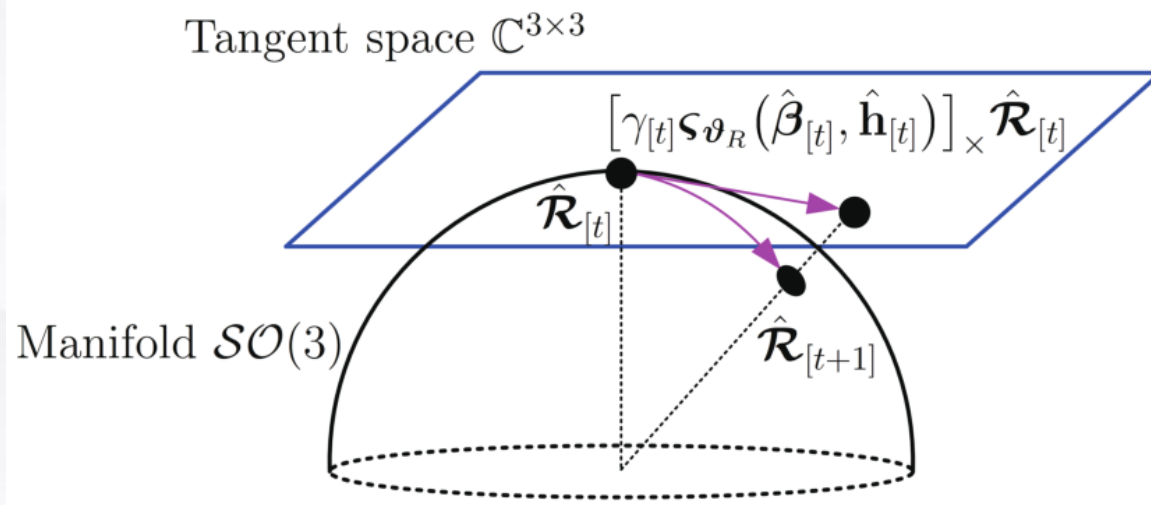
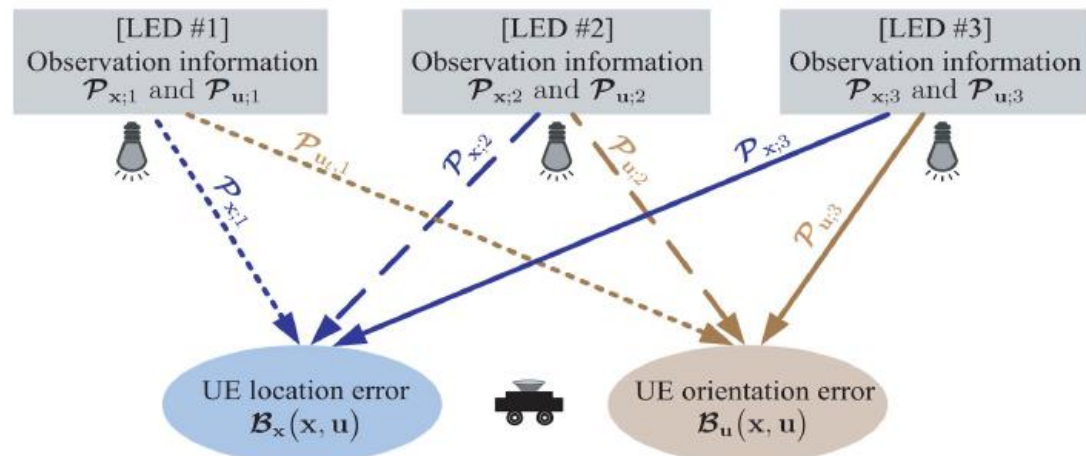
VLP Performance Limits

Problem Formulation

- UD location and pose tracking based on VLC aims to determine UD location α_R from varying samples $\{z_{m,n} | \forall m, \forall n\}$

$$\mathcal{P}_{\text{VLP}} : (\hat{\alpha}_R, \hat{\mathbf{h}}) = \arg \min_{\alpha_R} \min_{\mathbf{h}} \|\mathbf{z} - \mathbf{G}(\alpha_R) \mathbf{h}\|_2^2, \quad (1)$$

$$\text{s.t. } \mathcal{R}(\mathbf{u}_R) \in \mathcal{SO}(3), \quad (2)$$





VLP Performance Limits

Our Goal

- **VLP Performance Limits:** For a given scenario with fixed resource deployment and invariant fading, what is the performance limit of VLP?
- **Effect of Resource and Fading:** How do system resource and fading environment (esp. NLOS interference) affect the VLP performance?
- **Long-Term Performance Evolution:** How does VLP error evolution over time for a mobile user?

$$\mathcal{B}_{\alpha_{[k]}} \sim \text{scaling}(\text{bandwidth}), \text{ as bandwidth} \rightarrow 0$$

$$\mathcal{B}_{\alpha_{[k]}} \sim \text{scaling}(\text{NLOS interference}), \text{ as NLOS interference} \rightarrow 0$$

$$\mathcal{B}_{\alpha_{[k]}} \sim \text{scaling}(\text{channel variance}), \text{ as channel variance} \rightarrow 0$$

$$\mathcal{B}_{\alpha_{[k]}} \sim \text{scaling}(\text{RSU state error}), \text{ as RSU state error} \rightarrow 0$$



VLP Performance Limits

Challenge

- Localization, orientation and SPM calibration are **coupled** with each other, and thus their performance are dependent mutually.
- UD **mobility** is difficult to predict and quantification
- Instantaneous measurement information is difficult to quantify due to **nonlinear** models and complex calculations (integration over nonlinear).

[1] B. Zhou, A. Liu, and V. Lau, "Performance Limits of Visible Light-Based Positioning Using Received Signal Strength Under NLOS Propagation", IEEE Transactions on Wireless Communications, Vol. 18, No.11, 2019, pp. 5227-5241

[2] B. Zhou, Y. Cao, and Y. Zhuang, "On the Performance Gain of Harnessing Non-Line-Of-Sight Propagation for Visible Light-Based Positioning," IEEE Transactions on Wireless Communications, Vol. 19, No.7, 2020, pp. 4863-4878

[3] B. Zhou, A. Liu, V. Lau, J. Wen, S. Mumtaz, A. K. Bashir, and S. H. Ahmed, "Performance Limits of Visible Light-Based Positioning for Internet-of-Vehicles: Time-Domain Localization Cooperation Gain," IEEE Transactions on Intelligent Transportation Systems, vol. 22, no. 8, 2021, pp. 5374-5388.



VLP Performance Limits

Strategies:

- Schur complementary for information decoupling

$$\mathcal{J}_{\alpha_{[k]}^{(i)}} = \mathcal{I}_{\alpha_{[k]}^{(i)}, \alpha_{[k]}^{(i)}} - \mathcal{I}_{\alpha_{[k]}^{(i)}, \setminus \alpha_{[k]}^{(i)}} (\mathcal{I}_{\setminus \alpha_{[k]}^{(i)}, \setminus \alpha_{[k]}^{(i)}})^{-1} \mathcal{I}_{\setminus \alpha_{[k]}^{(i)}, \alpha_{[k]}^{(i)}},$$

- Laplacian approximation for complex statistical model and calculations

$$\tilde{\alpha}_{[k]}^{(j)} = \arg \max_{\alpha_{[k]}^{(j)}} \ln p(\alpha_{[k]}^{(j)} | \mathbf{z}_{[k]}^{\#})$$

$$\Psi_{[k]}^{(j)} = -(\nabla_{\alpha_{[k]}^{(j)}}^2 \ln p(\alpha_{[k]}^{(j)} | \mathbf{z}_{[k]}^{\#}))^{-1} \Big|_{\alpha_{[k]}^{(j)} = \tilde{\alpha}_{[k]}^{(j)}}$$

$$p(\alpha_{[k]}^{(j)}) \approx \mathcal{N}(\alpha_{[k]}^{(j)} | \tilde{\alpha}_{[k]}^{(j)}, \Psi_{[k]}^{(j)})$$



(1) VLP Error Bounds



(1) VLP Error Bounds

Two strategies to deal with NLOS interference

- LOS channel-based VLP

$$\mathcal{P}_{\text{LOS-VLP}} : (\hat{\mathbf{x}}_{\text{los}}, \hat{\mathbf{u}}_{\text{los}}) = \arg \min_{\mathbf{x}, \mathbf{u}} \|\mathbf{z} - \mathbf{G}_{\text{los}}(\mathbf{x})\boldsymbol{\mu}(\mathbf{u})\|_2^2.$$

- NLOS channel-based VLP

$$\mathcal{P}_{\text{NLOS-VLP}} : (\hat{\mathbf{x}}_{\text{nlos}}, \hat{\mathbf{u}}_{\text{nlos}}) = \arg \min_{\mathbf{x}, \mathbf{u}} \underbrace{\min\{\|\mathbf{z} - \mathbf{G}(\mathbf{x}, \boldsymbol{\beta}_S)\boldsymbol{\mu}(\mathbf{u})\|_2^2 : \forall \boldsymbol{\beta}_S\}}_{\text{Cost function } \vartheta(\mathbf{x}, \mathbf{u})},$$

- Different computational cost and prior knowledge, different performance



(1) VLP Error Bounds

- LOS channel-based VLP error bounds

Theorem 1 (LOS-Based VLP Error Bound) The LOS-based UD location and orientation estimate errors will be bounded from below, respectively, as follows,

$$\mathbb{E}\{\|\hat{\mathbf{x}}_{\text{los}} - \mathbf{x}\|_2^2\} \geq \text{trace}(\mathfrak{B}_{\mathbf{x}}^{\text{los}}(\mathbf{x}, \mathbf{u})) + v_{\mathbf{x}}^2, \quad (23)$$

$$\mathbb{E}\{\|\hat{\mathbf{u}}_{\text{los}} - \mathbf{u}\|_2^2\} \geq \text{trace}(\mathfrak{B}_{\mathbf{u}}^{\text{los}}(\mathbf{x}, \mathbf{u})) + v_{\mathbf{u}}^2, \quad (24)$$

$$\mathfrak{B}_{\mathbf{x}}^{\text{los}} = (\omega \mathbf{H}_{\text{los}}(\mathbf{x}) \mathbf{U}(\mathbf{u}) \mathbf{F}_{\text{los}}(\mathbf{x}) \mathbf{U}^{\top}(\mathbf{u}) \mathbf{H}_{\text{los}}^{\top}(\mathbf{x}))^{-1}, \quad (25)$$

$$\mathfrak{B}_{\mathbf{u}}^{\text{los}} = (\omega \mathcal{R}(\mathbf{u}) \mathbf{G}_{\text{los}}^{\top}(\mathbf{x}) \mathbf{V}_{\text{los}}(\mathbf{x}, \mathbf{u}) \mathbf{G}_{\text{los}}(\mathbf{x}) \mathcal{R}^{\top}(\mathbf{u}))^{-1}, \quad (26)$$

Theorem 2 (LOS-Based VLP Bias). The estimate biases $v_{\mathbf{x}}$ and $v_{\mathbf{u}}$ in LOS-based VLP are approximately given by

$$v_{\mathbf{x}} \approx \|\varsigma_{\text{bias}}\|_2 \|\mathbf{H}_{\text{los}}(\mathbf{x}) \mathbf{U}(\mathbf{u})\|_2^{-1}, \quad (35)$$

$$v_{\mathbf{u}} \approx \|\varsigma_{\text{bias}}\|_2 \|\mathcal{R}(\mathbf{u}) \mathbf{G}_{\text{los}}^{\top}(\mathbf{x})\|_2^{-1}, \quad (36)$$



Theorem 3 (LOS-Based VLP Error): The LOS-based UD location and orientation errors are approximately characterized, respectively, as follows,

$$\begin{aligned} \mathbb{E}\{\|\hat{\mathbf{x}}_{\text{los}} - \mathbf{x}\|_2^2\} &\approx (\|\varsigma_{\text{bias}}\|_2^2 + \mathbb{E}\{\|\epsilon\|_2^2\}) \|\mathbf{H}_{\text{los}}(\mathbf{x}) \mathbf{U}(\mathbf{u})\|_2^{-2}, \\ \mathbb{E}\{\|\hat{\mathbf{u}}_{\text{los}} - \mathbf{u}\|_2^2\} &\approx (\|\varsigma_{\text{bias}}\|_2^2 + \mathbb{E}\{\|\epsilon\|_2^2\}) \|\mathbf{G}_{\text{los}}(\mathbf{x}) \mathcal{R}^{\top}(\mathbf{u})\|_2^{-2}, \end{aligned}$$



(1) VLP Error Bounds

- NLOS interference-caused **error floor** for LOS channel-based VLP

Remark 3 (NLOS-Caused Error Floor in High SNR)

Combining corollaries 1 and 2 with theorem 2, it is implied that, as SNR increases (e.g., $\|\epsilon\|_2^2 \rightarrow 0$), the VLP error $\mathbb{E}\{\|\hat{\mathbf{x}} - \mathbf{x}\|_2^2\}$ and $\mathbb{E}\{\|\hat{\mathbf{u}} - \mathbf{u}\|_2^2\}$ will reduce and finally hit an error floor due to the non-ignorable NLOS link-caused VLP bias in the high SNR region (in this case, the NLOS component will become the dominant error source).

$$\begin{aligned}\mathbb{E}\{\|\hat{\mathbf{x}} - \mathbf{x}\|_2^2\} &\geq \text{trace}(\mathcal{B}_{\mathbf{x}}(\mathbf{x}, \mathbf{u})) + v_{\mathbf{x}}^2, \\ \mathbb{E}\{\|\hat{\mathbf{u}} - \mathbf{u}\|_2^2\} &\geq \underbrace{\text{trace}(\mathcal{B}_{\mathbf{u}}(\mathbf{x}, \mathbf{u}))}_{\mathcal{O}(\omega^{-1})} + \underbrace{v_{\mathbf{u}}^2}_{\mathcal{O}(1)},\end{aligned}$$

$$\text{trace}(\mathcal{B}_{\mathbf{x}}(\mathbf{x}, \mathbf{u})) \sim \mathcal{O}(\text{SNR}^{-1}),$$

$$\text{trace}(\mathcal{B}_{\mathbf{u}}(\mathbf{x}, \mathbf{u})) \sim \mathcal{O}(\text{SNR}^{-1}).$$

(1) VLP Error Bounds

- NLOS interference-caused **error floor** for LOS channel-based VLP

Corollary 2 (NLOS Link-Caused Error Floor in LOS-Based VLP): As the SNR increases infinitely, the LOS-based VLP error will tend to the following asymptotic limit:

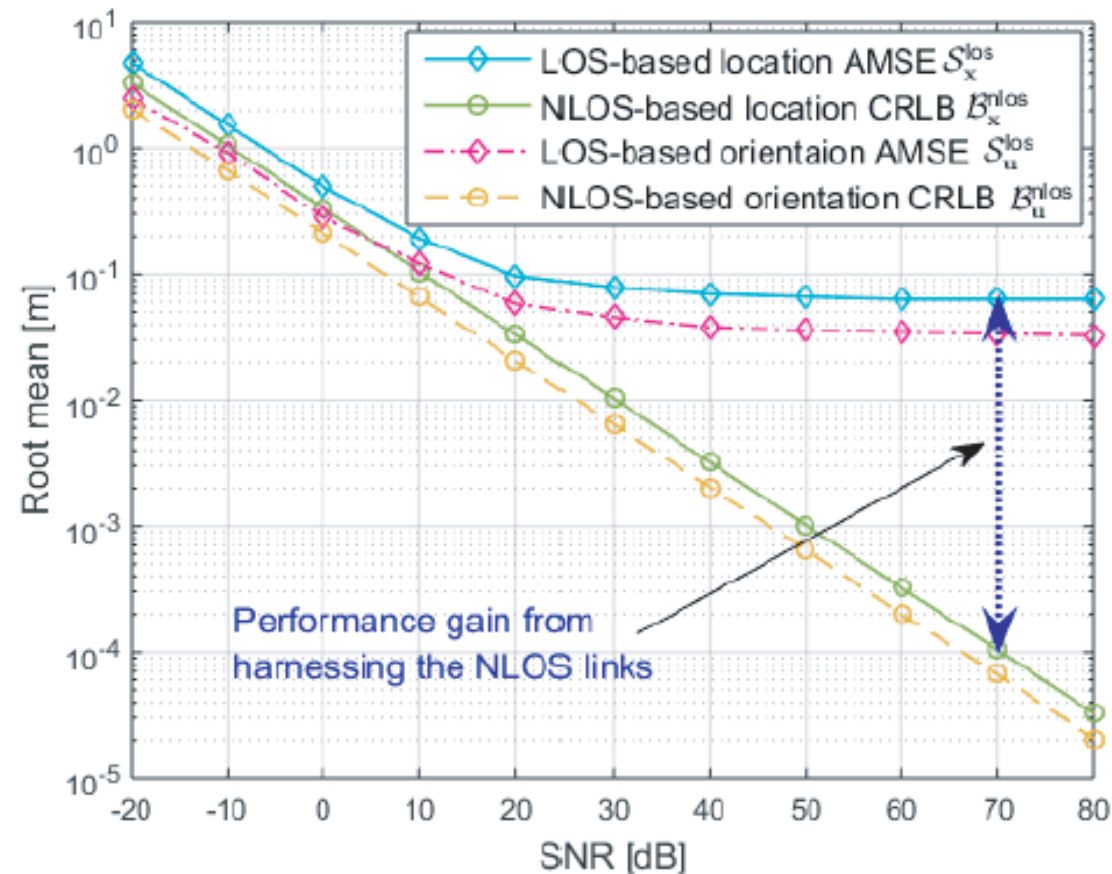
$$\lim_{\text{SNR} \rightarrow \infty} \mathbb{E}\{\|\hat{\mathbf{x}}_{\text{los}} - \mathbf{x}\|_2^2\} \approx \mathbb{E}\{\|\boldsymbol{\varsigma}_{\text{bias}}\|_2^2\} \|\mathbf{H}_{\text{los}}(\mathbf{x})\mathbf{U}(\mathbf{u})\|_2^{-2},$$

$$\lim_{\text{SNR} \rightarrow \infty} \mathbb{E}\{\|\hat{\mathbf{u}}_{\text{los}} - \mathbf{u}\|_2^2\} \approx \mathbb{E}\{\|\boldsymbol{\varsigma}_{\text{bias}}\|_2^2\} \|\mathbf{G}_{\text{los}}(\mathbf{x})\mathcal{R}^T(\mathbf{u})\|_2^{-2},$$

Corollary 1 (Scaling Rule of LOS-Based VLP Bias): The LOS-based VLP bias scales with $\|\boldsymbol{\varsigma}_{\text{bias}}\|_2$ as

$$\lim_{\|\boldsymbol{\varsigma}_{\text{bias}}\|_2 \rightarrow 0} \frac{v_{\mathbf{x}}}{\|\boldsymbol{\varsigma}_{\text{bias}}\|_2} \approx \|\mathbf{H}_{\text{los}}(\mathbf{x})\mathbf{U}(\mathbf{u})\|_2^{-1}, \quad (37)$$

$$\lim_{\|\boldsymbol{\varsigma}_{\text{bias}}\|_2 \rightarrow 0} \frac{v_{\mathbf{u}}}{\|\boldsymbol{\varsigma}_{\text{bias}}\|_2} \approx \|\mathcal{R}(\mathbf{u})\mathbf{G}_{\text{los}}^T(\mathbf{x})\|_2^{-1}, \quad (38)$$



(1) VLP Error Bounds

- NLOS channel-based VLP error bounds

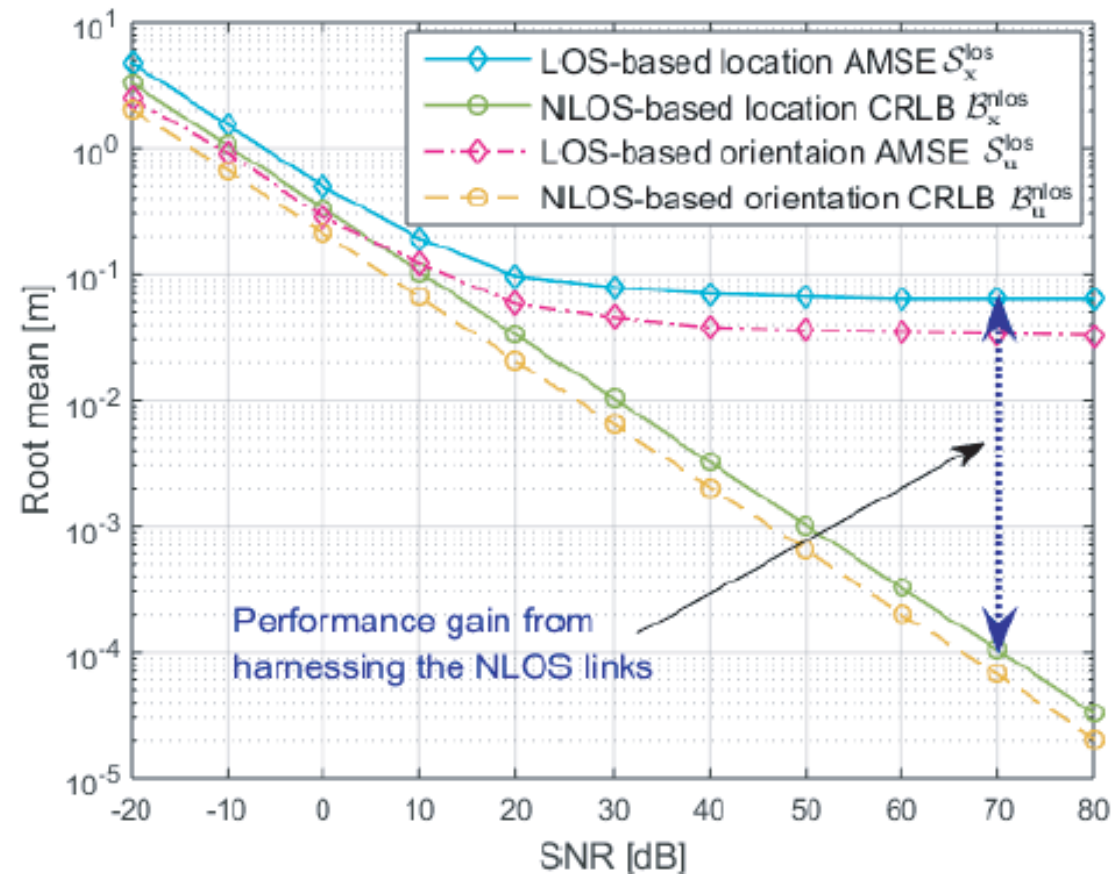
Theorem 4 (NLOS-Based VLP Error Bound): The NLOS-based UD location and orientation estimate errors will be bounded from below as follows,

$$\mathbb{E}\{\|\hat{\mathbf{x}}_{\text{nlos}} - \mathbf{x}\|_2^2 : \beta_S\} \geq \text{trace}(\mathfrak{B}_{\mathbf{x}}^{\text{nlos}}(\mathbf{x}, \mathbf{u}; \beta_S)), \quad (39)$$

$$\mathbb{E}\{\|\hat{\mathbf{u}}_{\text{nlos}} - \mathbf{u}\|_2^2 : \beta_S\} \geq \text{trace}(\mathfrak{B}_{\mathbf{u}}^{\text{nlos}}(\mathbf{x}, \mathbf{u}; \beta_S)), \quad (40)$$

$$\mathfrak{B}_{\mathbf{x}}^{\text{nlos}} = (\omega \mathbf{H}(\mathbf{x}) \mathbf{U}(\mathbf{u}) \mathbf{F}(\mathbf{x}) \mathbf{U}^\top(\mathbf{u}) \mathbf{H}^\top(\mathbf{x}) - \mathcal{L}_{\mathbf{x}}^{\text{nlos}}(\mathbf{x}, \mathbf{u}))^{-1},$$

$$\mathfrak{B}_{\mathbf{u}}^{\text{nlos}} = (\omega \mathcal{R}(\mathbf{u}) \mathbf{G}^\top(\mathbf{x}) \mathbf{V}(\mathbf{x}, \mathbf{u}) \mathbf{G}(\mathbf{x}) \mathcal{R}^\top(\mathbf{u}) - \mathcal{L}_{\mathbf{u}}^{\text{nlos}}(\mathbf{x}, \mathbf{u}))^{-1},$$



(1) VLP Error Bounds

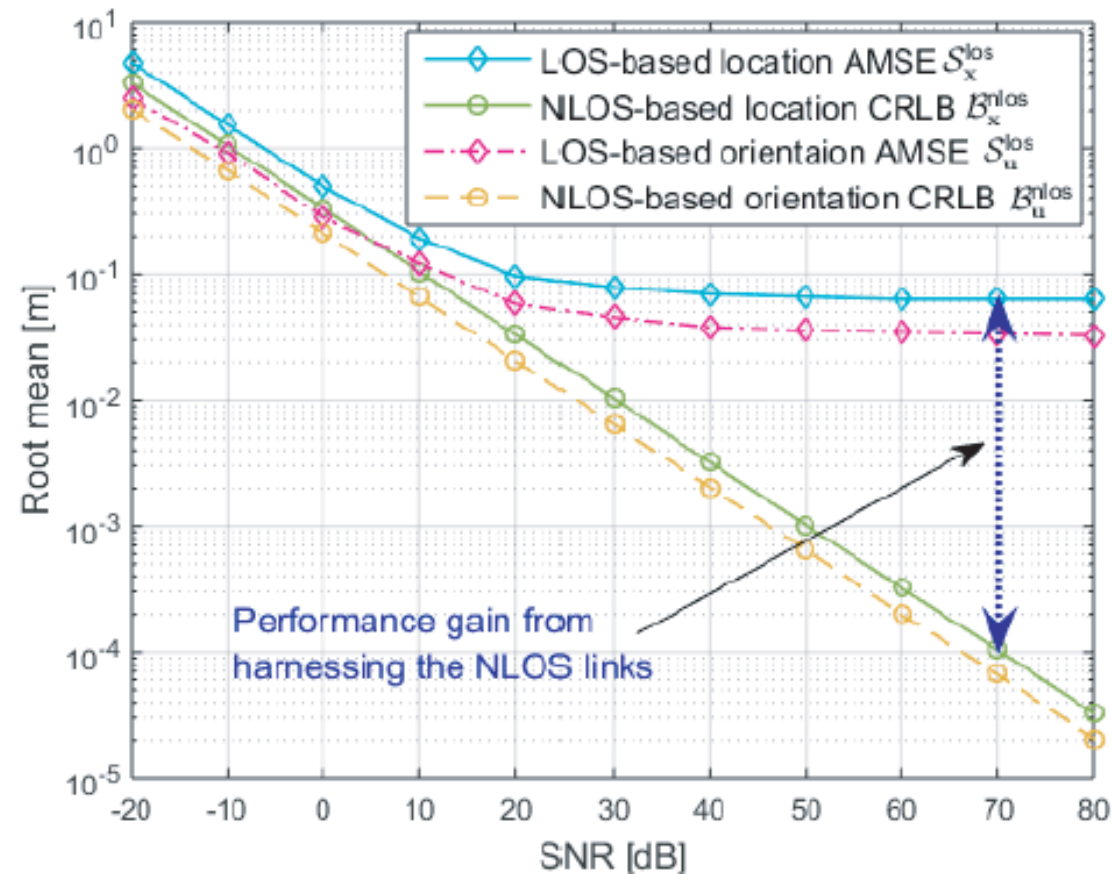
- NLOS channel-based VLP error bounds

Theorem 4 (NLOS-Based VLP Error Bound): The NLOS-based UD location and orientation estimate errors will be bounded from below as follows,

$$\mathbb{E}\{\|\hat{\mathbf{x}}_{\text{nlos}} - \mathbf{x}\|_2^2 : \beta_S\} \geq \text{trace}(\mathfrak{B}_{\mathbf{x}}^{\text{nlos}}(\mathbf{x}, \mathbf{u}; \beta_S)), \quad (39)$$

$$\mathbb{E}\{\|\hat{\mathbf{u}}_{\text{nlos}} - \mathbf{u}\|_2^2 : \beta_S\} \geq \text{trace}(\mathfrak{B}_{\mathbf{u}}^{\text{nlos}}(\mathbf{x}, \mathbf{u}; \beta_S)), \quad (40)$$

Remark 4 (Vanished Error Floor of NLOS-Based VLP): It should be noted that the information reduction $\mathcal{L}_{\mathbf{x}}^{\text{nlos}}$ and $\mathcal{L}_{\mathbf{u}}^{\text{nlos}}$ are proportional to ω . Therefore, when $\text{SNR} \rightarrow \infty$, the NLOS-based VLP error bound $\mathfrak{B}_{\mathbf{x}}^{\text{nlos}}$ and $\mathfrak{B}_{\mathbf{u}}^{\text{nlos}}$ will approach zero due to the exploitation of the NLOS propagation knowledge in the UD localization, as implied by Theorem 4. Hence, as SNR increases, there is no error floor in the VLP method after exploiting NLOS propagation knowledge. This implies a huge VLP performance gain from harnessing NLOS links. \square





(1) VLP Error Bounds

- NLOS channel-based VLP **performance gain**

Corollary 5 (NLOS-Based VLP Information Gain Over LOS-Based VLP): The performance gain of NLOS-based VLP over LOS-based VLP, from harnessing NLOS links, is given by

$$\mathcal{Q}_x^{\text{gain}}(\mathbf{x}, \mathbf{u}) = \mathcal{W}_x^{\text{los}}(\mathbf{x}, \mathbf{u}) + \mathcal{J}_x^{\text{nlos}}(\mathbf{x}, \mathbf{u}), \quad (60)$$

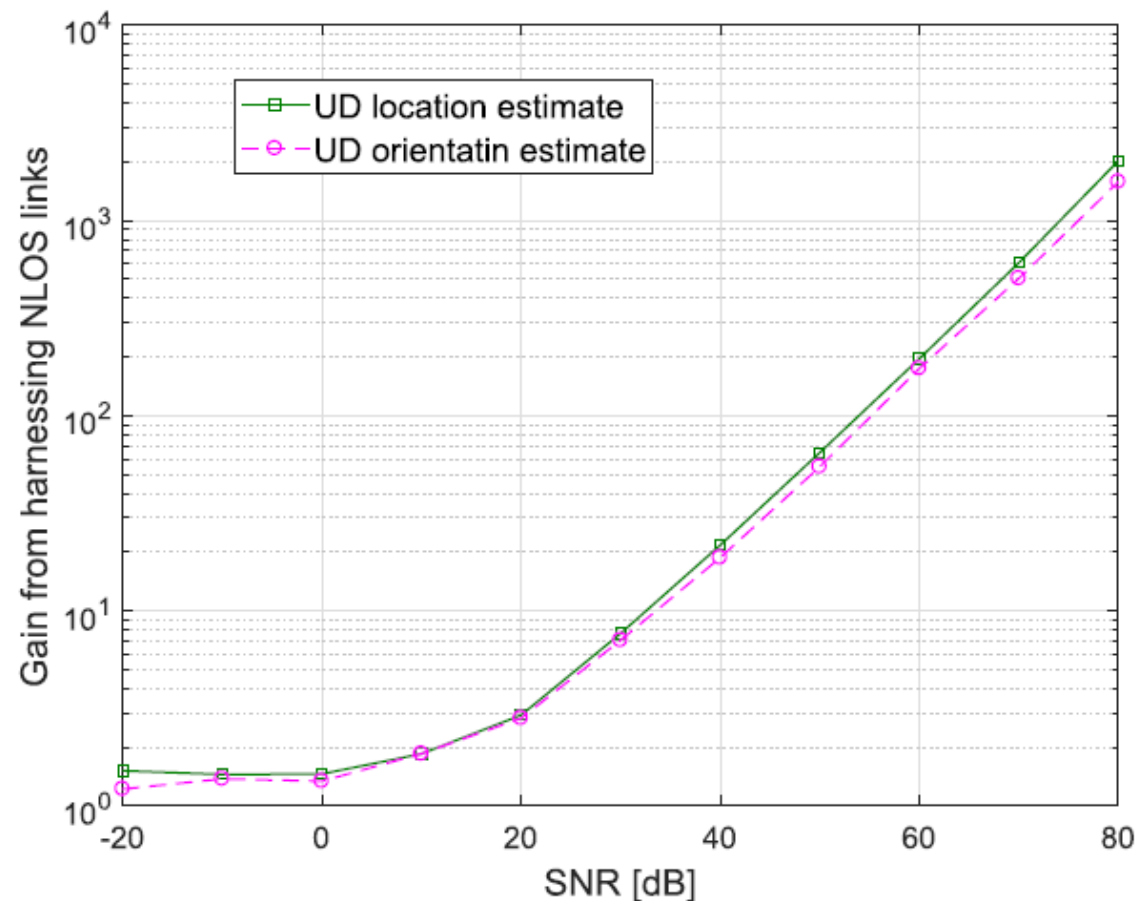
Gain from bias suppression

Gain from NLOS links

$$\mathcal{W}_x^{\text{los}}(\mathbf{x}, \mathbf{u}) = \left((\mathcal{J}_x^{\text{los}})^{-1} \mathcal{J}_x^{\text{bias}} (\mathcal{J}_x^{\text{los}})^{-1} + (\mathcal{J}_x^{\text{los}})^{-1} \right)^{-1}, \quad (54)$$

$$\mathcal{J}_x^{\text{bias}} = \|\varsigma_{\text{bias}}\|_2^{-2} \mathbf{H}_{\text{los}}(\mathbf{x}) \mathbf{U}(\mathbf{u}) \mathbf{U}^\top(\mathbf{u}) \mathbf{H}_{\text{los}}^\top(\mathbf{x}), \quad (52)$$

$$\mathcal{J}_x^{\text{los}} = \omega \mathbf{H}_{\text{los}}(\mathbf{x}) \mathbf{U}(\mathbf{u}) \mathbf{F}_{\text{los}}(\mathbf{x}) \mathbf{U}^\top(\mathbf{u}) \mathbf{H}_{\text{los}}^\top(\mathbf{x}), \quad (49)$$





(1) VLP Error Bounds

- LOS channel-based VLP Information structure

Lemma 1 (LOS-Based VLP's Equivalent FIM): The equivalent information matrix of the LOS-based VLP method is approximately given by

$$\tilde{\mathcal{Q}}_{\mathbf{x}}^{\text{los}}(\mathbf{x}, \mathbf{u}) \approx \underbrace{\left((\mathcal{J}_{\mathbf{x}}^{\text{los}}(\mathbf{x}, \mathbf{u}))^{-1} + (\mathcal{J}_{\mathbf{x}}^{\text{bias}}(\mathbf{x}, \mathbf{u}))^{-1} \right)^{-1}}_{\mathcal{Q}_{\mathbf{x}}^{\text{los}}(\mathbf{x}, \mathbf{u})}, \quad (53)$$

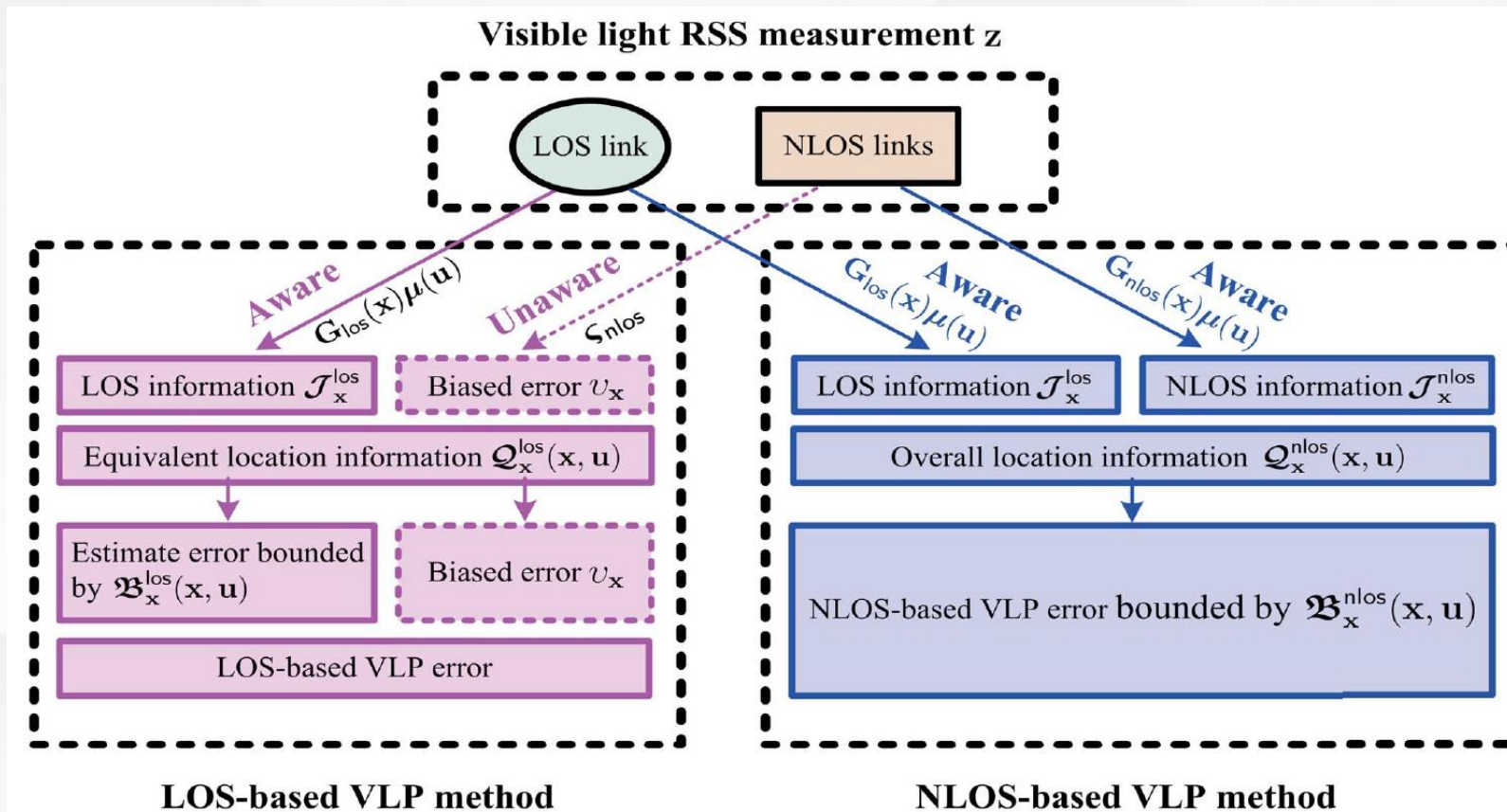
- NLOS channel-based VLP information structure

Lemma 2 (NLOS-based VLP information matrix): The equivalent FIM of NLOS channel-based VLP is given by

$$\mathcal{Q}_{\mathbf{x}}^{\text{nlos}}(\mathbf{x}, \mathbf{u}) = \mathcal{J}_{\mathbf{x}}^{\text{los}} + \mathcal{J}_{\mathbf{x}}^{\text{nlos}}$$

(1) VLP Error Bounds

- Information structure: full channel aware vs LOS channel-only aware





(2) Effect of Resource and Environment

(2) Effect of Resource Factor

- LOS channel-based CRLB on unbiased error

$$\mathcal{B}_x(\mathbf{x}, \mathbf{u}) = \left(\underbrace{\text{SNR} \cdot \mathcal{D}_x(\mathbf{x}, \mathbf{u})}_{\text{Observation information } \mathcal{H}_x^{\text{obs}}} + \chi_{\text{prior}} \right)^{-1}, \quad (18)$$

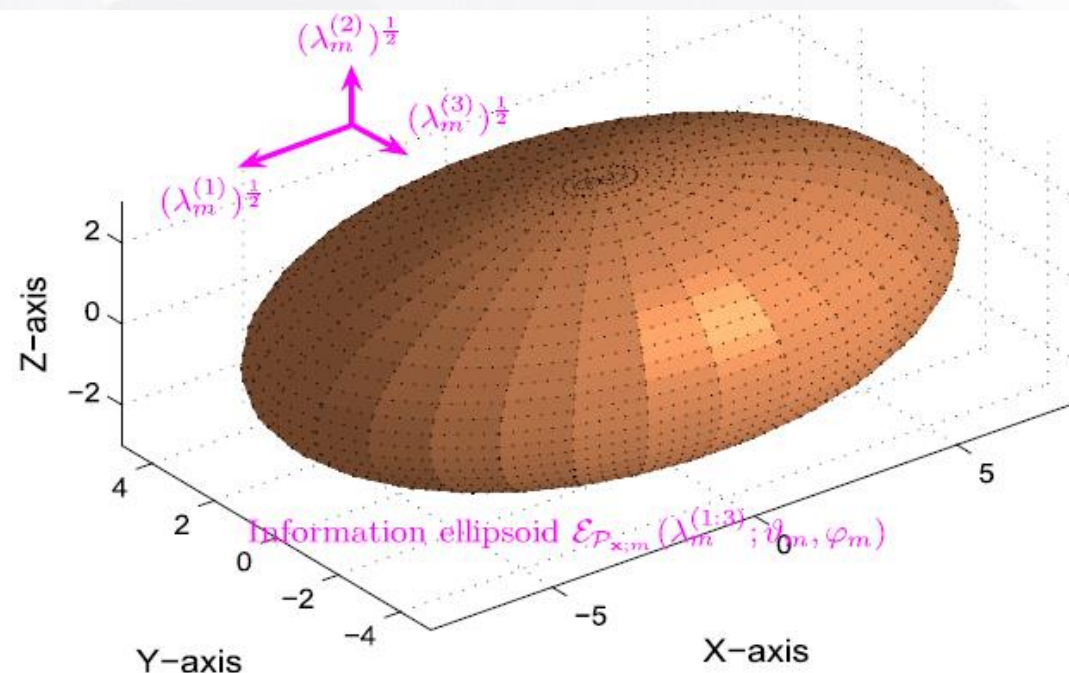
Total location information $\mathcal{J}_x(\mathbf{x}, \mathbf{u})$

$$\mathcal{B}_u(\mathbf{x}, \mathbf{u}) = \left(\underbrace{\text{SNR} \cdot \mathcal{D}_u(\mathbf{x}, \mathbf{u})}_{\text{Observation information } \mathcal{H}_u^{\text{obs}}} + \mathbf{U}_{\text{prior}} \right)^{-1}, \quad (19)$$

Total orientation information $\mathcal{J}_u(\mathbf{x}, \mathbf{u})$

$$\mathcal{D}_x(\mathbf{x}, \mathbf{u}) = \mathbf{H}(\mathbf{x})\mathbf{K}(\mathbf{u})\mathbf{F}(\mathbf{x}, \mathbf{u})(\mathbf{K}(\mathbf{u}))^\top (\mathbf{H}(\mathbf{x}))^\top, \quad (20)$$

$$\mathcal{D}_u(\mathbf{x}, \mathbf{u}) = \mathcal{R}(\mathbf{u})(\mathbf{G}(\mathbf{x}))^\top \mathbf{V}(\mathbf{x}, \mathbf{u})\mathbf{G}(\mathbf{x})\mathcal{R}^\top(\mathbf{u}), \quad (21)$$



Definition 1 (Information Ellipsoid): Given an information matrix $\mathcal{P}_{x;m}$, its information ellipsoid $\mathcal{E}_{\mathcal{P}_{x;m}}$ is defined as the set of points $\mathcal{E}_{\mathcal{P}_{x;m}} = \{\mathbf{x} \in \mathbb{R}^3 | \mathbf{x}^\top \mathcal{P}_{x;m} \mathbf{x} = 1\}$. \square



(2) Effect of Resource Factor

Remark 1 (VLP performance dependency)

- It is shown that the RSS-based VLP error performance depends on
 - the number of independent measurement sources, i.e., $|\Omega|$,
 - LED deployment $\{\mathbf{p}_m | \forall m \in \Omega\}$,
 - LED orientations $\{\mathbf{v}_m | \forall m \in \Omega\}$,
 - measurement resolution matrix $(\mathcal{D}_x(\mathbf{x}, \mathbf{u}), \mathcal{D}_u(\mathbf{x}, \mathbf{u}))$
 - SNR (inversely linear).
- (Resolution Information): The resolution information matrix depends on the choice of the measurement signal and it is essentially determined by the measurement function $h_m(\mathbf{x}, \mathbf{u})$. This metric indicates the capability to recognize the difference in α , for a given variation of measurement z_m .
- A zero-valued resolution information matrix means the unobservability of a parameter, since the measurement will remain invariant for different values of this parameter. Obviously, a measurement system with a high resolution (sensitivity) leads to a good VLP performance.



(2) Effect of Resource Factor

- The effect of **SNR**

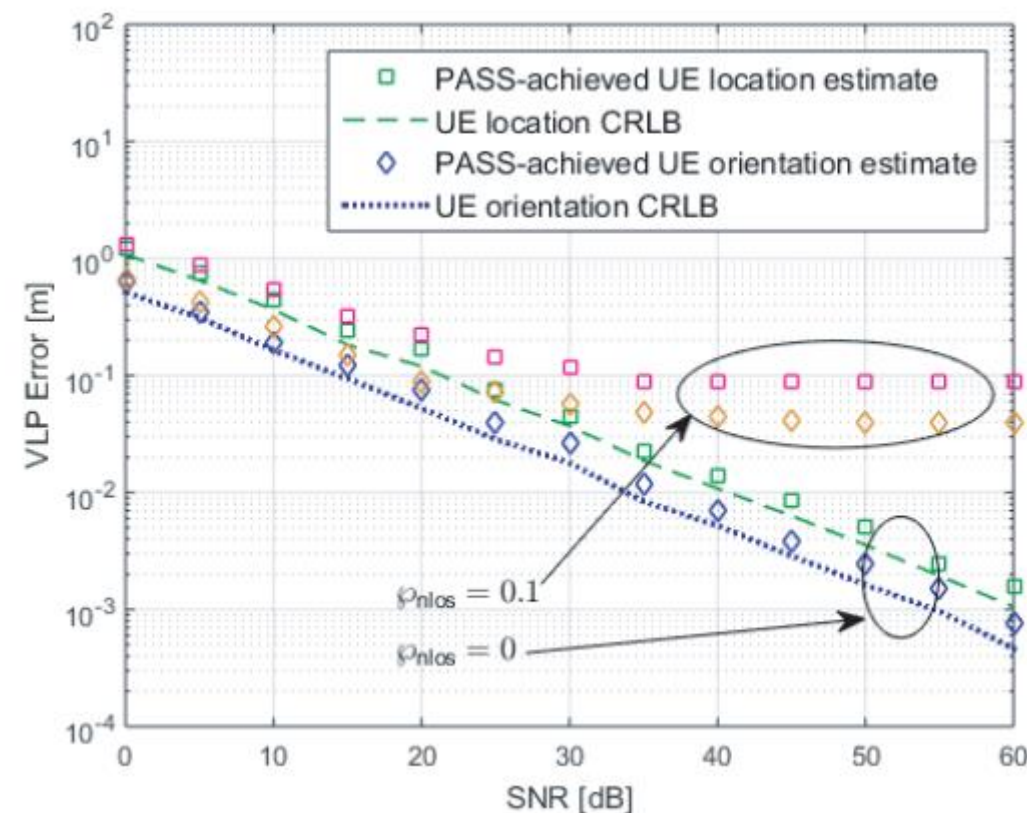
Corollary 2 (The Effect of SNR on VLP Error Bound): The UE location and orientation estimation error bounds scale with receiver-end SNR in the following manner: as $\text{SNR} \rightarrow \infty$,

$$\text{trace}(\mathcal{B}_{\mathbf{x}}(\mathbf{x}, \mathbf{u})) \sim \mathcal{O}(\text{SNR}^{-1}), \quad (35)$$

$$\text{trace}(\mathcal{B}_{\mathbf{u}}(\mathbf{x}, \mathbf{u})) \sim \mathcal{O}(\text{SNR}^{-1}). \quad (36)$$

Corollary 2 (The Effect of SNR on VLP Bias)

The UE location and orientation estimation biases are **independent** of SNR, i.e., $v_{\mathbf{x}} \sim \mathcal{O}(1)$ and $v_{\mathbf{u}} \sim \mathcal{O}(1)$, as $\text{SNR} \rightarrow \infty$.





(2) Effect of Resource Factor

- The effect of **transmission distance**

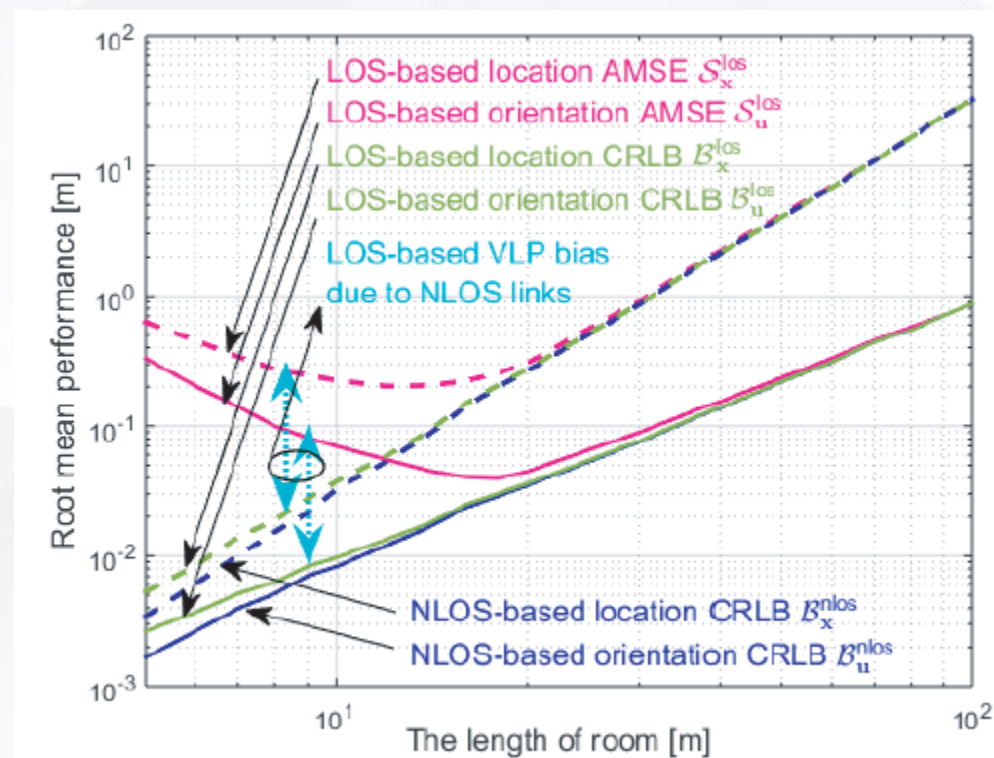
Corollary 1 (The Effect of Transmission Distance on VLP Error Bound): The VLP error bounds scale with the transmission distance between the LED and UE as⁴

$$\text{trace}(\mathcal{B}_x(\mathbf{x}, \mathbf{u})) \sim \mathcal{O}(\rho_{\max}^6), \quad (33)$$

$$\text{trace}(\mathcal{B}_u(\mathbf{x}, \mathbf{u})) \sim \mathcal{O}(\rho_{\max}^4), \quad (34)$$

as $\rho_{\min} \rightarrow \infty$, in which $\rho_{\min} = \min\{\rho_m | \forall m \in \Omega\}$ and $\rho_{\max} = \max\{\rho_m | \forall m \in \Omega\}$.

caused by Path loss and resolution





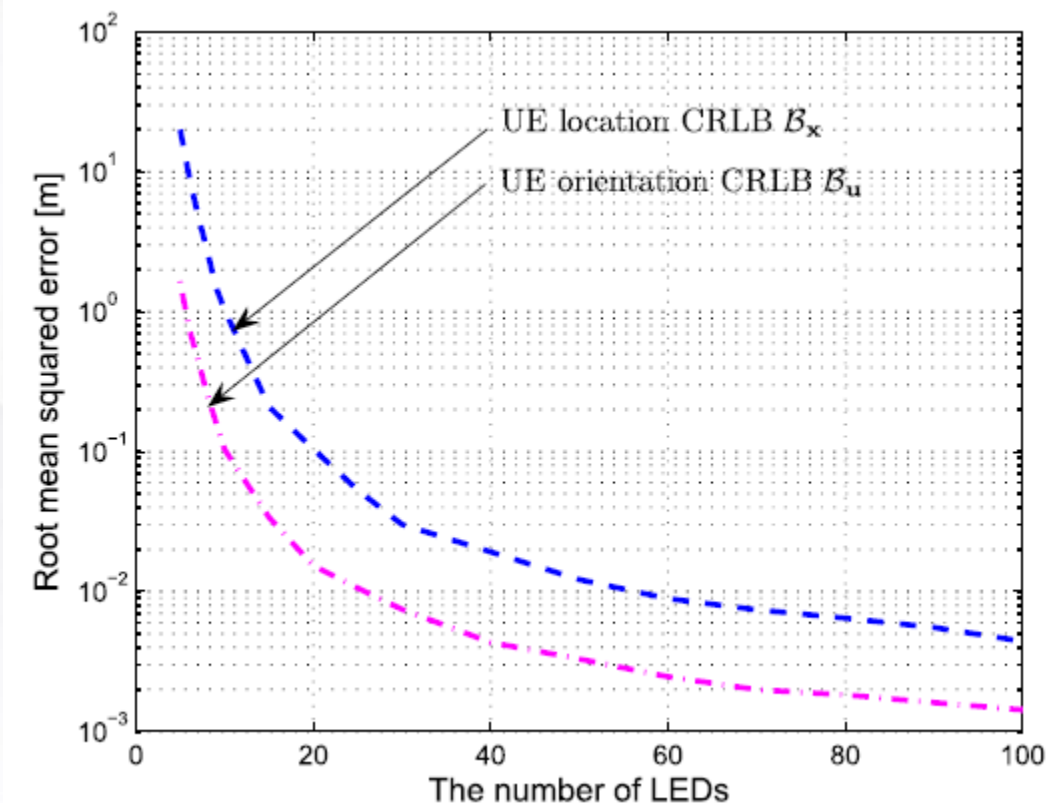
(2) Effect of Resource Factor

- The effect of **the number of LED sources**

Corollary 4 (The Effect of LED Set Size on CRLB): Assume the LEDs are uniformly distributed within the room. The UE location and orientation error bounds scale with the number of LEDs ($|\Omega|$) in the following manner: as $|\Omega| \rightarrow \infty$,

$$\text{trace}(\mathcal{B}_{\mathbf{x}}(\mathbf{x}, \mathbf{u})) \sim \mathcal{O}(|\Omega|^{-1}), \quad (37)$$

$$\text{trace}(\mathcal{B}_{\mathbf{u}}(\mathbf{x}, \mathbf{u})) \sim \mathcal{O}(|\Omega|^{-1}). \quad (38)$$





(2) Effect of Reflection Channel

- The effect of **reflection rate**

Corollary 9 (The Effect of Reflection Coefficient on NLOS-Based VLP Performance): The NLOS-based VLP error bounds $\mathfrak{B}_x^{\text{nlos}}(\mathbf{x}, \mathbf{u})$ and $\mathfrak{B}_u^{\text{nlos}}(\mathbf{x}, \mathbf{u})$ scale with the NLOS-path reflection coefficient as follows, as $\|\varphi\|_2 \rightarrow \infty$:¹¹

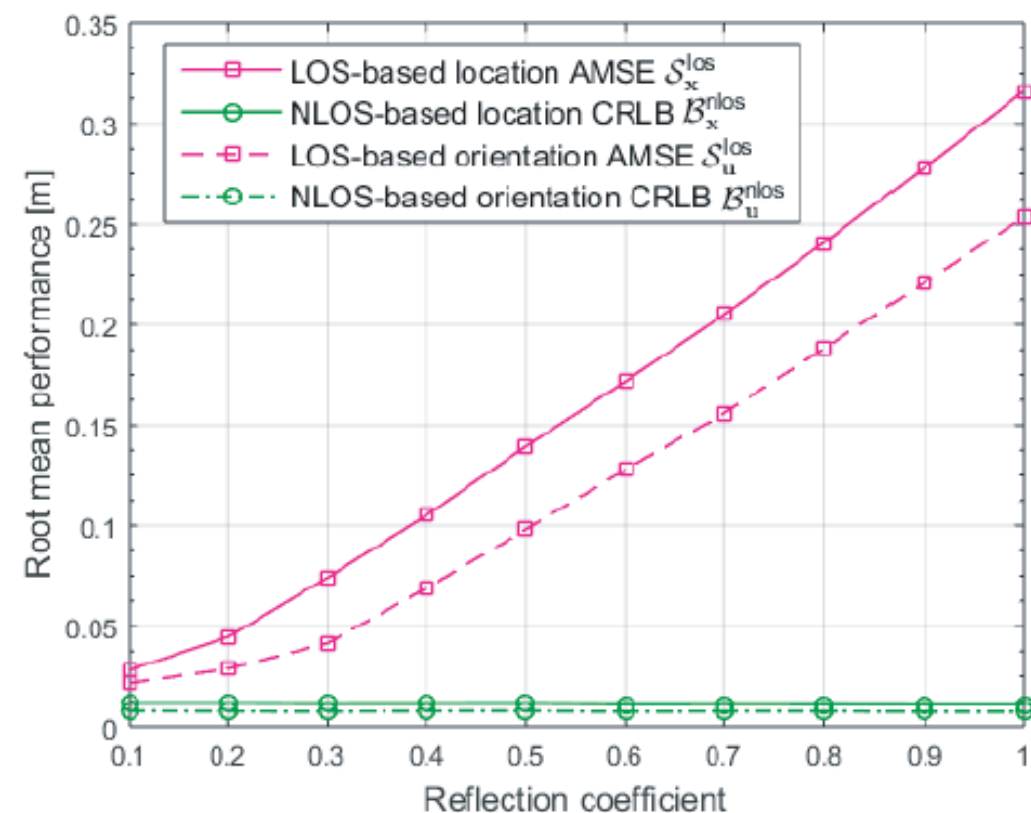
$$\text{trace}(\mathfrak{B}_x^{\text{nlos}}(\mathbf{x}, \mathbf{u})) \sim \Theta(\|\varphi\|_2^{-2}), \quad (68)$$

$$\text{trace}(\mathfrak{B}_u^{\text{nlos}}(\mathbf{x}, \mathbf{u})) \sim \Theta(\|\varphi\|_2^{-2}). \quad (69)$$

Corollary 10 (The Effect of Reflection Coefficient on LOS-Based VLP Performance): The LOS-based VLP error bounds $\mathfrak{B}_x^{\text{los}}(\mathbf{x}, \mathbf{u})$ and $\mathfrak{B}_u^{\text{los}}(\mathbf{x}, \mathbf{u})$ scale with the reflection coefficient strength $\|\varphi\|_2$ in the following manner, as $\|\varphi\|_2 \rightarrow \infty$:

$$\text{trace}(\mathfrak{B}_x^{\text{los}}(\mathbf{x}, \mathbf{u})) \sim \Theta(\|\varphi\|_2^2), \quad (70)$$

$$\text{trace}(\mathfrak{B}_u^{\text{los}}(\mathbf{x}, \mathbf{u})) \sim \Theta(\|\varphi\|_2^2). \quad (71)$$





(3) Information Alignment

(3) Information Alignment

- LOS channel-based CRLB on unbiased error

$$\mathcal{B}_x(\mathbf{x}, \mathbf{u}) = \left(\underbrace{\text{SNR} \cdot \mathcal{D}_x(\mathbf{x}, \mathbf{u})}_{\text{Observation information } \mathcal{H}_x^{\text{obs}}} + \chi_{\text{prior}} \right)^{-1}, \quad (18)$$

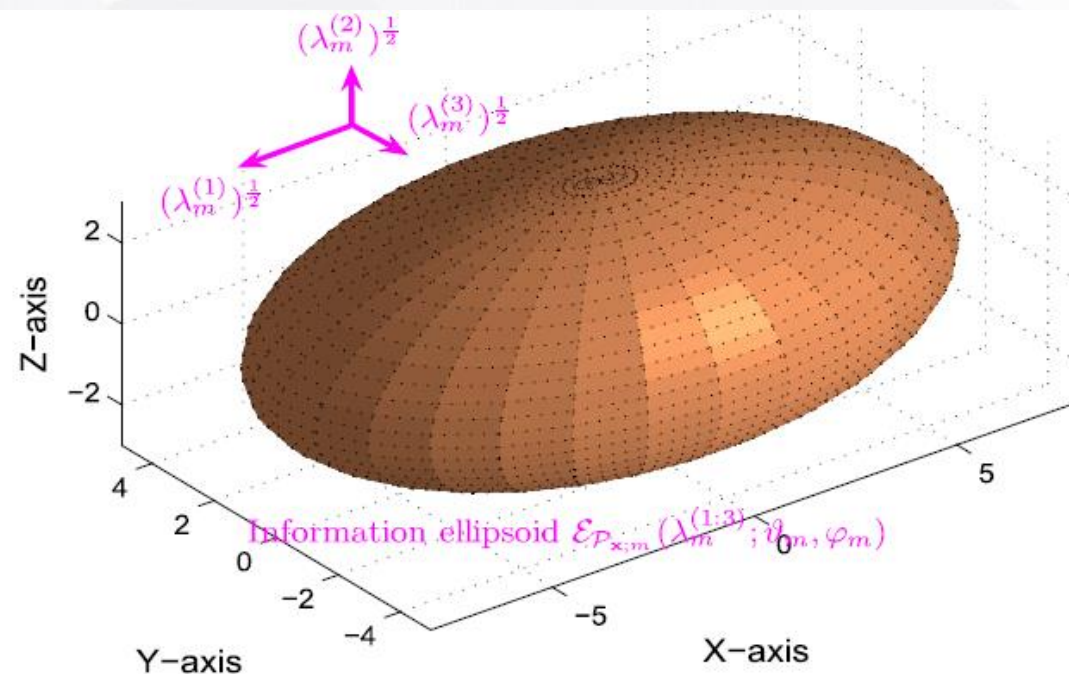
Total location information $\mathcal{J}_x(\mathbf{x}, \mathbf{u})$

$$\mathcal{B}_u(\mathbf{x}, \mathbf{u}) = \left(\underbrace{\text{SNR} \cdot \mathcal{D}_u(\mathbf{x}, \mathbf{u})}_{\text{Observation information } \mathcal{H}_u^{\text{obs}}} + \mathbf{U}_{\text{prior}} \right)^{-1}, \quad (19)$$

Total orientation information $\mathcal{J}_u(\mathbf{x}, \mathbf{u})$

$$\mathcal{D}_x(\mathbf{x}, \mathbf{u}) = \mathbf{H}(\mathbf{x})\mathbf{K}(\mathbf{u})\mathbf{F}(\mathbf{x}, \mathbf{u})(\mathbf{K}(\mathbf{u}))^\top (\mathbf{H}(\mathbf{x}))^\top, \quad (20)$$

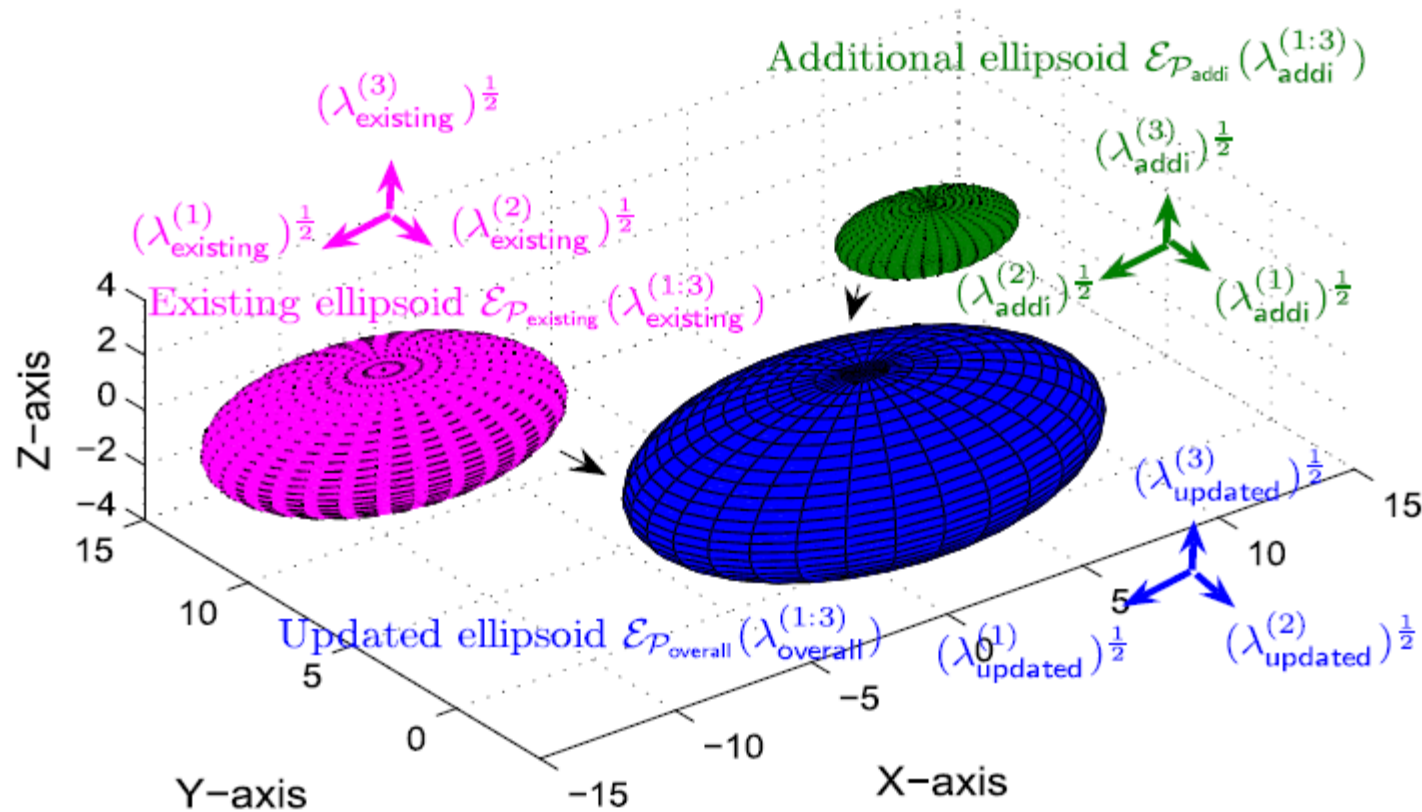
$$\mathcal{D}_u(\mathbf{x}, \mathbf{u}) = \mathcal{R}(\mathbf{u})(\mathbf{G}(\mathbf{x}))^\top \mathbf{V}(\mathbf{x}, \mathbf{u})\mathbf{G}(\mathbf{x})\mathcal{R}^\top(\mathbf{u}), \quad (21)$$



Definition 1 (Information Ellipsoid): Given an information matrix $\mathcal{P}_{x;m}$, its information ellipsoid $\mathcal{E}_{\mathcal{P}_{x;m}}$ is defined as the set of points $\mathcal{E}_{\mathcal{P}_{x;m}} = \{\mathbf{x} \in \mathbb{R}^3 | \mathbf{x}^\top \mathcal{P}_{x;m} \mathbf{x} = 1\}$. \square

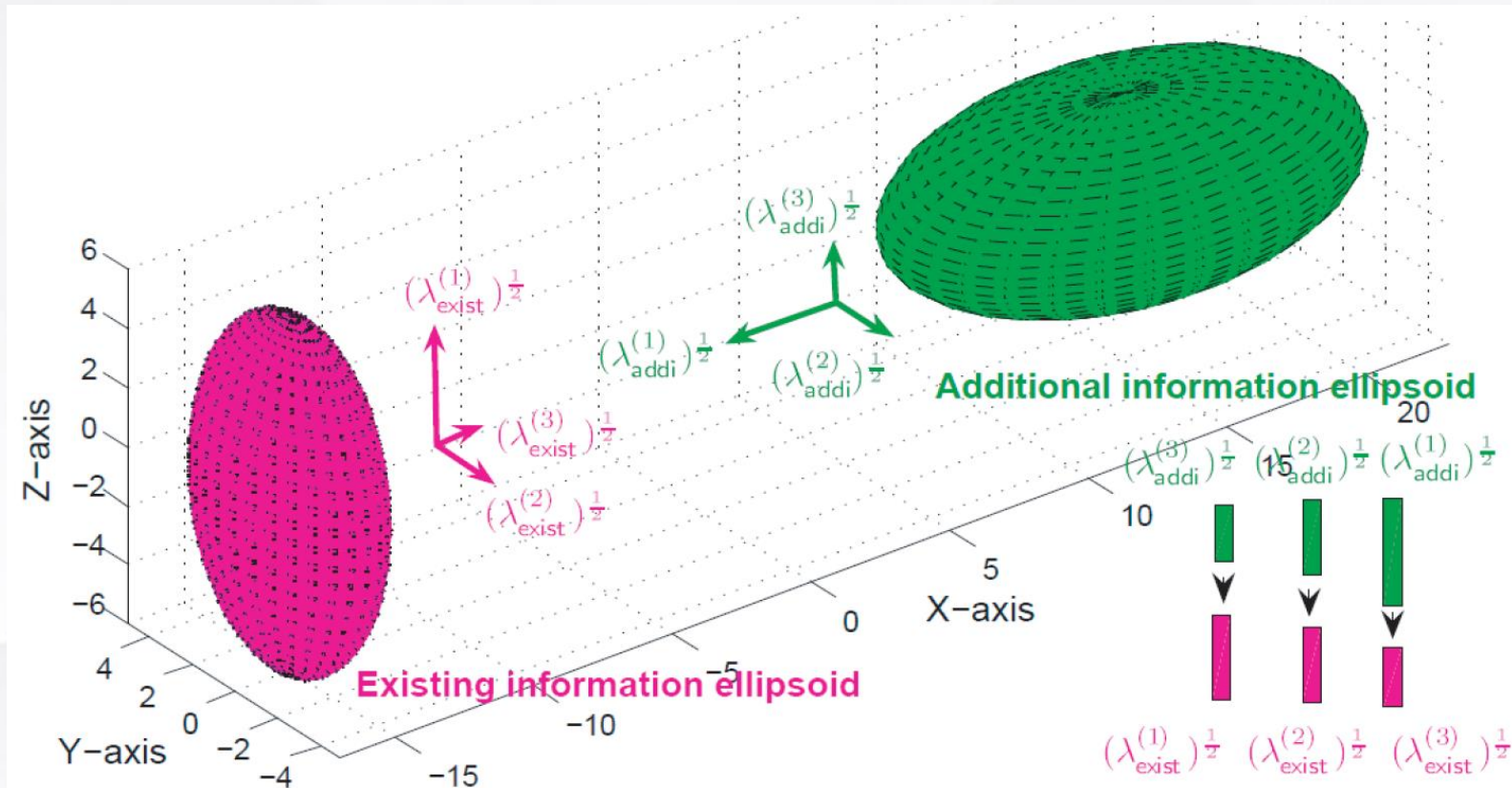
(3) Information Alignment

- localization cooperation => Information aggregation
- Spatial cooperation, multi-sensor fusion, mobility tracking



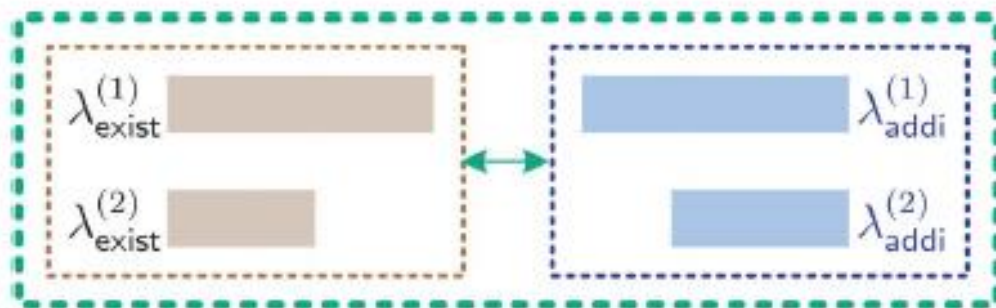
(3) Information Alignment

- Optimal cooperation => Best information alignment



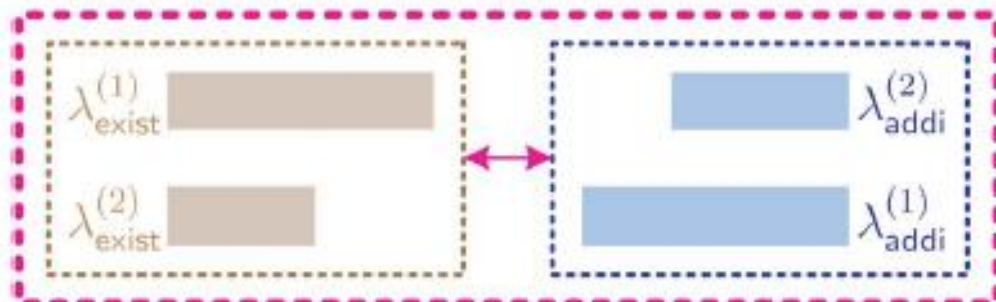
(3) Information Alignment

- Optimal cooperation => Best information alignment



The worst alignment:

$$\text{Overall } \mathcal{B}_{\max} = \frac{1}{\lambda_{\text{exist}}^{(1)} + \lambda_{\text{addi}}^{(1)}} + \frac{1}{\lambda_{\text{exist}}^{(2)} + \lambda_{\text{addi}}^{(2)}}$$



The best alignment:

$$\text{Overall } \mathcal{B}_{\min} = \frac{1}{\lambda_{\text{exist}}^{(1)} + \lambda_{\text{addi}}^{(2)}} + \frac{1}{\lambda_{\text{exist}}^{(2)} + \lambda_{\text{addi}}^{(1)}}$$



(4) Mobile UE Tracking



(4) Mobile UE Tracking

- Instantaneous UE tracking Problem formulation

$$\mathcal{P}_{\text{VLP}} : (\hat{\mathbf{x}}_t, \hat{\mathbf{u}}_t) = \arg \max_{\mathbf{x}_t, \mathbf{u}_t} p(\mathbf{x}_t, \mathbf{u}_t | \mathbf{z}_{1:t}, \tilde{\mathbf{x}}_{1:t}, \tilde{\mathbf{u}}_{1:t}), \quad (12)$$

$$p(\mathbf{x}_t, \mathbf{u}_t | \tilde{\mathbf{x}}_t, \tilde{\mathbf{u}}_t) = \underbrace{\mathcal{N}(\mathbf{x}_t | \tilde{\mathbf{x}}_t, \chi_{\text{prior}}) \mathcal{N}(\mathbf{u}_t | \tilde{\mathbf{u}}_t, \mathbf{U}_{\text{prior}})}_{\text{Inertial prior model}}, \quad (15)$$

$$p(\mathbf{z}_t | \mathbf{x}_t, \mathbf{u}_t) = \prod_{m \in \Omega_t} \mathcal{N}(z_{m,t} | h_m(\mathbf{x}_t, \mathbf{u}_t), \omega). \quad (17)$$



(4) Mobile UE Tracking

- Our Goal
- Establish error bounds for Instantaneous UE tracking error

$$\mathbb{E}_{\mathbf{z}_t} \{ \|\hat{\mathbf{x}}_t - \mathbf{x}_t\|_2^2 \} \geq \text{trace}(\mathcal{B}_{\mathbf{x}_t}(\mathbf{x}_t, \mathbf{u}_t)), \quad (18)$$

$$\mathbb{E}_{\mathbf{z}_t} \{ \|\hat{\mathbf{u}}_t - \mathbf{u}_t\|_2^2 \} \geq \text{trace}(\mathcal{B}_{\mathbf{u}_t}(\mathbf{x}_t, \mathbf{u}_t)), \quad (19)$$



(4) Mobile UE Tracking

- Instantaneous UE tracking error bounds

Theorem 1 (Single-Time-Slot CRLB): At the t th time slot, the CRLBs $\mathcal{B}_{\mathbf{x}_t}(\mathbf{x}_t, \mathbf{u}_t)$ and $\mathcal{B}_{\mathbf{u}_t}(\mathbf{x}_t, \mathbf{u}_t)$ of UE location and orientation, respectively, are given by

$$\mathcal{B}_{\mathbf{x}_t}(\mathbf{x}_t, \mathbf{u}_t) = \left(\underbrace{\text{SNR} \cdot \mathcal{D}_{\mathbf{x}_t}(\mathbf{x}_t, \mathbf{u}_t)}_{\text{Observation information } \mathcal{H}_{\mathbf{x}_t}^{\text{obs}}} + \chi_{\text{pred},t}^{\circ} \right)^{-1},$$

Total location information $\mathcal{J}_{\mathbf{x}_t}(\mathbf{x}_t, \mathbf{u}_t)$

(20)

$$\mathcal{B}_{\mathbf{u}_t}(\mathbf{x}_t, \mathbf{u}_t) = \left(\underbrace{\text{SNR} \cdot \mathcal{D}_{\mathbf{u}_t}(\mathbf{x}_t, \mathbf{u}_t)}_{\text{Observation information } \mathcal{H}_{\mathbf{u}_t}^{\text{obs}}} + \mathbf{U}_{\text{pred},t}^{\circ} \right)^{-1},$$

Total location information $\mathcal{J}_{\mathbf{u}_t}(\mathbf{x}_t, \mathbf{u}_t)$

1) *Prediction Information:* The overall prediction information matrices $\chi_{\text{pred},t}^{\circ}$ and $\mathbf{U}_{\text{pred},t}^{\circ}$ are given by

$$\chi_{\text{pred},t}^{\circ} = \chi_{\text{prior}} + \underbrace{\left(\chi_{\text{trans}}^{-1} + \mathcal{B}_{\mathbf{x}_{t-1}}(\alpha_{t-1}) \right)^{-1}}_{\text{Prediction information } \chi_{\text{pred},t}}, \quad (22)$$

Overall prediction information of UE location

$$\mathbf{U}_{\text{pred},t}^{\circ} = \mathbf{U}_{\text{prior}} + \underbrace{\left(\mathbf{U}_{\text{trans}}^{-1} + \mathcal{B}_{\mathbf{u}_{t-1}}(\alpha_{t-1}) \right)^{-1}}_{\text{Prediction information } \mathbf{U}_{\text{pred},t}}, \quad (23)$$

Overall prediction information of UE orientation

The essence of time-domain localization cooperation in mobile UE tracking is the **propagation** and **aggregation** of localization information, in an information-theoretic view.



(4) Mobile UE Tracking

- Evolution of VLP information/error

$$\mathcal{B}_{x_t} = (\mathcal{H}_{x_t}^{\text{obs}} + \chi_{\text{prior}} + (\chi_{\text{trans}}^{-1} + \mathcal{B}_{x_{t-1}})^{-1})^{-1}, \quad (32)$$

$$\mathcal{B}_{u_t} = (\mathcal{H}_{u_t}^{\text{obs}} + \mathbf{U}_{\text{prior}} + (\mathbf{U}_{\text{trans}}^{-1} + \mathcal{B}_{u_{t-1}})^{-1})^{-1}, \quad (33)$$

Theorem 2 (Convergence of TDEE): If A1 and A2 are satisfied, UE location and orientation error bounds \mathcal{B}_{x_t} and \mathcal{B}_{u_t} must converge to two certain fixed points \mathcal{B}_x^* and \mathcal{B}_u^* in \mathbb{S}^3 , respectively, at linear convergence rates, as $t \rightarrow \infty$, i.e.,⁵

$$\lim_{t \rightarrow \infty} \frac{\|\mathcal{B}_{x_{t+1}} - \mathcal{B}_{x_t}\|_F}{\|\mathcal{B}_{x_t} - \mathcal{B}_{x_{t-1}}\|_F} = 1 - \kappa_x \in (0, 1), \quad (36)$$

$$\lim_{t \rightarrow \infty} \frac{\|\mathcal{B}_{u_{t+1}} - \mathcal{B}_{u_t}\|_F}{\|\mathcal{B}_{u_t} - \mathcal{B}_{u_{t-1}}\|_F} = 1 - \kappa_u \in (0, 1), \quad (37)$$



(4) Mobile UE Tracking

- Evolution of VLP information/error

Theorem 4 (Monotonically Non-Increasing Of TDEE): If the observation information matrices $\mathcal{H}_{x_t}^{\text{obs}}$ and $\mathcal{H}_{u_t}^{\text{obs}}$ are non-decreasing over time and bounded from above by their limit states $\mathcal{H}_{x^*}^{\text{obs}}$ and $\mathcal{H}_{u^*}^{\text{obs}}$, respectively, i.e.,

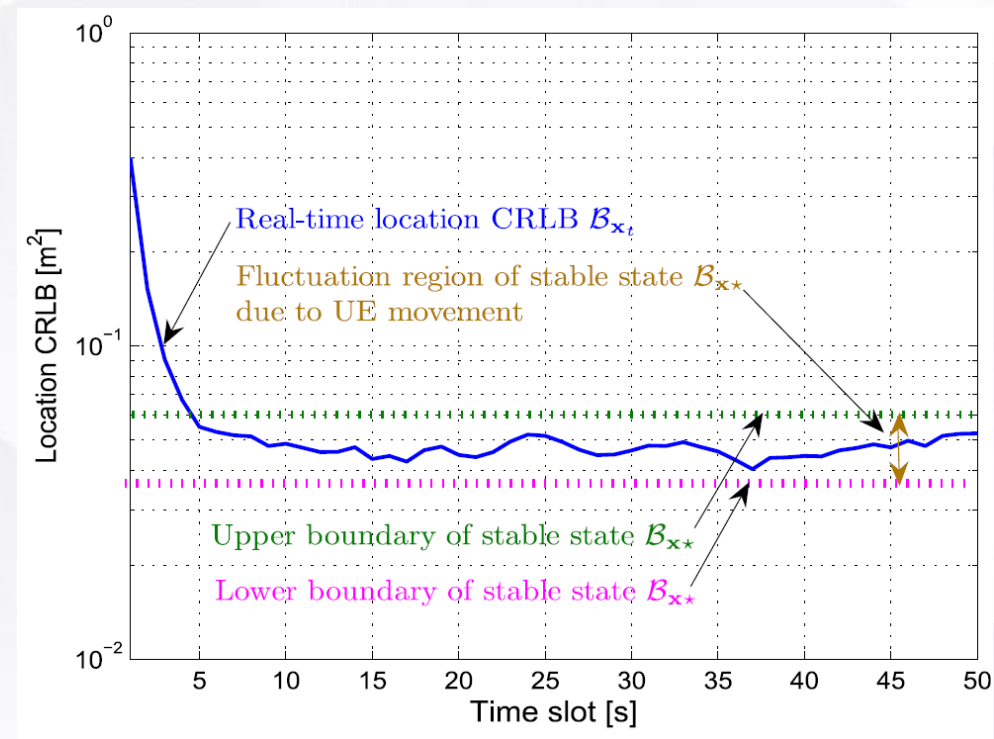
- (B1) $\mathcal{H}_{x_{t-1}}^{\text{obs}} \leq \mathcal{H}_{x_t}^{\text{obs}} \leq \mathcal{H}_{x^*}^{\text{obs}}, \forall t > 0,$

- (B2) $\mathcal{H}_{u_{t-1}}^{\text{obs}} \leq \mathcal{H}_{u_t}^{\text{obs}} \leq \mathcal{H}_{u^*}^{\text{obs}}, \forall t > 0,$

then the VLP error bounds \mathcal{B}_{x_t} and \mathcal{B}_{u_t} are both monotonically non-increasing over time, i.e.,

$$\mathcal{B}_{x_t} \leq \mathcal{B}_{x_{t-1}}, \quad \forall t > 0 \quad (40)$$

$$\mathcal{B}_{u_t} \leq \mathcal{B}_{u_{t-1}}, \quad \forall t > 0. \quad (41)$$



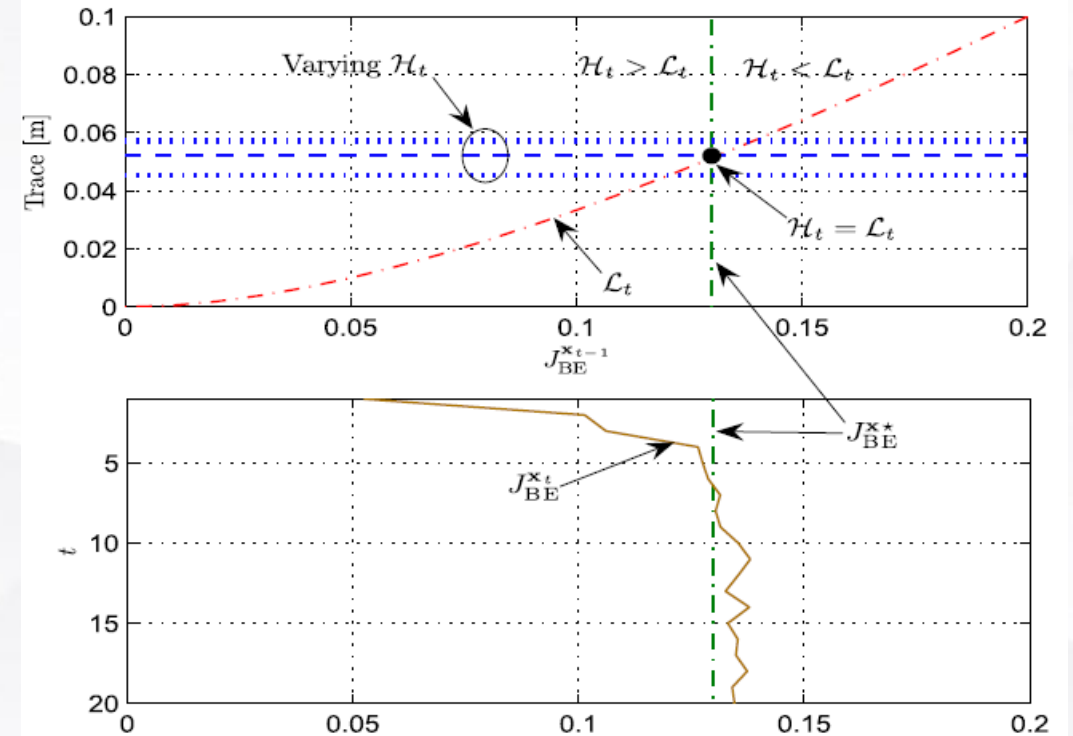
(4) Mobile UE Tracking

- VLP Error Evolution: steady state

Theorem 3 (Closed-Form Stable State Of TDEE): If A1 and A2 are satisfied, the closed-form expressions of the stable states (limit points) \mathcal{B}_x^* and \mathcal{B}_u^* of \mathcal{B}_{x_t} and \mathcal{B}_{u_t} , respectively, as $t \rightarrow \infty$, are given by

$$\mathcal{B}_x^* = \frac{1}{2} \chi_{\text{trans}}^{-\frac{1}{2}} \left(\mathbf{I}_3 + 4 \chi_{\text{trans}}^{\frac{1}{2}} (\mathcal{H}_{x^*}^{\#})^{-1} \chi_{\text{trans}}^{\frac{1}{2}} \right)^{\frac{1}{2}} \chi_{\text{trans}}^{-\frac{1}{2}} - \frac{1}{2} \chi_{\text{trans}}^{-1}$$

$$\mathcal{B}_u^* = \frac{1}{2} \mathbf{U}_{\text{trans}}^{-\frac{1}{2}} \left(\mathbf{I}_3 + 4 \mathbf{U}_{\text{trans}}^{\frac{1}{2}} (\mathcal{H}_{u^*}^{\#})^{-1} \mathbf{U}_{\text{trans}}^{\frac{1}{2}} \right)^{\frac{1}{2}} \mathbf{U}_{\text{trans}}^{-\frac{1}{2}} - \frac{1}{2} \mathbf{U}_{\text{trans}}^{-1}$$





Outline

- Background
- System Model
- Robust VLP Algorithm
- Performance Limits
- Resource Allocation & System Configuration
- Conclusions



System Configuration

Intuition:

- VLP error bounds dependent on resource factors
- Performance limits of VLP systems can be fundamentally improved via

$$\mathcal{B}_{\mathbf{x}}(\mathbf{x}, \mathbf{u}) = \left(\underbrace{\text{SNR} \cdot \mathcal{D}_{\mathbf{x}}(\mathbf{x}, \mathbf{u})}_{\text{Observation information } \mathcal{H}_{\mathbf{x}}^{\text{obs}}} + \chi_{\text{prior}} \right)^{-1}, \quad (18)$$

Total location information $\mathcal{J}_{\mathbf{x}}(\mathbf{x}, \mathbf{u})$

$$\mathcal{B}_{\mathbf{u}}(\mathbf{x}, \mathbf{u}) = \left(\underbrace{\text{SNR} \cdot \mathcal{D}_{\mathbf{u}}(\mathbf{x}, \mathbf{u})}_{\text{Observation information } \mathcal{H}_{\mathbf{u}}^{\text{obs}}} + \mathbf{U}_{\text{prior}} \right)^{-1}, \quad (19)$$

Total orientation information $\mathcal{J}_{\mathbf{u}}(\mathbf{x}, \mathbf{u})$

$$\mathcal{B}_{\alpha_{[k]}} \sim \text{scaling}(\text{bandwidth}), \text{ as bandwidth} \rightarrow 0$$

$$\mathcal{B}_{\alpha_{[k]}} \sim \text{scaling}(\text{NLOS interference}), \text{ as NLOS interference} \rightarrow 0$$

$$\mathcal{B}_{\alpha_{[k]}} \sim \text{scaling}(\text{channel variance}), \text{ as channel variance} \rightarrow 0$$

$$\mathcal{B}_{\alpha_{[k]}} \sim \text{scaling}(\text{RSU state error}), \text{ as RSU state error} \rightarrow 0$$

- [1] B. Zhou, A. Liu, and V. Lau, "Performance Limits of Visible Light-Based Positioning Using Received Signal Strength Under NLOS Propagation", IEEE Transactions on Wireless Communications, Vol. 18, No.11, 2019, pp. 5227-5241
- [2] B. Zhou, Y. Cao, and Y. Zhuang, "On the Performance Gain of Harnessing Non-Line-Of-Sight Propagation for Visible Light-Based Positioning," IEEE Transactions on Wireless Communications, Vol. 19, No.7, 2020, pp. 4863-4878
- [3] B. Zhou, A. Liu, V. Lau, J. Wen, S. Mumtaz, A. K. Bashir, and S. H. Ahmed, "Performance Limits of Visible Light-Based Positioning for Internet-of-Vehicles: Time-Domain Localization Cooperation Gain," IEEE Transactions on Intelligent Transportation Systems, vol. 22, no. 8, 2021, pp. 5374-5388.



(1) Resource Allocation

- Solution 1: Upper bound minimization

• **Upper Bound Minimization:** The first method is to minimize the associated CRLB via worst-case minimization. In such a case, sensing-driven ICAS power allocation can be formulated as

$$\hat{\mathbf{p}} = \arg \min_{\mathbf{p}} \max_{\beta} \text{trace}(\mathcal{B}_{\beta}(\mathbf{p}; \beta)), \quad (60)$$

$$\text{s.t. } \|\mathbf{p}\|_2 = 1, \quad (61)$$



(1) Resource Allocation

- Solution 2: Stochastic Average

• **Statistical Average:** If prior knowledge of vehicle state is available, e.g., from inertial measurements or GPS, RADAR, etc, the following statistical average of CRLB over prior knowledge can be used,

$$\mathcal{B}_{\beta}^{\#}(\mathbf{p}) = \int p(\beta) \mathcal{B}_{\beta}(\mathbf{p}; \beta) d\beta, \quad (62)$$

where $p(\beta)$ denotes the prior distribution of β .



$$\mathcal{B}_{\beta}^{\#}(\mathbf{p}) \approx \sum_{i=1:N_S} \frac{p(\beta_{[i]})}{q(\beta_{[i]})} \mathcal{B}_{\beta}(\mathbf{p}; \beta_{[i]}), \quad (66)$$



$$\hat{\mathbf{p}} = \arg \min_{\mathbf{p}} \text{trace}(\mathcal{B}_{\beta}^{\#}(\mathbf{p})), \quad (63)$$

$$\text{s.t. } \|\mathbf{p}\|_2 = 1, \quad (64)$$



(1) Resource Allocation

- Solution 3: Alternate Optimization

- **Alternating Optimization:** This approach is to use a hybrid criterion-driven optimization objective for guiding alternating iterations between resource parameter and state variable,

$$\left\{ \begin{array}{l} \mathcal{P}_{\text{resource}} : \mathbf{p}^* = \arg \min_{\mathbf{p}} \text{trace}(\mathcal{B}_{\beta}(\beta^*, \mathbf{p})), \\ \quad \quad \quad \downarrow \quad \text{(alternating iterations)} \quad \downarrow \\ \mathcal{P}_{\text{sensing}} : \beta^* = \arg \min_{\beta} \|\mathbf{z} - \mathbf{g}(\beta; \mathbf{p}^*)\|_2. \end{array} \right.$$

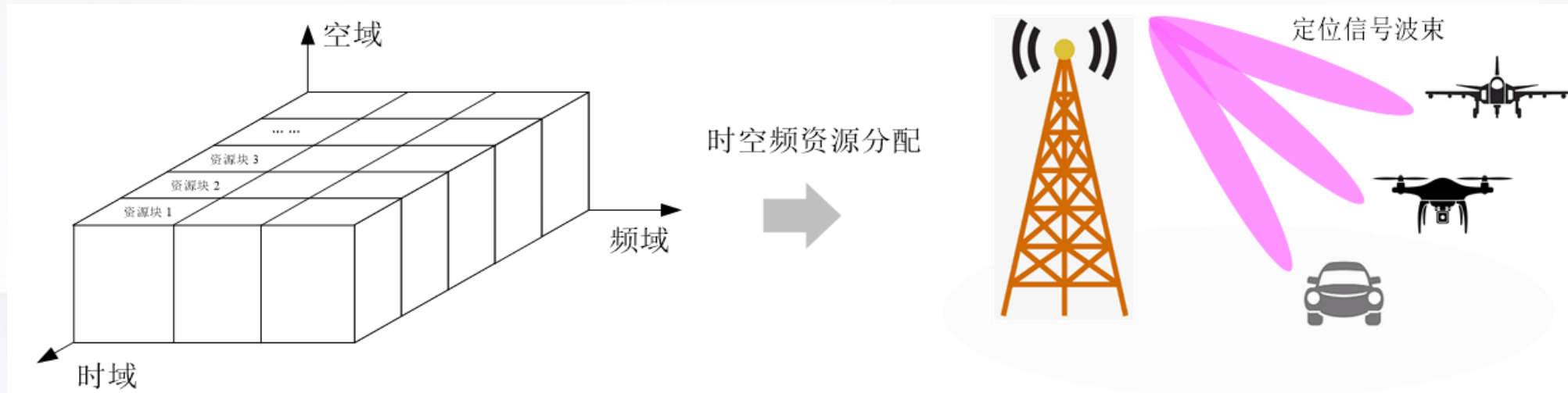
Shanshan Ma, and Bingpeng Zhou, "Asymptotic Performance Limits of Vehicular Location and Velocity Detection towards 6G mmWave Integrated Communication and Sensing," China Communications, 2023.

B. Zhou, A. Liu, and V. Lau, "Successive Localization and Beamforming in 5G mmWave MIMO Communication Systems", IEEE Transactions on Signal Processing, Vol.67, No.6, 2019, pp.1620-1635.

(2) Localization Beam Tracking

- Generate a sensing beam to continuously cover the vehicle

$$\begin{aligned}\hat{\mathbf{U}} = \arg \min_{\mathbf{U}} \max_{\beta} \{ & \text{trace}(\mathcal{B}_{\text{xUE}}(\mathbf{U}; \beta)), \mathcal{B}_{v\text{UE}}(\mathbf{U}; \beta) \}, \\ \text{s.t. } & \|\mathbf{U}\|_2 = 1.\end{aligned}\quad (67)$$





(3) Communication vs Sensing

- Comm & Sensing performance tradeoff via budgeting resource

$$\hat{N}_T = \arg \min_{N_T} \varrho(N_T, N_R), \quad (68)$$

$$\text{s.t. } N_T + N_R = N_{\text{total}}, \quad (69)$$

$$N_T \geq 0, N_R \geq 0, \quad (70)$$

$$\varrho(N_T, N_R) = \frac{\text{trace}(\mathcal{B}_{\text{xUE}}(N_T, N_R))}{\mathcal{R}(N_T)}, \quad (71)$$

$$\mathcal{R}(N_T) = B_{\text{width}} \ln(1 + \gamma_{\text{UE}}(N_T)), \quad (72)$$



Conclusion

- Demand end: intelligence-driven communication and sensing
- Supply end: consistent software and hardware
- Solution: integrated VLC and sensing
- Challenge: NLOS, fading, non-convex nature, resource allocation
- Our work:
 - Robust VLP algorithm design: stochastic sampling, VLC-assisted VLP, DL-driven VLP
 - Insightful analysis: closed-form error bound, the effect of resource and fading
 - Dynamic resource management: resource, beam tracking, C&S tradeoff
- Environment interference of VLP can be reduced via **elegant cooperation between communication and sensing.**



Future works

- Model based + data driven VLP
- UD velocity detection
- Multi-Target Detection
- Communication + localization for VLC
 - Multiband aggregation for VLP
 - Beam Focusing for near-field VLP
 - Sensing-assisted communication



Reference list

- [1] B. Zhou, Y. Cao, and Y. Zhuang, "On the Performance Gain of Harnessing Non-Line-Of-Sight Propagation for Visible Light-Based Positioning," IEEE Transactions on Wireless Communications, Vol. 19, No.7, 2020, pp. 4863-4878.
- [2] B. Zhou, A. Liu, V. Lau, et al, "Performance Limits of Visible Light-Based Positioning for Internet-of-Vehicles: Time-Domain Localization Cooperation Gain," IEEE Transactions on Intelligent Transportation Systems, vol. 22, no. 8, 2021, pp. 5374-5388.
- [3] B. Zhou, A. Liu, and V. Lau, "Successive Localization and Beamforming in 5G mmWave MIMO Communication Systems", IEEE Transactions on Signal Processing, Vol.67, No.6, 2019, pp.1620-1635.
- [4] B. Zhou, A. Liu, and V. Lau, "Performance Limits of Visible Light-Based Positioning Using Received Signal Strength Under NLOS Propagation", IEEE Transactions on Wireless Communications, Vol. 18, No.11, 2019, pp. 5227-5241.
- [5] B. Zhou, A. Liu, and V. Lau, "Joint User Location and Orientation Estimation in Visible Light Communication Systems with Unknown Power Emission", IEEE Transactions on Wireless Communications, Vol.18, No.11, 2019, pp. 5181-5195
- [6] B. Zhou, V. Lau, Q. Chen, and Y. Cao, "Simultaneous Positioning and Orientating (SPA0) for Visible Light Communications: Algorithm Design and Performance Analysis", IEEE Transactions on Vehicular Technology, Vol.67, No.12, 2018, pp.11790-11804.
- [7] Shanshan Ma, and Bingpeng Zhou, "Asymptotic Performance Limits of Vehicular Location and Velocity Detection towards 6G mmWave Integrated Communication and Sensing," China Communications, 2023



Bingpeng Zhou

zhoubp3@mail.sysu.edu.cn

**School of Electronics and Communication Engineering
Sun Yat-sen University, Shenzhen**